MOLECULAR CHARACTERIZATION OF BIOGENIC SECONDARY ORGANIC AEROSOL WITH VARIOUS ANALYTICAL TECHNIQUES

by

Peijun Tu

A dissertation submitted to the Faculty of the University of Delaware in partial fulfillment of the requirements for the degree of Doctor of Philosophy in Chemistry and Biochemistry

Fall 2017

MOLECULAR CHARACTERIZATION OF BIOGENIC SECONDARY ORGANIC AEROSOL WITH VARIOUS ANALYTICAL TECHNIQUES

by

Peijun Tu

Approved: _____

Brian J. Bahnson, Ph.D.
Chair of the Department of Chemistry and Biochemistry

Approved: _____

George Watson, Ph.D.
Dean of the College of Arts and Sciences

Approved: _____

Ann L. Ardis, Ph.D.
Senior Vice Provost for Graduate and Professional Education

I certify that I have read this dissertation and that in my opinion it meets the academic and professional standard required by the University as a dissertation for the degree of Doctor of Philosophy.

Signed: _____

Murray V. Johnston, Ph.D.
Professor in charge of
dissertation

I certify that I have read this dissertation and that in my opinion it meets the academic and professional standard required by the University as a dissertation for the degree of Doctor of Philosophy.

Signed: _____

Barbara S. Larsen, Ph.D.
Member of dissertation
committee

I certify that I have read this dissertation and that in my opinion it meets the academic and professional standard required by the University as a dissertation for the degree of Doctor of Philosophy.

Signed: _____

Karl S. Booksh, Ph.D.
Member of dissertation
committee

I certify that I have read this dissertation and that in my opinion it meets the academic and professional standard required by the University as a dissertation for the degree of Doctor of Philosophy.

Signed: _____

Douglas P. Ridge, Ph.D.
Member of dissertation
committee

ACKNOWLEDGMENTS

The financial support was provided by the National Science Foundation through grant numbers 1110554 and 1408455.

I would like to express the sincere gratitude to my advisor Prof. Murray Johnston who guides me to the wonderful world of science. His guidance and support throughout my graduate study help me become an independent and critical researcher. I am also very grateful to all my committee members, Dr. Barbara S. Larsen, Dr. Douglas P. Ridge and Dr. Karl S. Booksh for their valuable suggestions on my research and work.

I am also grateful to all the Johnston group members for their generous assistance. It's been an unforgettable experience to work and collaborate with them at UD. And I would particularly like to single out Dr. Andrew Horan. He has showed me patiently how the group and the lab operated by starting from every single piece of equipment in the lab, also provided me very useful advices throughout my research.

Last but not the least, this work would never be accomplished without the support from my family and friends. My father always encouraged me and shared his precious experience with me. My mother, stays far away from me though, supported me as best she can. And I would like to particularly thank my fiancé for his encouragement and patience throughout my academic years. Thanks for all the colleagues and friends I met during the study at UD, you made my graduated life meaningful and unforgettable and help me become a stronger one.

TABLE OF CONTENTS

LIST OF TABLES

LIST OF FIGURES

ABSTRACT

Secondary organic aerosol (SOA), which is produced by the oxidation of volatile organic compounds (VOCs) emitted from biogenic and anthropogenic sources, has great impact on the environment and human health. In this dissertation, SOA particles derived from biogenic precursors were characterized with various mass spectrometry techniques for molecular level analysis. Differences in the chemical compositions of these particles at different formation stages were used to gain insight into the formation and fate of SOA in the atmosphere. While not pursued in this dissertation, the changes studied here may also provide significant information about SOA toxicity and harm to human health.

SOA derived from ozonolysis of biogenic precursors was generated in a flow tube reactor and then sent into a photo chamber where the OH radicals could be produced to simulate further aging (fresh SOA oxidation with OH radicals to produce aged SOA). The molecular compositions of both fresh and aged SOA were studied with high resolution ESI-MS, and thousands of unique molecular formulas were characterized. Among these, a class of highly oxidized multifunctional (HOM) components, which are believed to contribute significantly to the formation of SOA, were identified and compared with previously reported Extremely Low-Volatility Organic Compounds (ELVOC) detected in the gas phase and Low Volatility Organic Oxygenated Aerosol (LV-OOA) measurements of the particle phase. HOMs in fresh SOA consisted mostly of monomers and dimers, which are consistent with condensation of ELVOCs reported from a separate study. Aging caused an increase in the average number of carbon atoms per molecule of the HOMs, which is consistent

with particle phase oxidation of (less oxidized) oligomers already existing in fresh SOA. For the biogenic precursors and experimental conditions studied, HOMs in fresh biogenic SOA have molecular formulas more closely resembling LVOOA than HOMs in aged SOA, suggesting that aging of biogenic SOA is not a good surrogate for ambient LVOOA.

In a separate set of experiments, SOA particles were size-selected in the 30-100 nm range with a Differential Mobility Analyzer (DMA) and analyzed by both on- and off-line mass spectrometry techniques. The chemical composition was found to change significantly with particle size. Both the average oxygen-to-carbon (O/C) ratio and carbon oxidation state (OSc) were found to decrease with increasing particle size, while the change of relative abundance of oligomers was opposite as the particle size increases. These changes allowed the relative contributions of condensation, partitioning, and particle phase oligomerization to be determined at various stages of particle formation and growth. Condensation of non-/low- volatility, highly oxidized species dominates the formation/growth of smaller SOA particles, while the partitioning of semi-volatile, less oxidized species tends to play an important role in the growth of larger SOA particles. The formation of oligomers that primarily takes place in the particle phase (accretion reactions) becomes more favored as the volume to surface area ratio of the particle increases.

Additionally, due to the complex molecular components of atmospheric nanoparticles, Reverse Phase Liquid Chromatography (RPLC) and Ion-Mobility Separation (IMS)- Mass Spectrometry were employed for molecular separation. Compositions partially separated based on their size, shape and polarity were subjected to tandem mass spectrometry for structure elucidation. In some cases, isomers/ isobars were identified and separated with the help of HPLC using gradient elution method.

Chapter 1

INTRODUCTION

1.1 Secondary Organic Aerosol (SOA) in the Atmosphere

Aerosol, which refers to solid particles/liquid droplets suspended in the surrounding air or another gas, has drawn great attention by environment scientists. A suspended aerosol particle is usually categorized based on its aerodynamic diameter. Respirable particles are those with diameters smaller than 10 μm. Those with diameters between 2.5 and 10 μm are coarse particles, while those with aerodynamic size ≤ 2.5 μm are fine particles and can penetrate more deeply into the respiratory system. Among these, ultrafine particles, with diameters ≤ 0.1 μm, are found to be closely related to the initial formation/nucleation and growth of aerosol in the atmosphere and are of special interest to the scientist. Ultrafine particles constitute the largest number of particles in the atmosphere and are of interest owing to their disproportionate influence on climate and human health.[1–6] Some fine and ultrafine particles have a strong ability to absorb and scatter light, thus will affect the amount of incoming/outcoming (scatter back) solar radiation between the sun and the earth surface.[7,8] Also important is their role as cloud condensation nuclei (CCN) and subsequent effect on cloud formation.[1,9,10] Together, the optical and CCN properties of these particles can substantially affect climate.[11,12] Additionally, fine and ultrafine particles that are breathed into human body cause irritation to throats first, followed by the deposition inside the human respiratory system, and might potentially cause heart and lung disease.[13–15]

In the atmosphere, primary aerosols are those directly emitted from anthropogenic (e.g. biomass burning, vehicle emission) and biogenic (e.g. sea spray, volcanic eruption) sources. This type of aerosol tends to have many particles with aerodynamic diameters >1 μm. In contrast, secondary aerosol, which is formed by the oxidation of small volatile species that can form very small nuclei (<5 nm) that subsequently grow into ultrafine and eventually fine particles. Of particular interest are volatile organic species that, when released from their sources, will be oxidized and eventually form Secondary Organic Aerosol (abbreviated as SOA in the following chapters). On a global scale, organic aerosol constitutes a substantial fraction of the total aerosol mass[1,16,17] in the atmosphere and most of it is secondary.[17,18] On a molecular level, the chemical composition of ambient organic aerosol is very complex, encompassing hundreds to thousands of individual compounds[1,19,20]. Laboratory generated SOA, which is formed inside a photo chemical chamber that mimics atmospheric conditions, is of similar complexity. A variety of oxidation and degradation pathways are proposed to explain molecular formation mechanism and product distributions.[1,21–23]

The atmospheric lifecycle of SOA includes particle formation, growth, aging and ultimately removal by volatilization or wet and dry deposition. During the initial formation and subsequent growth stages, organic molecules (i.e. SVOCs, NVOCs) are thought to enter the particle phase mainly by a combination of condensation and partitioning.[24,25] Condensation occurs when the gas phase mixing ratio of a compound is larger than its equilibrium vapor pressure and the "on" rate determined by collisions of gas phase molecules with the particle surface exceeds the "off" rate determined by re-evaporation of molecules from the particle phase. Partitioning occurs when the gas phase mixing ratio is smaller than the equilibrium vapor pressure and the compound distributes between the gas and particle phases. Accretion reaction, defined as the

formation of oligomers in the particle phase, is also found to make a great contribution to SOA production and will be described later in this dissertation. At the other end of the lifecycle, the end products of SOA oxidation ultimately would be carbon dioxide and water, though wet and dry deposition are usually too fast to reach this endpoint. Once SOA is freshly formed, it might undergo further aging in the atmosphere. Here, aging refers to further oxidation of particle phase organics with OH radicals, which are highly reactive, short lived and generated by the reaction of excited atomic oxygen with water (discussed in Chapter 2) in the upper troposphere[26]:

$$O_3 + h\nu\ (\lambda \leq 310\ \text{nm}) \rightarrow O(^1D_2) + O_2 \quad (1)$$

$$O(^1D_2) + H_2O \rightarrow 2OH \quad (2)$$

As SOA undergoes the aging process in the atmosphere, it is subjected to both functionalization and fragmentation.[27] Functionalization occurs because oxidation leads to the formation of new functional groups such as acids and carbonyls. Fragmentation occurs because carbon-carbon bonds are broken, leading to the formation of smaller molecules that are also functionalized, but because of their lower molecular mass they may partition back to the gas phase. As aging proceeds, functionalization can initially lead to the formation of additional SOA mass because the insertion of functional groups lowers the vapor pressure, though eventually fragmentation leads to the loss of SOA mass through volatilization.[27,28] Therefore, the organic matter remaining in the particle phase after aging tends to be more highly oxidized and less volatile than the fresh SOA. The aging process studied in my work specifically focuses on the photooxidation of fresh SOA with OH radicals. With the presence of OH in the atmosphere, RO_2 radicals are formed by H abstraction and O_2 addition, followed by further reaction between RO_2 or with other species such as HO_2 and NO_2. Photolysis and other photochemical reactions take place as well producing some oxygenated organic compounds (e.g. peroxides and carbonyls[29]).

1.2 SOA from Oxidation of Biogenic Precursors

On a regional and global scale, a great fraction of SOA is emitted into the atmosphere from biogenic sources of which most are vegetation [30,31]. Due to their high chemical reactivity and large amount of emission, Biogenic Volatile Organic Compounds (BVOCs) play an important role in the chemistry of lower troposphere and atmospheric boundary layer. These organic compounds include monoterpenes ($C_{10}H_{16}$), isoprene (C_5H_8), sesquiterpenes ($C_{15}H_{24}$) and a variety of oxygenated compounds including hexane derivatives and methane.[32,33] Among these, monoterpenes account for a substantial fraction of nonmethane hydrocarbons emitted from the terrestrial biosphere[30,31], with an estimated global contribution to SOA of ~10%, and of this α-pinene (35% of monoterpene SOA) and β-pinene (23% of monoterpene SOA) are main contributors.[31,34] These two compounds are structural isomers (the two most abundant terpenes in the troposphere) and have been studied widely by the atmospheric scientist over several decades.

The oxidants that evolve in the formation of SOA include O_3, NO_3 and OH radical of which the reactions produce a variety of oxygenated compounds. In the troposphere, the most significant formation source of O_3 is the photolysis of NO_2:

$$NO_2 + h\nu \rightarrow NO + O(^3P) \quad (1)$$

$$O(^3P) + O_2 + M \rightarrow O_3 + M \ (M = \text{air}) \quad (2)$$

The ambient concentration of O_3 is typically on the ppb level. In contrast, NO_3 (< 1 ppt) and OH (<1 ppt) radicals are found to have a much lower concentration in the troposphere due to their relatively short lifetime and certain formation time range (OH radical is only formed during the day-time under the irradiation of UV light[35] while NO_3 is mostly involved in night-time chemistry when OH concentration is zero[36]). Ozone and OH are the most important atmospheric oxidants due to their high chemical

potentials, abundance, and negative effects on human health. Laboratory studies were performed to investigate the formation of SOA derived from ozonolysis of α- and β-pinene due to their high reaction rates (second order rate constants (0.28–3.3) x 10^{-16} cm^3 $molecule^{-1}$ s^{-1} for a-pinene and (1.2–6.5) x 10^{-17} cm^3 $molecule^{-1}$ s^{-1} for b-pinene)[37]. The current understanding of gas phase alkene- ozone reaction was proposed by Criegee and following studies were performed in the condensed phase.[38,39]

The reaction between O_3 and α- or β-pinene is initiated by the attachment of ozone onto the double bond followed by the formation of a primary ozonide[39]. The excited primary ozonide subsequently undergoes unimolecular isomerization (for α-pinene) or decomposition (for β-pinene) to yield chemically activated carbonyl oxides or Criegee intermediates (CIs) and aldehydes (for β-pinene). As shown in Figure 1.1 (adapted from a separate study[40]), during the reaction of ozone and β-pinene, most of the CIs have enough internal energy and are subjected to further unimolecular reactions or collisional stabilization. There are two main pathways for the CIs to stabilized and form monomers. One is the 'Ester Channel' of which produce some C_{10} species (e.g. ketopinic acid, pinanediol) through ring-closure and further isomerization. The other reaction pathway is 'Hydroperoxide Channel'. H migration on CIs and subsequent isomerization or decomposition lead to formation of acids, carbonyls, and a variety of C_9 monomers (e.g. pinic acid, pinonic acid). In general, both reaction pathways yield a great variety of SOA monomers containing functional groups (e.g. hydroxyl, carbonyl, carboxyl, hydroperoxyl). Some of the monomers undergo subsequent formation of dimers, trimers or even higher orders oligomers through bonding with others by the oxygen containing functional groups. There have been a variety of studies investigating the dominant reactions that form the oligomeric component of SOA. For instance, aldol condensation, formation of hemiacetal as well as the hydroperoxide ester (e.g. formed by reaction of SCI and carboxylic acid) are reported to play

important roles in oligomerization.[41,42] Recently, particle phase chemistry, specifically accretion reactions in the particle phase that form higher MW lower volatility oligomers from higher volatility lower MW monomers[43], have been proposed as an additional pathway for SOA formation.

Figure 1.1. Reaction mechanism of β-pinene ozonolysis.

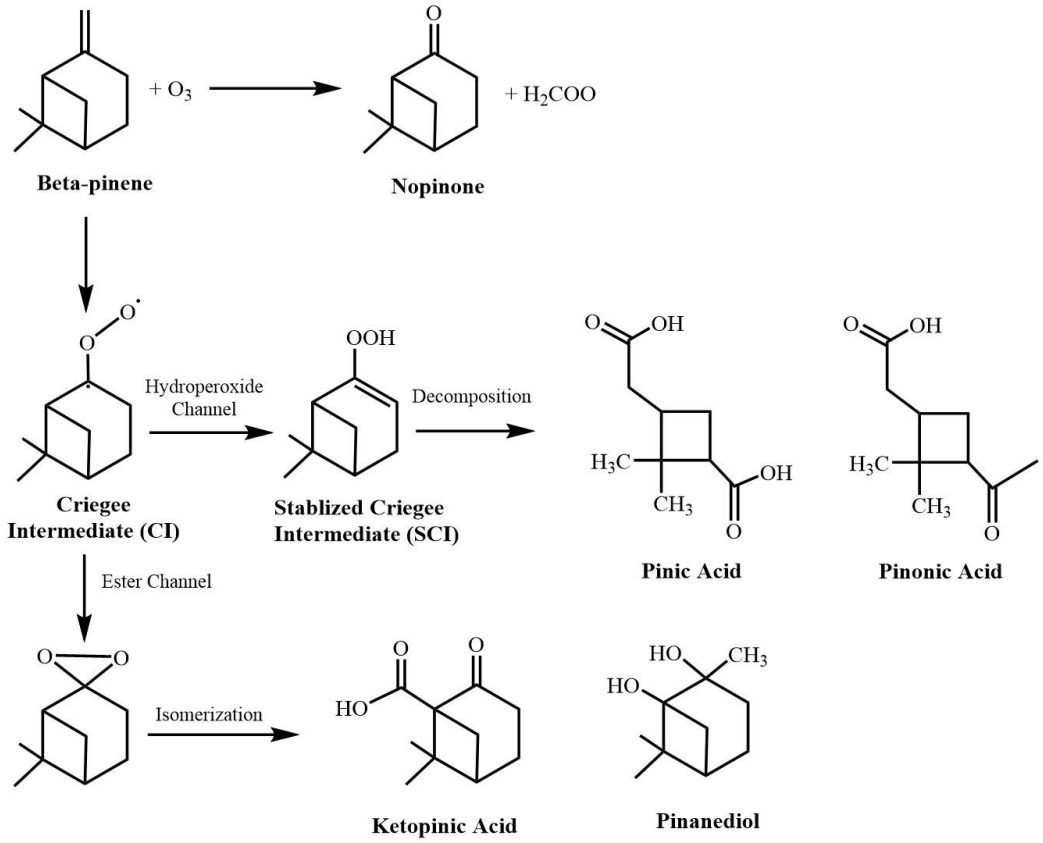

1.3 Chemical Analysis of SOA

As mentioned above, both ambient and laboratory organic aerosol are very complex on a molecular level. Both number and types of their components change with the identity of the VOC precursor and the manner and extent to which oxidation occurs.[20,40,44–47] The chemical composition analysis of SOA covers a wide range of analytical instrument techniques and each of them has its own strengths and weaknesses. For example, thermal- optical EC/OC analyzer is able to quantify the amount (mass) of elemental carbon and organic carbon contained in SOA, but lacks the capability to determine molecular formulas[1]; Fourier Transform Infrared (FTIR) and Nuclear Magnetic Resonance (NMR) spectroscopy provide detailed information on functional groups/elemental compositions[48,49] in SOA but generally require large amounts of sample with long collection time, and therefore are difficult to apply to ultrafine particles and size selection. Gas Chromatography mass spectrometry (GC-MS) provides the molecular speciation and sensitivity needed, but it is only able to characterize thermally stable compounds, which represent only a small mass fraction of SOA in the atmosphere.[50] Generally, the optimal analytical techniques need to meet the requirements of high chemical resolution, short collection/detection time, good particle size resolution and the ability to characterize nonvolatile compounds.

Aerosol Mass Spectrometry (AMS) has been widely used as an online technique for bulk measurements of SOA (i.e. overall elemental composition of the sample) and provides good sensitivity and hence the ability for high time and size resolution.[51,52] With this method, a particle beam is aerodynamically transmitted into the EI source under vacuum using capillaries, nozzles or aerodynamic lenses. Once in the source, particles are then vaporized and ionized. Ions are analyzed with a quadrupole, ion trap or time-of-flight (TOF). The energy of EI source (70 eV) causes extensive fragmentation of individual molecules, and the fragment ions from the

various molecules in the particle overlap in the particle mass spectrum. As a result, only the bulk aerosol elemental composition is obtained from the ions observed in the mass spectrum. One strength of AMS is that it offers real-time, online analysis, without problems due to contamination and side reactions during sample storage when samples are collected for offline analysis. However, the high vaporization temperature (~ 600 ˚C) of particle beam tends to induce the thermal decomposition and evaporation of the analytes especially the relatively volatile ones.[1,53] Therefore, the elemental composition measured by AMS is derived from the decomposition products after losing small neutral fragments (e.g. CO_2, CO, H_2O) from carboxylic acid/alcohol molecules, thus results in the potential bias of the elemental ratio (e.g. O/C, H/C ratio) measurements.[53]

Molecular analysis of laboratory SOA is usually performed with off-line techniques. SOA samples are generated in the reaction chamber, collected onto filters and extracted with solvents for further analysis with high resolution mass spectrometry. Various ionization sources (e.g. CI, APCI, MALDI, EI) and mass analyzers (e.g. TOF, FTICR, Triple Quadrupole) have been used to perform chemical analysis of SOA on a molecular level. Electrospray ionization (ESI), which is the soft ionization technique that produces mostly molecular ions, is coupled with high resolution mass analyzers to obtain elemental formulas of individual molecules. Generally, due to its high resolution and mass accuracy, electrospray ionization high resolution mass spectrometry (ESI-HRMS) typically detects 1000 or more unique molecular formulas in a given SOA sample (e.g. ozonolysis of β-pinene as shown in Figure 1.2 with negative ion detection). As shown in the figure, multiple groups of peaks which can be classified as monomers, dimers and other high order oligomers are detected. Timers and tetramers, which hardly seen due to their low signal intensity, are displayed in an expanded spectrum. It is noted that ions are detected at almost

each nominal mass. Figures in Chapter 2 and further discussion will display the existence of multiple ions detected within one nominal mass (isobaric species), which means that the molecular composition is even more complex that it looks in Figure 1.2.

Figure 1.2. An example of SOA (β-pinene ozonolysis) sample detected with high resolution mass spectrometry in the negative ion mode.

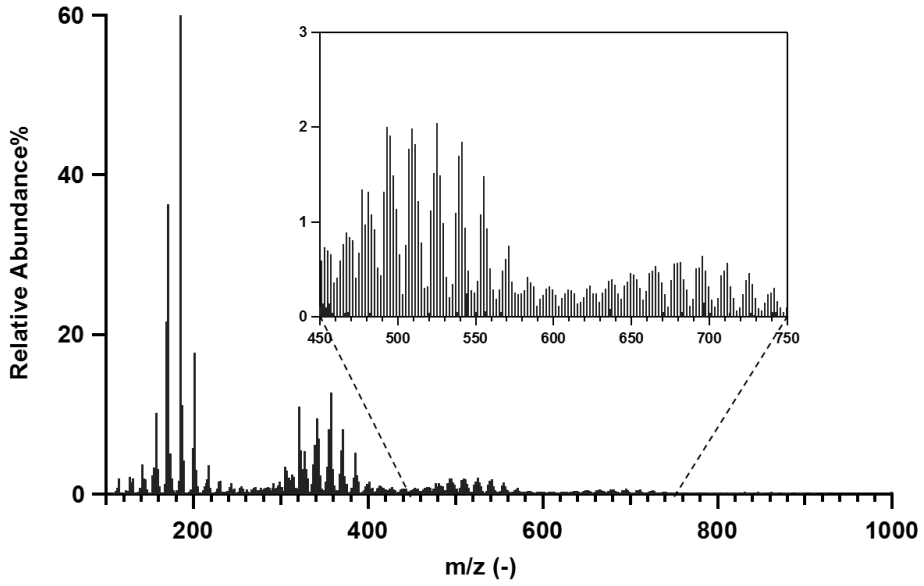

The determination of individual molecular formulas allows SOA to be assessed on a molecule-by-molecule basis or by combining the formulas from the various compounds to reconstruct average/bulk parameters for the entire SOA sample such as oxygen to carbon (O/C) and hydrogen to carbon (H/C) elemental ratios that are determined with AMS.[53,54] Also of interest is the average Oxidation State of Carbon (OSc), which is defined in terms of O/C and H/C elemental mole ratios[55]:

$$OSc = 2\,(O/C) - (H/C)$$

The goal of my research is to study the chemical composition of SOA at

different formation stages. This includes study of photooxidation of freshly formed SOA derived from ozonolysis of biogenic precursors including α-pinene, β-pinene and limonene. In Chapter 2, the chemical composition of both fresh and aged SOA (the latter photo-oxidized by OH radical) were assessed off-line using high resolution MS. Highly Oxidized Multifunctional (HOM) components, based on their important role in the SOA, were studied in particular as an indicator to the degree of oxidation of SOA. Chapter 3 investigates the growth mechanism of SOA particles in the size range of 10-100 nm. Size-resolved SOA particles were classified with a Differential Mobility Analyzer (DMA) and collected with a nano aerosol sampler (NAS), which allowed very small sample amounts to be analyzed. The chemical composition of SOA at each size was assessed with high resolution mass spectrometry similar to that in Chapter 2. However, one of the weaknesses for off-line analysis is the errors brought in during sample collection, extraction and storage. Therefore, a combination of both on- and off-line analysis techniques was used to investigate and rule out the bias that could result from either method. On-line analysis was performed with the Nano Aerosol Mass Spectrometer (NAMS), which was developed by our group.

As mentioned above, a great number of molecular formulas are detected from a single SOA sample with HR-MS and some of them have been reported to have various isomers that are not distinguished by MS alone.[56,57] Therefore, hyphenated methods combining powerful chromatography and tandem mass spectrometry techniques are essential for the molecular separation, identification and structure elucidation. In Chapter 4, Reverse Phase Liquid Chromatography (RPLC) is coupled with high resolution MS/MS^2 for SOA analysis. Methods to separate complex SOA samples were developed and the separation results are discussed. It is shown that some of the isomeric and isobaric components can be separated during the interaction with the mobile/stationary phase in the LC column. The separation efficiency of RPLC is also

compared with that of Ion Mobility Separation (IMS)-MS, of which the separation principle is based on size/shape of the molecules. In these experiments, Tandem Mass Spectrometry was coupled for the structure elucidation. A series of isomeric species identified as mono/dicarboxylic acid and peroxy acid are displayed and their relative abundance during different SOA formation stages (e.g. fresh vs. aged, 30-110 nm) are discussed as well.

In summary, molecular level analysis including non-target screening, HOM analysis, size-segregated nanoparticles, isomeric/isobaric components separation and structure elucidation of monoterpene derived SOA during different formation stages were investigated in my research. The results give insight into the evolution and fate of monoterpene derived SOA in the atmosphere.

REFERENCES

(1) Hallquist, M.; Wenger, J. C.; Baltensperger, U.; Rudich, Y.; Simpson, D.; Claeys, M.; Dommen, J.; Donahue, N. M.; George, C.; Goldstein, A. H.; Hamilton, J. F. *Atmos. Chem. Phys. Atmos. Chem. Phys.* **2009**, *9*, 5155–5236.

(2) Ramanathan, V. *Science.* **2001**, *294* (5549), 2119–2124.

(3) Kaufman, Y. J.; Tanré, D.; Boucher, O. *Nature* **2002**, *419* (6903), 215–223.

(4) Lelieveld, J.; Crutzen, P. J.; Ramanathan, V.; Andreae, M. O.; Brenninkmeijer, C. M.; Campos, T.; Cass, G. R.; Dickerson, R. R.; Fischer, H.; J Hansel, A.; Jefferson, A.; Kley, D.; de Laat, A. T.; Lal, S.; Lawrence, M. G.; Lobert, J. M.; Mayol- Bracero, O. L.; Mitra, A. P.; Novakov, T.; Oltmans, S. J.; Prather, K. A.; Reiner, T.; Rodhe, H.; Scheeren, H. A.; Sikka, D.; Williams, J. *Science* **2001**, *291* (5506), 1031-1036.

(5) Andreae, M. O.; Crutzen, P. J. *Science* **1997**, *276* (5315), 1052–1058.

(6) Haywood, J.; Boucher, O. *Reviews of Geophysics*. **2000**, 513-543.

(7) Barker, T. *Change* **2007**, *446*, 12–17.

(8) Finlayson-Pitts, B. J.; Pitts, J. N. *Chemistry of the Upper and Lower Atmosphere: Theory, Experiments, and Applications*; **2000**.

(9) Rissman, T. a.; Varutbangkul, V.; Surratt, J. D.; Topping, D. O.; McFiggans, G.; Flagan, R. C.; Seinfeld, J. H. *Atmos. Chem. Phys. Discuss.* **2006**, *6* (6), 13251–13305.

(10) Dinar, E.; Anttila, T.; Rudich, Y. *Environ. Sci. Technol.* **2008**, *42* (3), 793–799.

(11) Kulmala, M.; Suni, T.; Lehtinen, K. E. J.; Dal Maso, M.; Boy, M.; Reissell, A.; Rannik, Ü.; Aalto, P.; Keronen, P.; Hakola, H.; Bäck, J.; Hoffmann, T.; Vesala, T.; Hari, P. *Atmos. Chem. Phys.* **2004**, *4*, 557–562.

(12) Adams, P. J.; Seinfeld, J. H. *J. Geophys. Res. Atmos.* **2002**, *107* (19).

(13) Davidson, C. I.; Phalen, R. F.; Solomon, P. A. *Aerosol Sci. Technol.* **2005**, *39* (8), 737–749.

(14) Pope, C. A.; Dockery, D. W. *J. Air Waste Manage. Assoc.* **2006**, *56* (6), 709–742.

(15) Harrison, R. M.; Yin, J. *Science of the Total Environment*. **2000**, 85–101.

(16) Kanakidou, M.; Seinfeld, J. H.; Pandis, S. N.; Barnes, I.; Dentener, F. J.; Facchini, M. C.; Van Dingenen, R.; Ervens, B.; Nenes, A.; Nielsen, C. J.; Swietlicki, E.; Putaud, J. P.; Balkanski, Y.; Fuzzi, S.; Horth, J.; Moortgat, G. K.; Winterhalter, R.; Myhre, C. E. L.; Tsigaridis, K.; Vignati, E.; Stephanou, E. G.; Wilson, J. *Atmos. Chem. Phys.* **2005**, *5*, 1053–1123.

(17) Jimenez, J. L.; Canagaratna, M. R.; Donahue, N. M.; Prevot, a. S. H.; Zhang, Q.; Kroll, J. H.; DeCarlo, P. F.; Allan, J. D.; Coe, H.; Ng, N. L.; Aiken, A. C.; Dorcherty; K. S.; Ulbrich, I. M.; Grieshop, A. P.; Robinson, a. L.; Duplissy, J.; Smith, J. D.; Wilson, K. R.; Lanz, V. a.; Hueglin, C.; Sun, Y. L.; Tian, J.; Laaksonen, A.; Raatikainen, T.; Rautiainen, J.; Vaattovaara, P.; Ehn, M.; Kulmala, M.; Tomlinson, J. M.; Collins, D. R.; Cubison, M. J.; Dunlea, J.; Huffman, J. A.; Onasch, T. B.; Alfarra, M. R.; Williams, P. I.; Bower, K.; Kondo, Y.; Schneider, J.; Drewnick, F.; Borrmann, S.; Weimer, S.; Demerjian, K.; Salcedo, D.; Cottrell, L.; Griffin, R.; Takami, a.; Miyoshi, T.; Hatakeyama, S.; Shimono, A.; Sun, J. Y.; Zhang, Y. M.; Dzepina, K.; Kimmel, J. R.; Sueper, D.; Jayne, J. T.; Herndon, S. C.; Trimborn, a. M.; Williams, L. R.; Wood, E. C.; Middlebrook, A. M.; Kolb, C. E.; Baltensperger, U.; Worsnop, D. R. *Science.* **2009**, *326* (5959), 1525–1529.

(18) Ng, N. L.; Canagaratna, M. R.; Zhang, Q.; Jimenez, J. L.; Tian, J.; Ulbrich, I. M.; Kroll, J. H.; Docherty, K. S.; Chhabra, P. S.; Bahreini, R.; Murphy, S. M.; Seinfeld, J. H.; Hildebrandt, L.; Donahue, N. M.; Decarlo, P. F.; Lanz, V. A.; Prévôt, A. S. H.; Dinar, E.; Rudich, Y.; Worsnop, D. R. *Atmos. Chem. Phys.* **2010**, *10* (10), 4625–4641.

(19) Chan, A. W. H.; Isaacman, G.; Wilson, K. R.; Worton, D. R.; Ruehl, C. R.; Nah, T.; Gentner, D. R.; Dallmann, T. R.; Kirchstetter, T. W.; Harley, R. A.; Gilman, J. B.; Kuster, W. C.; De Gouw, J. A.; Offenberg, J. H.; Kleindienst, T. E.; Lin, Y. H.; Rubitschun, C. L.; Surratt, J. D.; Hayes, P. L.; Jimenez, J. L.; Goldstein, A. H. *J.*

Geophys. Res. Atmos. **2013**, *118* (12), 6783–6796.

(20) Goldstein, A. H.; Galbally, I. E. *Environ. Sci. Technol.* **2007**, *41* (5), 1514–1521.

(21) Donahue, N. M.; Epstein, S. A.; Pandis, S. N.; Robinson, A. L. *Atmos. Chem. Phys.* **2011**, *11* (7), 3303–3318.

(22) Hall IV, W. A.; Johnston, M. V. *J. Am. Soc. Mass Spectrom.* **2012**, *23* (6), 1097–1108.

(23) Perraud, V.; Bruns, E. a; Ezell, M. J.; Johnson, S. N.; Yu, Y.; Alexander, M. L.; Zelenyuk, A.; Imre, D.; Chang, W. L.; Dabdub, D.; Pankow, J. F.; Finlayson-Pitts, B. J. *Proc. Natl. Acad. Sci. U. S. A.* **2012**, *109* (8), 2836–2841.

(24) Odum, J. R.; Hoffmann, T.; Bowman, F.; Collins, D.; Flagan, R. C.; Seinfeld, J. H. *Environ. Sci. Technol.* **1996**, *30* (8), 2580–2585.

(25) Pankow, J. F. *Atmos. Environ.* **1994**, *28* (2), 185–188.

(26) Rohrer, F.; Berresheim, H. *Nature* **2006**, *442* (7099), 184–187.

(27) Kroll, J. H.; Smith, J. D.; Che, D. L.; Kessler, S. H.; Worsnop, D. R.; Wilson, K. R. *Phys. Chem. Chem. Phys.* **2009**, *11*, 8005–8014.

(28) Chhabra, P. S.; Lambe, A. T.; Canagaratna, M. R.; Stark, H.; Jayne, J. T.; Onasch, T. B.; Davidovits, P.; Kimmel, J. R.; Worsnop, D. R. *Atmos. Meas. Tech.* **2015**, *8* (1), 1–18.

(29) Henry, K. M.; Donahue, N. M. *J. Phys. Chem. A* **2012**, *116*, 5932−5940.

(30) Guenther, A.; Geron, C.; Pierce, T.; Lamb, B.; Harley, P.; Fall, R. *Atmospheric Environment*. **2000**, 2205–2230.

(31) Guenther, A.; Hewitt, C. N.; Erickson, D.; Fall, R.; Geron, C.; Graedel, T.; Harley, P.; Klinger, L.; Lerdau, M.; McKay, W. A.; Pierce, T.; Scholes, B.; Steinbrecher, R.; Tallamraju, R.; Taylor, J.; Zimmerman, P. *J. Geophys. Res.* **1995**, *100*, 8873.

(32) Beech, O. I. F. a; With, F.; Ursinum, A.; Konig, G. *Environment* **1997**, *31* (2), 291–294.

(33) Griffin, R. J.; Cocker, R.; Flagan, C. *Journal of Geophysical Research*. **1999**, 3555–

3567.

(34) Zhang, D.; Zhang, R. *J. Chem. Phys.* **2005**, *122* (11), 114308.

(35) Di Carlo, P.; Brune, W. H.; Martinez, M.; Harder, H.; Lesher, R.; Ren, X.; Thornberry, T.; Carroll, M. A.; Young, V.; Shepson, P. B.; Riemer, D.; Apel, E.; Campbell, C. *Science*. **2004**, *304* (5671), 722–725.

(36) Gligorovski, S.; Strekowski, R.; Barbati, S.; Vione, D. *Chem. Rev.* **2015**, *115* (24), 13051–13092.

(37) Zhang, D.; Zhang, R. *J. Chem. Phys.* **2005**, *122* (11).

(38) Criegee, R. *Angew. Chemie Int. Ed. English* **1975**, *14* (11), 745–752.

(39) Johnson, D.; Marston, G. *Chem. Soc. Rev.* **2008**, *37* (4), 699–716.

(40) Ma, Y.; Marston, G. *Phys. Chem. Chem. Phys.* **2008**, *10* (40), 6115–6126.

(41) DePalma, J. W.; Horan, A. J.; Hall, W. A.; Johnston, M. V. *Phys. Chem. Chem. Phys.* **2013**, *15* (18), 6935–6944.

(42) Kristensen, K.; Bilde, M.; Aalto, P. P.; Petäjä, T.; Glasius, M. *Atmos. Environ.* **2016**, 130, 35-53.

(43) Barsanti, K. C.; Pankow, J. F. *Atmos. Environ.* **2005**, *39* (35), 6597–6607.

(44) Putman, A. L.; Offenberg, J. H.; Fisseha, R.; Kundu, S.; Rahn, T. A.; Mazzoleni, L. R. *Atmos. Environ.* **2012**, *46*, 164–172.

(45) Mutzel, A.; Poulain, L.; Berndt, T.; Iinuma, Y.; Rodigast, M.; Böge, O.; Richters, S.; Spindler, G.; Sipilä, M.; Jokinen, T.; Kulmala, M.; Herrmann, H. *Environ. Sci. Technol.* **2015**, *49* (13), 7754–7761.

(46) Heaton, K. J.; Sleighter, R. L.; Hatcher, P. G.; Hall IV, W. A.; Johnston, M. V. *Environ. Sci. Technol.* **2009**, *43* (20), 7797–7802.

(47) Walser, M. L.; Desyaterik, Y.; Laskin, J.; Laskin, A.; Nizkorodov, S. A. *Phys. Chem. Chem. Phys.* **2008**, *10* (7), 1009–1022.

(48) Maria, S. F.; Russell, L. M.; Turpin, B. J.; Porcja, R. J.; Campos, T. L.; Weber, R. J.;

Huebert, B. J. *J. Geophys. Res.* **2003**, *108* (D23), 8637.

(49) Decesari, S.; Mircea, M.; Cavalli, F.; Fuzzi, S.; Moretti, F.; Tagliavini, E.; Facchini, M. C. *Environ. Sci. Technol.* **2007**, *41* (7), 2479–2484.

(50) Williams, B. J.; Goldstein, A. H.; Kreisberg, N. M.; Hering, S. V. *Aerosol Sci. Technol.* **2006**, *40* (8), 627–638.

(51) DeCarlo, P. F.; Dunlea, E. J.; Kimmel, J. R.; Aiken, A. C.; Sueper, D.; Crounse, J.; Wennberg, P. O.; Emmons, L.; Shinozuka, Y.; Clarke, A.; Zhou, J.; Tomlinson, J.; Collins, D. R.; Knapp, D.; Weinheimer, A. J.; Montzka, D. D.; Campos, T.; Jimenez, J. L. *Atmos. Chem. Phys.* **2008**, *8* (14), 4027–4048.

(52) Aiken, A. C.; Decarlo, P. F.; Kroll, J. H.; Worsnop, D. R.; Huffman, J. A.; Docherty, K. S.; Ulbrich, I. M.; Mohr, C.; Kimmel, J. R.; Sueper, D.; Sun, Y.; Zhang, Q.; Trimborn, A.; Northway, M.; Ziemann, P. J.; Canagaratna, M. R.; Onasch, T. B.; Alfarra, M. R.; Prevot, A. S. H.; Dommen, J.; Duplissy, J.; Metzger, A.; Baltensperger, U.; Jimenez, J. L. *Environ. Sci. Technol.* **2008**, *42* (12), 4478–4485.

(53) Canagaratna, M. R.; Jimenez, J. L.; Kroll, J. H.; Chen, Q.; Kessler, S. H.; Massoli, P.; Hildebrandt Ruiz, L.; Fortner, E.; Williams, L. R.; Wilson, K. R.; Surratt, J. D.; Donahue, N. M.; Jayne, J. T.; Worsnop, D. R. *Atmos. Chem. Phys.* **2015**, *15* (1), 253–272.

(54) Aiken, A. C.; DeCarlo, P. F.; Jimenez, J. L. *Anal. Chem.* **2007**, *79* (21), 8350–8358.

(55) Kroll, J. H.; Donahue, N. M.; Jimenez, J. L.; Kessler, S. H.; Canagaratna, M. R.; Wilson, K. R.; Altieri, K. E.; Mazzoleni, L. R.; Wozniak, A. S.; Bluhm, H.; Mysak, E. R.; Smith, J. D.; Kolb, C. E.; Worsnop, D. R. *Nat. Chem.* **2011**, *3* (2), 133–139.

(56) Yasmeen, F.; Szmigielski, R.; Vermeylen, R.; Gõmez-González, Y.; Surratt, J. D.; Chan, A. W. H.; Seinfeld, J. H.; Maenhaut, W.; Claeys, M. *J. Mass Spectrom.* **2011**, *46* (4), 425–442.

(57) Steimer, S. S.; Kourtchev, I.; Kalberer, M. *Anal. Chem.* **2017**, *89* (5), 2873–2879.

Chapter 2

OFF-LINE ANALYSIS OF FRESH AND AGED SOA WITH HIGH RESOLUTION MASS SPECTROMETRY

2.1 Introduction

As mentioned in Chapter 1, the chemical composition of SOA is very complex on a molecular level. The assigned molecular formulas change with the type of VOC precursor and the manner and extent to which oxidation occurs.[1–4] For example, the aging process alters the properties of newly formed ("fresh") SOA in both chemical and physical ways.[5,6] Particularly, the aging process (e.g. functionalization, fragmentation) affects the volatility and degree of oxidation of SOA and significantly contributes to the formation of highly oxidizes species. Among the complex chemical compositions of SOA, there is a class of Highly Oxidized Multifunctional organic compounds (HOMs)[7] that have drawn great attention by the scientists. They were found to significantly affect the formation/growth of SOA, and further photochemical activity.[8–11] Various ambient measurements and laboratory studies utilizing both on- and off-line mass spectrometry techniques characterized the chemical compositions of them and discussed their role in the evolution of SOA in the atmosphere.[7–10,12]

While HOMs are important throughout the SOA lifecycle, the distribution of molecules is likely to change as aging proceeds,[22] which requires the molecular level analysis of the chemical compositions to understand how the highly-oxidized components of SOA undergo the aging process. The rapidly developing high resolution mass spectrometry, with its high-resolving power to distinguish the peaks with slight m/z difference, has been widely used to investigate the complex

constituents of aerosols. In the work discussed in this chapter, molecular level analysis with ESI-HR-MS was employed to characterize the chemical composition of both freshly formed SOA derived from biogenic precursors.

Although compositions of SOA were as a whole not highly oxidized, molecular analysis identified a significant number of HOMs embedded within it. Further work studying the aging process of fresh SOA was performed by passing fresh SOA through a photochemical reactor where it reacted with hydroxyl radicals to explore how the highly-oxidized species change during the aging process. β-Pinene and limonene which were chosen as precursors in this work are regarded as important biogenic sources of SOA due to their considerable potential for SOA formation and the significant large-scale emissions.[13] In addition, collision-induced dissociation (CID) applied to the multiple-stage mass spectrometry (MS^2) helps with the characterization of the molecular formulas based on the fragment ions detected.

2.2 Laboratory Generation of Fresh and Aged SOA

The chemical composition and formation pathways of SOA particles can be studied by investigating ambient nanoparticles collected during field campaigns or lab generated SOA samples derived from specific precursors. In this work, fresh and aged SOA derived from biogenic precursors were generated with flow tube reactor (FTR) and photochemical chamber (PC) as shown in Figure 2.1. Similar as summarized previously[6], lab generated air flows containing the biogenic precursor (e.g. β-pinene, limonene) and ozone were mixed in the FTR which is a 125cm long Teflon-coated stainless-steel tube. Flowrates of 100 CPM (cm^3/min) for precursor and 675 CPM for ozone ensure the laminar flow inside the tube and give approximate concentrations of 1 ppm (precursor), 20 ppm (ozone) and a reaction time of ~ 20s. Particle losses during SOA generation due to the walls are insignificant as reported from previous results[14,15].

Figure 2.1. Summary of fresh and aged SOA experiments. BVOC = biogenic volatile organic carbon precursor. The photo of photochemical chamber was given as well. Adapted with permission from (Tu, P.; Hall, W. A.; Johnston, M. V. *Anal. Chem.* **2016**, *88* (8), 4495–4501). © 2016 American Chemical Society.

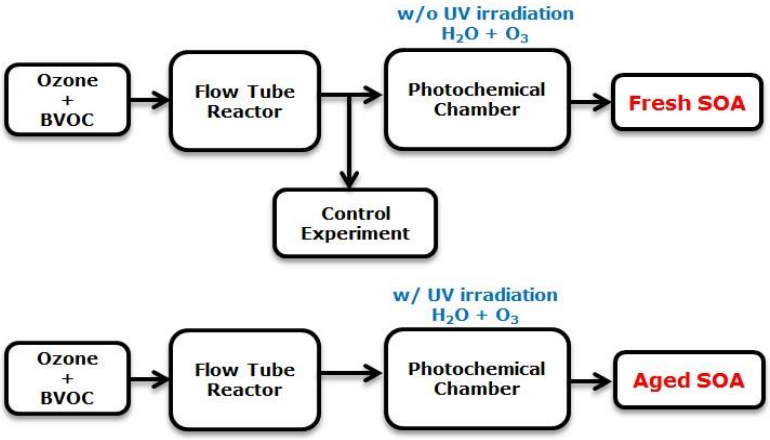

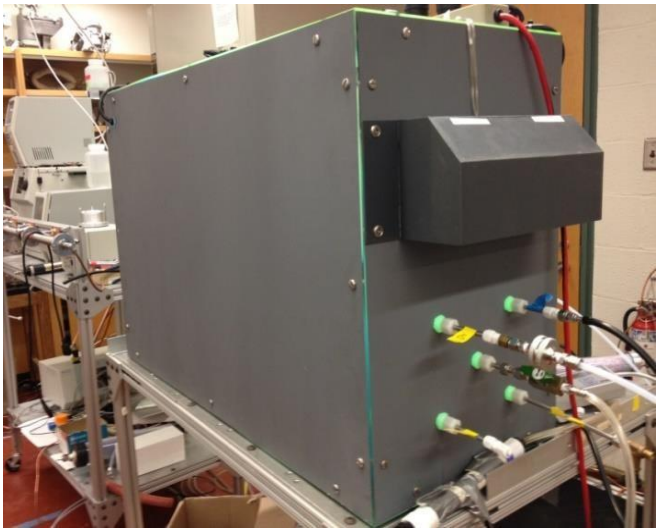

The aerosol exiting the FTR was combined with a flow of humidified air (35% or 70% RH depending on the experiment monitored with the Thermometer) containing additional ozone (~ 775 CPM) and sent into the Photo Chamber (PC). The volume of the PC and gas flow was such that the residence time in the PC was ~30 min. The configuration of PC was introduced in detail in a previous paper by another group member[6]. It consisted of a 50L, box-shaped (251 × 251 × 800 mm) inner chamber made from thick perfluoroalkoxy copolymer (Welch Fluorocarbon, Dover, NH), suspended inside a larger outer chamber (419× 610 × 978 mm, WxHxL). The inside walls of the outer chamber were coated with a reflective material, and four 36" (914 mm) long UV lamps, coated to transmit radiation only around 254 nm ran along the top length of the chamber.[6] When the lamps were turned on, OH was produced by the reaction of photolyzed ozone with water vapor (equations were given in Chapter 1). The magnitude of the OH concentration in the PC was controlled by adjusting the relative humidity and intensity of ultraviolet lamps and was estimated to be ~10^9 molecules/cm^3 by feeding a known concentration and excess amount of SO_2 into the PC. The reaction rate to produce sulfuric acid (H_2SO_4) aerosol was monitored with Scanning Mobility Particle Sizer (SMPS) which will be discussed later. The concentration of OH radicals could be calculated through the second order rate equations assuming all the sulfuric acid formed aerosol with negligible wall loss. This estimation method does not take into account that oxidation of organic vapors in the PC may have produced additional OH[16].

Since no OH scavenger was added, it is possible that some products in the SOA exiting the FTR arose from the reaction of OH with the biogenic precursor. For the work described here, "fresh" SOA is defined as the aerosol exiting the PC when the ultraviolet lamps were turned off. "Aged" SOA is defined as the aerosol exiting the

PC when the ultraviolet lamps were turned on. Control experiment was performed as the aerosol exiting the FTR prior to mixing with humidified air. It should be noted that aging in the PC was performed in the presence of both gas and particle phase organics exiting the FTR. When a HEPA filter was inserted between the FTR and PC to remove particles from the air flow entering the PC, no new particle mass was observed in the gas flow exiting the PC (UV lamps on). This experiment showed that gas phase organics exiting the FTR were not capable of nucleating and growing new particles in the PC, though it cannot be ruled out the possibility that oxidation of these vapors in the PC led to uptake and heterogeneous reaction when the particle phase from fresh SOA was present.

Most experiments were performed with β-pinene as the SOA precursor, though several experiments were also performed with limonene as the precursor. Table 2.1 gives the experimental conditions used in this study. Experiments with β-pinene precursor, discussed in detail below, consisted of 4 separate experiments: fresh SOA with lower/higher RH and aged SOA with lower/higher RH. A total of 5 samples (3 lower RH, 2 higher RH) were analyzed each for fresh and aged SOA (10 samples total). Three replicates (one at 25% RH and two at 75% RH) were performed for fresh and aged SOA from limonene. A total of 6 SOA samples derived from limonene precursor (3 fresh, 3 aged) were generated in the similar way (2 lower RH, 1 higher RH). For each SOA sample, particle size distribution and concentration were monitored with Scanning Mobility Particle Sizer (SMPS: TSI Incorporated, St. Paul, MN). A fused silica diffusion dryer was added at the exit of the PC before entering SMPS to remove water prior to analysis. Measurement with SMPS is performed by coupling a Differential Mobility Analyzer (DMA) with a Condensation Particle Counter (CPC). Aerosol particles are firstly charged by the unipolar charger (^{210}Po Aerosol Neutralizer, TSI Incorporated, Shoreview, MN) and classified in DMA based

on their electrical mobility. The electrical mobility of a particle is determined by its number of charge and size. The charging method used in this work produces mostly singly charged particles. Therefore, particles with various sizes are separated and sent to CPC for number and mass concentration measurement.

Figure 2.2 shows example size distributions of fresh and aged SOA from β-pinene measured with SMPS. Their number, mass concentration and mode diameters were summarized based on SMPS data. Fresh SOA typically had a mode diameter in the number size distribution just above 100 nm. Upon aging, the size distribution broadened and the mode diameter increased (Figure 2.2), and both the number and mass concentrations of aerosol decreased (Table 2.2). The gas phase concentrations, aerosol loadings and OH exposures are higher than ambient levels but the relative proportions are similar[13,17]. High aerosol loadings were needed to facilitate sample collection and analysis. Its effect on SOA compositions would be discussed in Chapter 3. Figure 2.3 shows the change of mass and number concentration of SOA particles inside the photochemical chamber under two modes of aging experiment. As shown in Figure 2.3a, freshly formed SOA in the FTR was injected into PC at the beginning of the experiment and allowed to mix well in the chamber which takes ~100 min; then the UV lights were turned on to generate OH radical for aging. It is evident that both mass and number concentration inside the chamber take a while to stabilized during aging process. As shown in Figure 2.3b, the other aging mode is to turn the UV lights on first followed by the injection of freshly formed SOA. In both cases, the generation of OH radicals in PC and further aging process took hours to reach the equilibrium state. The resulting mass concentration of aged SOA measured at the exit of the chamber was found to decrease by ~50% which is also shown in Figure 2.2.

Table 2.1. Experimental conditions and concentrations of particles measured by SMPS.

Precursor (ppmv)	[O_3] (ppmv)	Exp. No.	Relative Humidity	[OH] (molecules cm^{-3})	Number Concentration (# cm^{-3})	Mass Concentration (µg m^{-3})
β-Pinene (≤1)	>20	1	25%	N/A	2.2E+05	4.9E+02
		2	75%	N/A	2.0E+05	5.1E+02
		3	25%	2.9E+09	2.5E+04	2.2E+02
		4	75%	8.9E+09	2.4E+04	3.1E+02
Limonene (≤1)	>20	1	25%	N/A	4.7E+05	7.9E+02
		2	75%	N/A	6.2E+05	7.6E+02
		3	25%	2.6E+09	5.2E+04	5.0E+02
		4	75%	9.2E+09	4.6E+04	4.2E+02

Figure 2.2. Size distribution of fresh and aged SOA monitored by SMPS. Adapted with permission from (Tu, P.; Hall, W. A.; Johnston, M. V. *Anal. Chem.* **2016**, *88* (8), 4495–4501). © 2016 American Chemical Society.

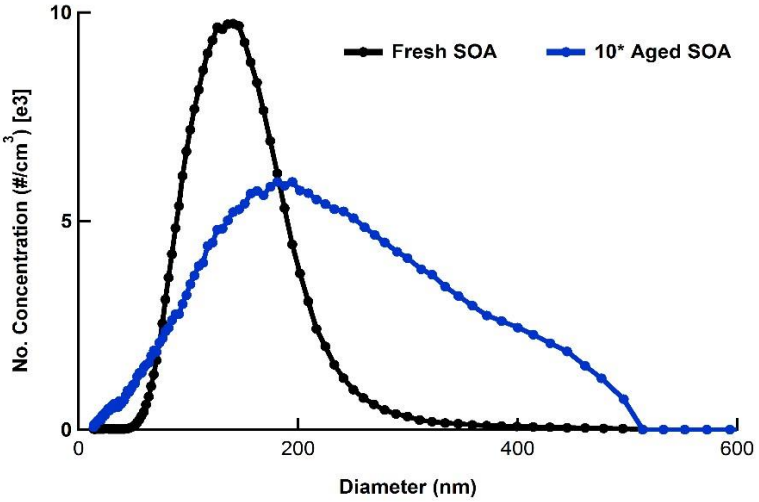

Figure 2.3. Mass and number concentration in the photochemical chamber during the aging experiment measured with SMPS. Shaded region in plot a) show the experiment performed under the dark condition with the UV lights off. Plot b) displays the aging experiment starting from the generation of OH radicals in the chamber followed by the injection of freshly formed SOA after ~175 min (after the mass and number concentration of OH radicals reach the steady state).

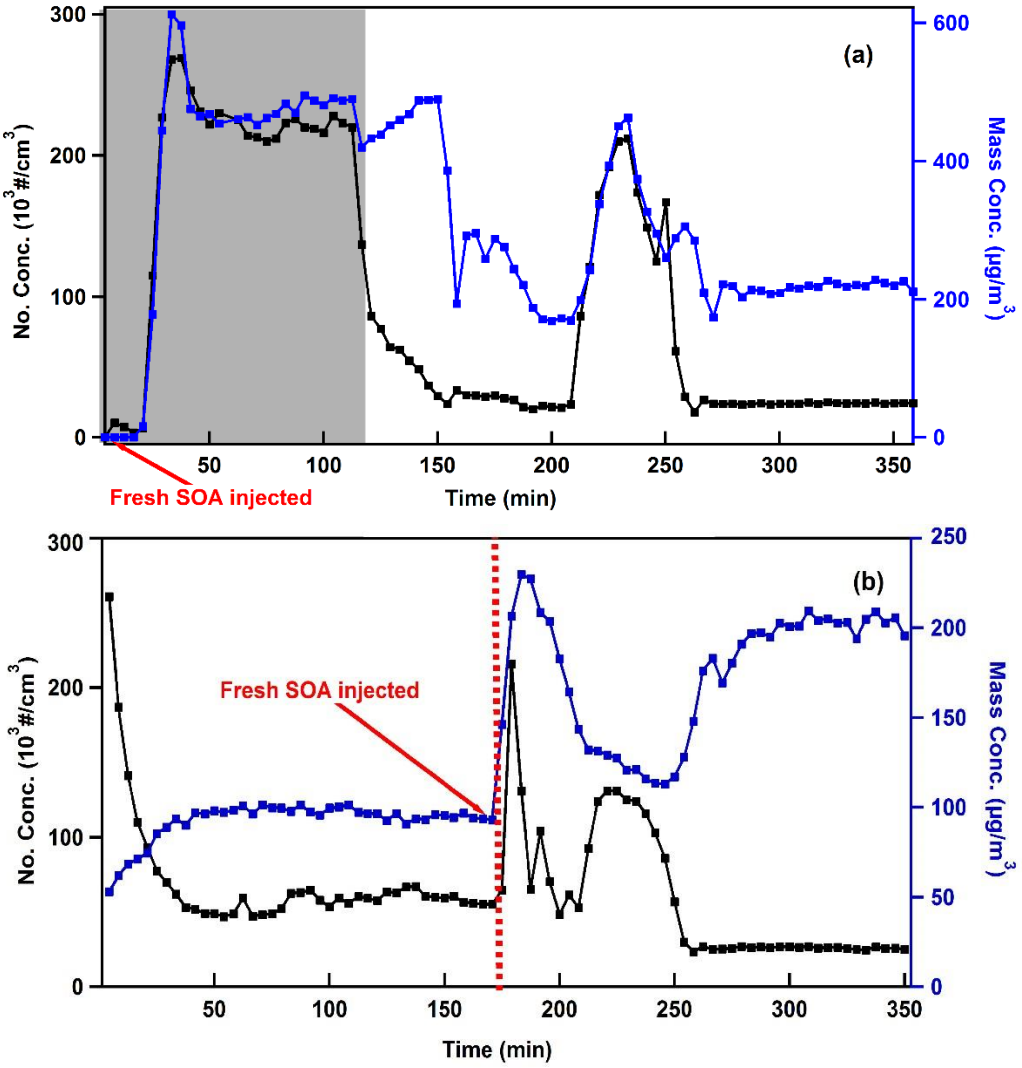

Table 2.2. Peaks and assigned formulas in SOA samples from β-pinene and limonene. Shown are average numbers and standard deviations for replicate measurements (5 for β- pinene and 3 for limonene).

Precursor	Sample Type	Ion Mode	Peaks Detected	Peaks Analyzed	Ions Assigned (Percentage)	Unique Molecular Formulas[a]
β-Pinene	Fresh	(+)	5473 ± 466	2767 ± 180	2654 ± 108 (95.9%)	1293 ± 83
	Aged	(+)	4037 ± 157	1921 ± 106	1808 ± 87 (94.1%)	1089 ± 75
	Fresh	(-)	3725 ± 317	2074 ± 248	1918 ± 119 (92.5%)	1096 ± 82
	Aged	(-)	4939 ± 326	2615 ± 242	2500 ± 235 (95.6%)	1517 ± 156
Limonene	Fresh	(+)	5308 ± 231	4577 ± 145	4261 ± 68 (93.1%)	1864 ± 78
	Aged	(+)	5964 ± 289	4191 ± 101	3617 ± 45 (86.3%)	2559 ± 50
	Fresh	(-)	3750 ± 223	2390 ± 65	2295 ± 66 (96.0%)	1408 ± 77
	Aged	(-)	5273 ± 381	1320 ± 85	2218 ± 71 (95.6%)	1805 ± 98

[a] Approximately 70% of the assigned peaks in the positive ion spectra contained sodium after removing redundancies from the spectra. None contained potassium was detected in the spectrum.

Both fresh and aged samples were collected and prepared for further analysis in a similar manner to each other and to the Johnston group's previous work.[6] Particles were collected on a Teflon coated, glass fiber filter (GF/D, CAT No.1823-025, Whatman, GE Healthcare, Piscataway, NJ) by passing aerosol (gas and particle phase organics) through the filter for about 24 hours so that the total amount of particulate matter collected was about 1000 µg assuming particle density of 1.3 g cm^{-3}. The filter was sonicated and extracted with ~8 mL ACN/H_2O (50%/50%). The extraction was repeated a total of 3 times (30 min each) and the extraction efficiency after this was achieved to be as high as >97%.[18] Acetonitrile was used instead of methanol to remove the possibility of esterification of acid groups.[19] The extraction solutions were combined and evaporated to near dryness in a concentrator (Savant™, SpeedVac™ Plus, Model: SC110A), followed by reconstitution in acetonitrile/water solution to give a final concentration of 100 µg/ mL, which was found to be optimal for the detection of both major and minor components in relevant test samples (e.g. pinic acid, pinanediol, etc.) by the high resolution mass spectrometry under the conditions used. A chamber blank was also collected by flowing air through the PC without fresh SOA injection. Prior to each experiment, the PC was cleaned by introducing ozone (~20 ppmv) into the chamber with the UV lights on for days and monitored with the SMPS. The mass concentration of photochemically produced aerosol in the cleaned chamber was much less than 1 µg/m^3.

2.3 Molecular Level Characterization of SOA with High Resolution MS

SOA samples collected on filters were analyzed with a Q-Exactive Hybrid Quadrupole-Orbitrap Mass Spectrometer (Thermo Scientific, Waltham, MA) coupled with a heated-electrospray ionization (HESI) probe using a spray voltage of 3.5 kV and capillary temperature of 275 ˚C. While direct infusion suffers quantitatively from

competitive ionization effects, it tends to detect many more compounds than LC/MS.[20] In the Johnston group's previous work with a different ESI source, a 5 eV in-source collision energy was applied to break the noncovalent bond of the clusters in the standard solution (pinonic acid) for SOA detection.[21] In the current work, 5 eV and even higher (10-20 eV) in-source collision energy were applied to compare with the original spectra (no in-source collision energy applied) to identify and remove artifacts from in-source clustering. Full MS scan was acquired over the range 100-1000 *m/z* with a mass resolving power of 70000. Each spectrum was obtained by averaging ~100 scans over a period of approximately 0.8 min.

The mass spectra were processed with Xcalibur software supplied with the mass spectrometer. As mentioned above, mass spectrum lists averaging over ~ 100 single scans were exported from the software into Excel for further analysis. Initially, background subtraction was performed to remove contaminant and other background peaks. Peaks with either <0.1% intensity relative to the base peak or S/N <5 were removed from the peak lists. The remaining peaks were assigned molecular formulas with atomic constraints based on likely products of monoterpene oxidation in combination with the 'Seven Golden Rules' for molecular formulas described elsewhere.[22] Table 2.3 summarizes all the criteria that applied for formula assignment. Note that potassiated molecules were not observed in the positive ion mode, so the potassium was not in the analysis. Also, only one ^{13}C atom was included considering the extremely low abundances of formulas having more than one isotopic substitution. Due to the high mass accuracy of the instrument, most of the peaks could be assigned within 5 ppm mass error tolerance from the expected m/z in both ion modes and more than 90% of the peaks were assigned reasonable molecular formulas. The few unassigned peaks generally had peak intensities <<1% relative to the base peak. About 10% of the peaks had more than one reasonable formula assigned to them.

Additionally, elemental ratios (i.e. O/C and H/C) and RDB value (number of rings and double bonds contained in the formula) could be used exclude unlikely formulas. RDB-O value which serves as a better indicator for the degree of unsaturation of the carbon skeleton was considered as well (-10<RDB-O > 10 was used based on previous studies[23]). In the rare case that more than one reasonable formula remained after these considerations, all formulas were included in the subsequent analysis. Finally, redundancies due to ionization (i.e. $[M+Na]^+$ and $[M+H]^+$) and isotopic substitutions were removed, typically leaving over 1000 non-redundant assigned molecular formulas for each sample. Table 2.2 summarizes the total number of peaks detected and number of assigned formulas for each experiment. Note that I am only focused on the closed-shell products (with even number of H atoms in its neutral formula) so ions with even number of hydrogen atoms are removed as well.

Table 2.3. Criteria that applied during formula assignment and analysis.

Odd/even electron ions	Closed shell products (even electron ions)
Isotopes	^{12}C and ^{13}C included and combined as C atoms
Elements	C, H, O (Na for positive mode) atoms
Ring and Double Bond	0-20 (-10 < RDB-O <10)
Dynamic Range	100-1000 m/z
Mass Error Tolerance	< 5 ppm
Signal to Noise Ratio Relative Abundance	> 5 < 0.1%
O/C	< 2
H/C	> 0.45
OSc	< 2

In some cases, Kendrick Mass analysis is performed to get rid of some unreasonable formulas. Kendrick mass defect (KMD), was known to identify homologous compounds differing only by a number of base units in high resolution mass spectra.[24,25] Therefore, KMD is found to be very helpful to filter out those species from background interference especially for those SOA samples with relatively small mass loading (e.g. monodisperse SOA samples which would be discussed in Chapter 3). Figure 2.4 provides an example of how KMD analysis involved in the spectra analysis. In this case, the repeating unit of CH_2 was used to convert the IUPAC mass of SOA components to the Kendrick Mass.[26] And the homologous series of ions (the same class and type) with increasing extent of alkylation were displayed in the figure. The formulas with same numbers of CH_2 groups yield the same KMD value thus will be aligned in a horizontal line in the figure. Additionally, the expanded panel clearly shows how the KMD value of the ions changes with the addition of two hydrogen atoms (indicated by the linear line). In contrast, the dots on the lower right corner in the figure, which do not belong to any group, were regarded as unreasonable formulas thus can be removed. Because of a small experiment-to-experiment variation in the distribution of molecular formulas that is inherent to this type of experiment,[6,1] only those formulas detected in all samples of a given type (e.g. in all 5 fresh samples or all 5 aged samples from β-pinene precursor) are considered below.

Figure 2.4. Kendrick Mass Defect (KMD) plot used for removing the non-homologous ions detected in positive/negative spectra during data analysis. The embedded panel shows the expanded spectrum (-) and the detected molecular formulas.

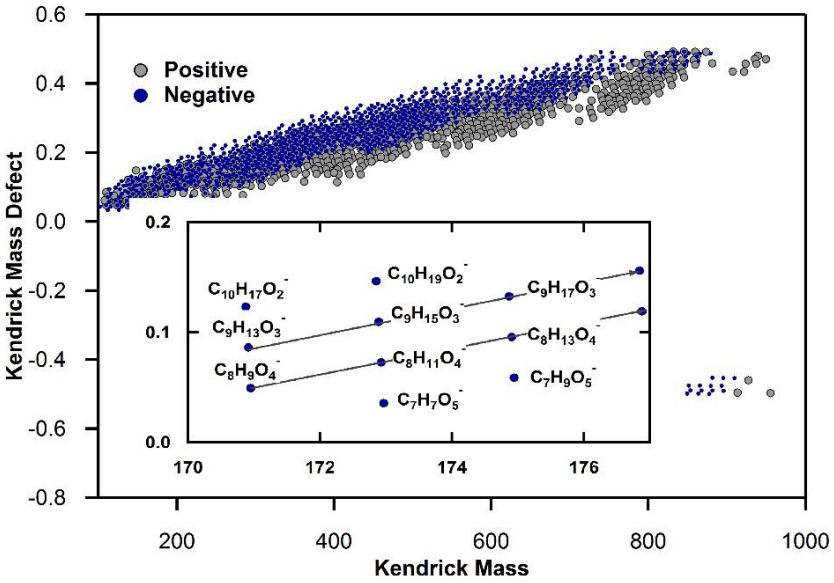

2.4 Fresh and Aged SOA in the Atmosphere

With the methods mentioned above, up to thousands of unique molecular formulas in each fresh/aged SOA sample were assigned and kept for further analysis. The molecular composition of SOA generated in control experiments (collected before entering the chamber) was compared to that from the fresh SOA experiments (collected at the exit of the chamber). More than 96% of the molecular formulas were reproduced between the two experiments and the remaining formulas accounted for a very small fraction of the total signal intensity. This result suggests that the molecular composition of fresh SOA is not significantly affected by exposure to excess amount of ozone in the dark, so the change of fresh SOA after flowing through the chamber

(lamps off) was negligible. A similar result was reported by a separate study investigating the dark aging of SOA in the presence of ozone in the chamber and they claimed that subsequent aging in the dark in the presence of residual ozone did not provide an observable effect on molecular composition of the aerosols and their oxygen extent.[20] Figure 2.5 shows the mass spectra after combing all five spectra of fresh SOA in positive and negative ion mode. A series of monomers, dimers and even high orders of oligomers with relatively low abundance were detected. A series of species were detected and reported previously. For example, pinic acid ($C_9H_{13}O_4^-$) and pinanediol ($C_{10}H_{17}O_2^-$), as labelled in the spectrum, were found to be prevalent organic component of SOA in the atmosphere. Some components such as nopinone ($C_9H_{14}O$), were detected in both polarities. Although the SOA produced in laboratory experiments, on average, has relatively low O/C ratio and OSc, highly oxidized compounds are embedded within it. Not surprisingly, formulas having lower O/C ratios are more prevalent in positive ion spectra, while formulas having higher O/C ratios are more prevalent in negative ion spectra where molecules containing carboxylic acid groups tend to be more highly represented than those containing only carbonyls, peroxides and/or alcohols.

Figure 2.5. Mass spectra after combing all five spectra of fresh SOA in positive and negative ion mode. The embedded panel shows the expanded spectrum and the molecular formulas assigned to the highly abundant peaks.

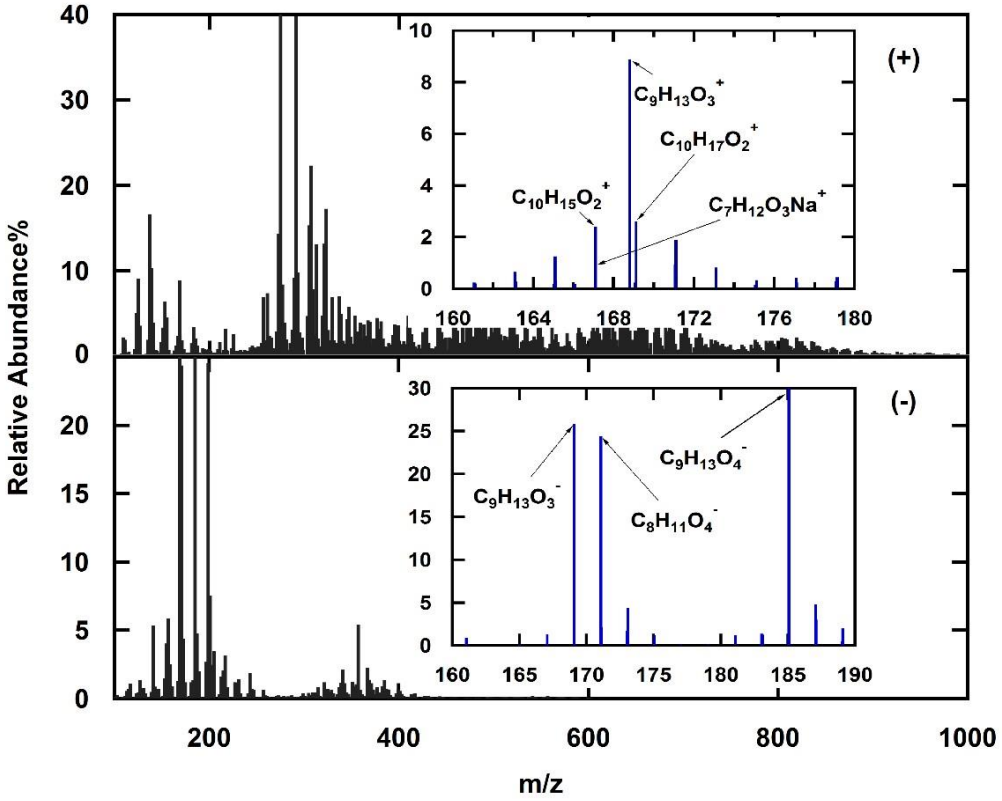

Under the conditions used in this work, both fragmentation and functionalization are observed after aging process of SOA. Fragmentation is evidenced by a decrease in aerosol mass, see Figure 2.2. Functionalization is evidenced by an increase in oxidation. Figure 2.6 and 2.7 combining the mass spectra of fresh and aged SOA (±) for a comparison. Elemental ratio of O/C for each formula was displayed with a color scale. Highly oxidized species with color red are found to be more prevalent after aging in both positive and negative mode. Some of them that are found to exist in fresh SOA are found to be more abundant in aged SOA. Additionally,

Figure 2.8 shows a combination van Krevelen diagram comparing fresh and aged SOA from β-pinene in which data from both positive and negative ion spectra are combined. Van Krevelen diagram, which was devised by van Krevelen[27], namely, a plot of the molar ratio of H/C as the ordinate and O/C ratio as the abscissa[28], has been widely used in the atmospheric aerosol analysis. The diagram with elemental ratios (i.e. H/C and O/C) of molecular shown helps to clearly exhibit the extent of oxidation of the analytes especially for those with complicated components like SOA. In this figure, assigned formulas in red were observed either in aged SOA but not fresh SOA or in both samples but with higher relative abundance in aged SOA. Assigned formulas in black were observed either in fresh SOA but not aged SOA or in both samples but with higher relative abundance in fresh SOA. It shows that there is a virtual continuum of formulas extending from an O/C ratio of ~0.1 to ~1.0. And almost all formulas above O/C=0.4 are either unique to or more intensely detected in aged SOA relative to fresh SOA.

Figure 2.6. (a) Positive ion mode spectra comparison between fresh and aged SOA from β- pinene and (b) expanded spectra showing m/z 226-230 as an example. Abundance is plotted relative to the base peak. Adapted with permission from (Tu, P.; Hall, W. A.; Johnston, M. V. *Anal. Chem.* **2016**, *88* (8), 4495–4501). © 2016 American Chemical Society.

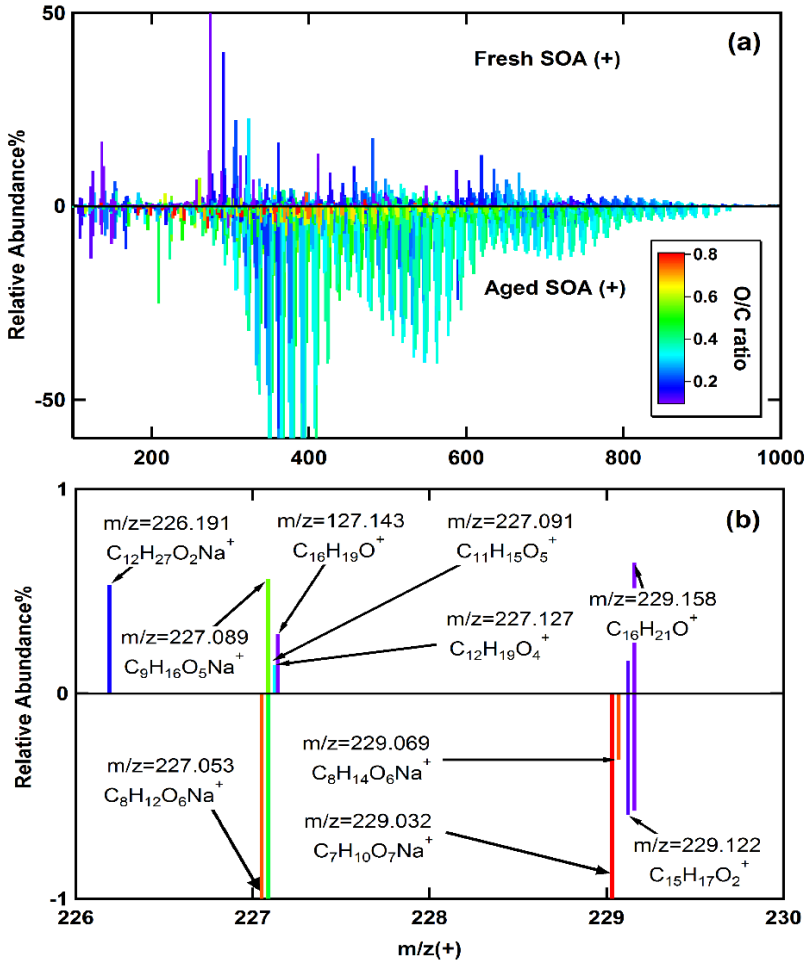

Figure 2.7. (a) Negative ion mode spectra comparison between fresh and aged SOA from β- pinene and (b) expanded spectra showing m/z 261.00-261.20 as an example. Abundance is plotted relative to the base peak. Adapted with permission from (Tu, P.; Hall, W. A.; Johnston, M. V. *Anal. Chem.* **2016**, *88* (8), 4495–4501). © 2016 American Chemical Society.

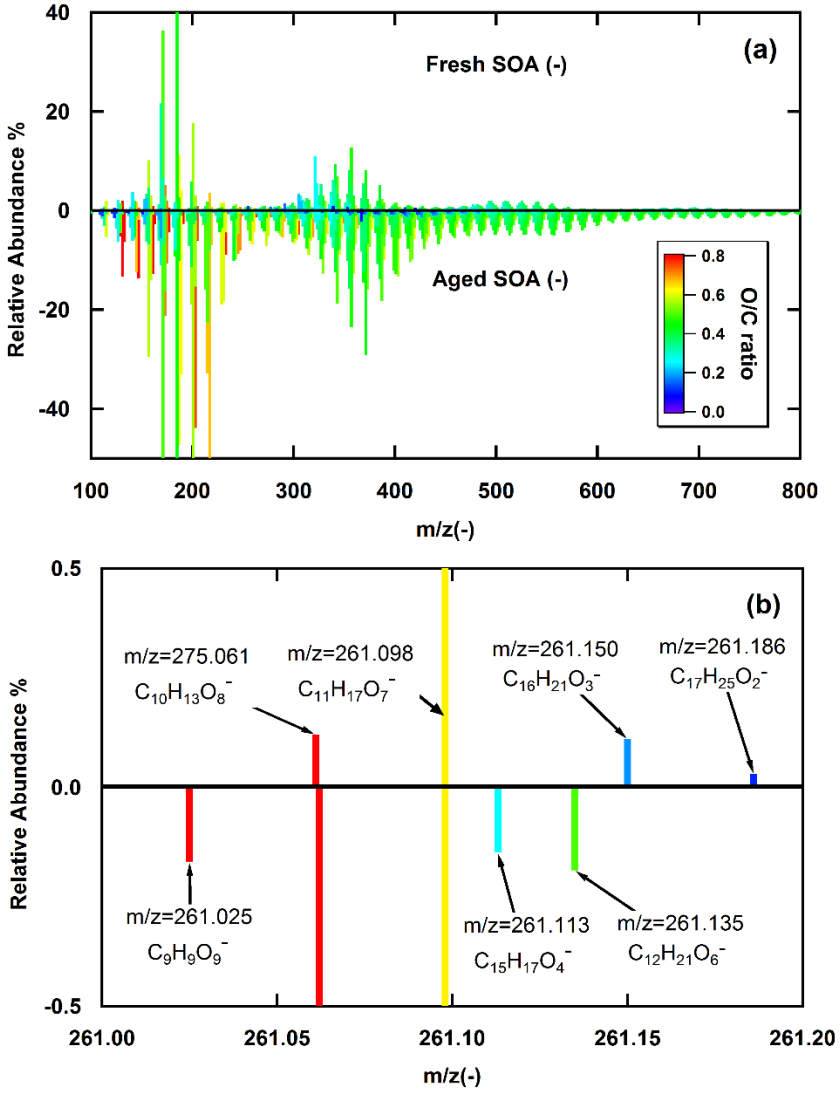

Figure 2.8. van Krevelen diagram of formulas in fresh and aged SOA (positive and negative ion spectra combined). Black dots represent formulas that were observed either in fresh SOA but not aged SOA or in both samples but with higher relative abundance in fresh SOA. Red dots represent formulas that were observed either in aged SOA but not fresh SOA or in both samples but with higher relative abundance in aged SOA. The two lines with different slopes are added for later discussion. Adapted with permission from (Tu, P.; Hall, W. A.; Johnston, M. V. *Anal. Chem.* **2016**, *88* (8), 4495–4501). © 2016 American Chemical Society.

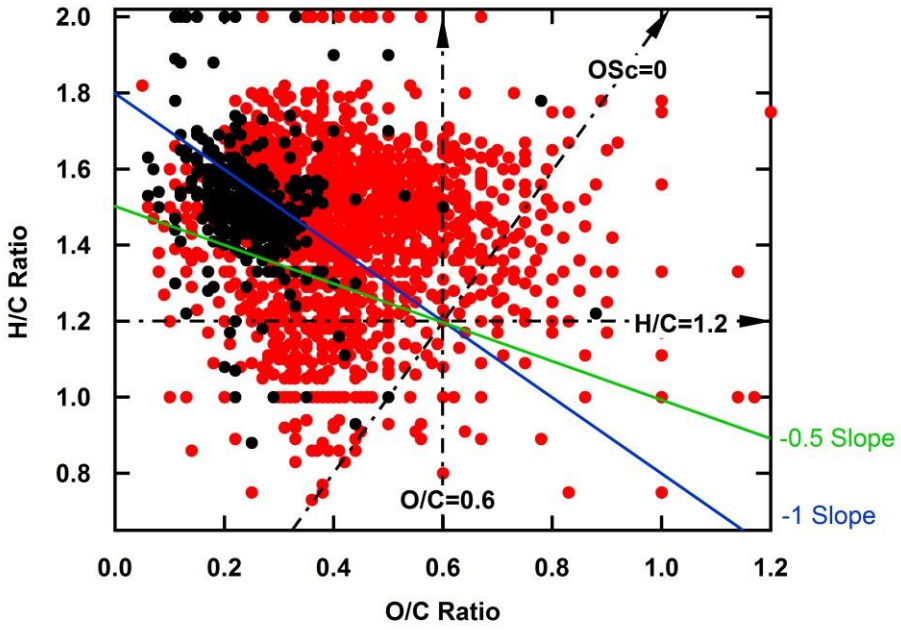

2.5 Highly Oxidized Multifunctional (HOMs) Components of SOA

HOMs in the Atmosphere. The atmospheric lifecycle of SOA includes particle formation, growth, aging and ultimately removal by volatilization or wet and dry deposition. Important components of SOA throughout its lifecycle are highly oxidized multifunctional molecules (HOMs).[29,8,10,7] At the beginning of the lifecycle, particle formation is thought to be assisted by so-called extremely low volatility

organic compounds (ELVOCs), which have been detected in the gas phase by online sampling into a mass spectrometer.[8] ELVOCs consist of organic molecules that have sufficiently low volatility to condense onto a particle surface. ELVOCs are produced by oxidation of a VOC precursor in a manner that leads to the rapid incorporation of many oxygen atoms,[8,30] which may be accompanied by the coupling of two oxidized precursors together to produce dimers and sometimes higher order oligomers. Condensation of ELVOCs provides a reasonable explanation of why oligomers are detected in the particle phase almost immediately after particle formation.[31] Once particles are formed, they can continue to grow by condensation of additional ELVOC molecules or by partitioning of more volatile oxidation products of the precursor molecules.[32] The partitioned compounds may also be highly oxidized, but do not possess a sufficiently low vapor pressure to simply condense, and therefore distribute between the gas and particle phases. Once in the particle phase, both condensed and partitioned molecules can continue to react, for example to form higher order oligomers. It is estimated that approximately half of the mass of laboratory generated SOA from biogenic precursors consists of oligomers.[18] The organic matter remaining in the particle phase after aging tends to be more highly oxidized and less volatile than its fresh SOA counterpart, and in ambient measurements is identified as low volatility oxygenated organic aerosol (LVOOA).[33]

While HOMs are important throughout the SOA lifecycle, the distribution of molecules is likely to change as aging proceeds.[6] From a measurement perspective, defining what is meant by HOM is difficult. ELVOC is based on a gas phase measurement of individual molecules.[8] The formulas distribute over a wide range of van Krevelen space (H/C ratio vs. O/C ratio) and not all can be regarded as highly oxidized. The actual range of molecular formulas that contribute to LVOOA is unknown since it is identified through an average composition measurement[33–35]

though the average compositions reported for LVOOA do fit within the van Krevelen space encompassed by HOMs in biogenic SOA. In some studies, LVOOA has been detected and characterized in ambient measurements[34–39] where substantial aging has occurred. However, a suitable laboratory surrogate for LVOOA has not been found, perhaps in part because it is based on an average measurement and the entire aerosol must be highly oxidized for it to be identified.

HOMs in Lab-generated SOA Derived from β-pinene. Whether in the context of ELVOC or LVOOA, HOMs are characterized by high O/C ratio and/or high average carbon oxidation state (OSc). In the work reported here, high performance mass spectrometry is used to search for and characterize HOMs embedded within fresh and aged biogenic SOA and assess how closely these HOMs conform to ELVOC-like and LVOOA-like material. Among the thousands of formulas in fresh SOA, the highly oxidized multifunctional organic components (HOMs) were characterized based on multiple criteria determined from associated studies on the characterization of highly oxidized components during field measurements and related AMS data analysis.[7,33–36,40,41] Firstly, the O/C ratio of HOM formulas might not be lower than a specific value which was determined by the mechanism of monoterpenes' ozonolysis (O_3 was attached to form Criegee Intermediate/ release of OH radicals/ amounts of O_2 added during the further auto-oxidation). Here we set the boundary of O/C ratio to 0.6 while other papers have used similar but higher standards (0.7 reported by Mutzel et al, 2015; O/C > 1 in monomer region and O/C > 0.55 in dimer region reported by Rissanen et al, 2014)[7,42]. Secondly, carbon oxidation state, which was believed to separate LV-OOA (highly oxidized) and SV-OOA according to the field campaigns,[35] was set to be greater than or equal to zero for HOMs. Lastly, H/C ratio of the formulas should be greater than or equal to 1.2. HOMs are defined as assigned formulas having either O/C≥0.6 and/or OSc≥0.

Figure 2.9 shows the van Krevelen plots of assigned formulas from fresh SOA produced by ozonolysis of β-pinene under positive and negative ion mode respectively. Formulas that are detected in all five samples are shown. As an aid to understanding the molecular characteristics of HOMs, three lines are drawn in the plots: one showing O/C=0.6, another showing OSc=0, and a third showing H/C=1.2. To explore the relative importance of oxygen content vs. oxidation state, three specific regions of interest are then defined based on these lines: O/C≥0.6 and OSc≥0 (region 1, both highly oxygenated and highly oxidized), O/C≥0.6 but OSc<0 (region 2, highly oxygenated but less oxidized owing to a relatively high H/C ratio), and OSc≥0 but H/C<1.2 (region 3, highly oxidized for a moderate level of oxygenation owing to a relatively low H/C ratio). Characteristics of the HOMs in each of these regions are summarized in Table 2.4. HOMs identified in SOA derived from α-pinene and limonene are also included in this table and would be discussed later.

Figure 2.9. van Krevelen diagrams of the formulas in fresh SOA under a) positive and b) negative modes of ESI. HOMs considered in this study were defined by the three lines drawn in this plot: O/C=0.6, H/C=1.2, OSc=0. Region 1 HOMs are in dark blue. Region 2 HOMs are in light blue. Region 3 HOMs are in gray. Adapted with permission from (Tu, P.; Hall, W. A.; Johnston, M. V. *Anal. Chem.* **2016**, *88* (8), 4495–4501). © 2016 American Chemical Society.

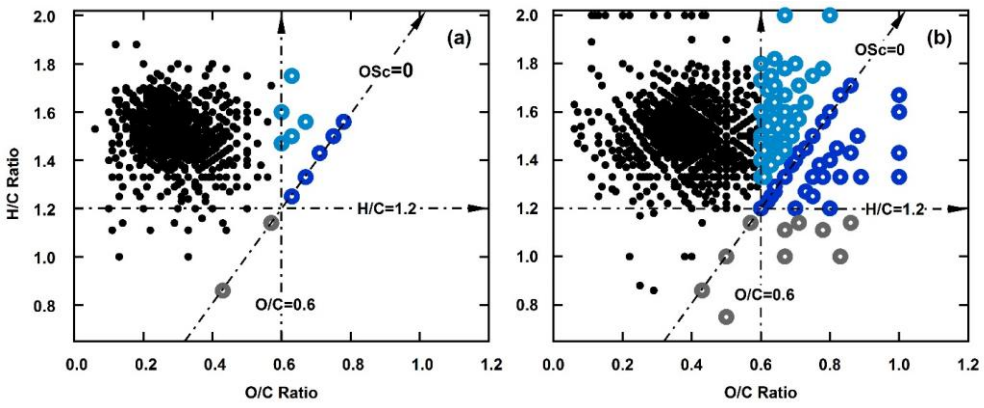

Table 2.4. Summary of HOM assigned formulas in fresh and aged SOA.

BVOC Precursor	Region	Fresh SOA			Aged SOA		
		HOM Formulas	RA%[c]	Avg. Formula	HOM Formulas	RA%[c]	Avg. Formula
β-Pinene[a]	1	40	1.5	$C_{9.9}H_{13.1}O_{7.0}$	109	3.7	$C_{12.8}H_{16.9}O_{9.5}$
	2	49	1.9	$C_{12.6}H_{19.6}O_{8.1}$	65	4.1	$C_{14.3}H_{21.5}O_{9.1}$
	3	11	0.2	$C_{7.3}H_{7.1}O_{4.6}$	111	0.9	$C_{12.8}H_{13.4}O_{8.1}$
Limonene[a]	1	76	2.8	$C_{11.8}H_{16.6}O_{8.9}$	315	2.1	$C_{14.4}H_{20.5}O_{12.4}$
	2	172	5.8	$C_{15.6}H_{25.0}O_{10.2}$	242	1.4	$C_{17.7}H_{28.1}O_{12.2}$
	3	40	0.3	$C_{11.9}H_{11.0}O_{8.6}$	650	6.0	$C_{20.9}H_{18.2}O_{11.4}$
α-Pinene[b]	1	64	2.5	$C_{11.0}H_{15.2}O_{8.4}$	211	8.7	$C_{17.0}H_{22.4}O_{12.9}$
	2	83	5.3	$C_{17.3}H_{26.8}O_{11.4}$	87	6.4	$C_{19.9}H_{28.8}O_{12.7}$
	3	71	0.8	$C_{11.4}H_{10.2}O_{6.9}$	387	4.6	$C_{19.4}H_{20.2}O_{13.4}$

[a]This work.
[b]From Hall et al (2013).
[c]Summed intensity of HOM formulas divided by summed intensity of all assigned formulas.

HOMs of all three regions of fresh and aged SOA are summarized in Figure 2.10 as OSc of each formula vs. the number of carbon atoms contained in it. Similarly, the aging process facilitates the generation of highly oxidized species with relatively high OSc value (represented by the red dots). In fresh SOA, HOMs in region 1 have molecular formulas most similar to LVOOA. The mass and intensity weighted average formula for these species ($C_{9.9}H_{13.1}O_{7.0}$) is quite similar to the reported average formula of LVOOA from 10 different field measurement sites ($C_{10.5}H_{13.4}H_{7.3}$)[33] though the ambient sites were strongly impacted by anthropogenic as well as biogenic SOA precursors. Results from the similar publications studying the

highly-oxidized species are summarized in Table 2.5. Among the ten bulk measurements listed, summer time emitted aerosols in Paris assessed by HR-ToF-AMS showed the most similar result (OSc= 0.13, O/C = 0.73 and H/C = 1.33) as ours.[38] In another study, elemental ratios calculated by AMS had been corrected due to potential bias from vaporization and fragmentation during the ionization process. With the Improved-Ambient Method, ambient LV-OOA (averaged over a series of data sets) were calculated to give an average OSc of 0.1, O/C of 0.8 and H/C of 1.4.[43] To my knowledge, ambient LV-OOA with the highest oxygen extent that had been reported was from the field measurement of Mexico City at 2010.[37] 10% of region 1 formulas have previously been reported for gas phase ELVOCs from various biogenic precursors[8,42,12,9,44] and another 10% have been reported in SOA from other precursors including isoprene[45] and aqueous-phase reaction between phenols and OH radical[41]. The similarity between HOMs in region 1 and these other experiments suggests that extensive oxidation of a variety of molecular precursors can lead to a common set of products. HOMs in region 1 constitute about half of the total signal intensity of all HOMs in regions 1-3.

Figure 2.10. Carbon oxidation state vs. carbon number for the HOM assigned formulas from β-pinene SOA. Grey dots represent assigned formulas observed in fresh SOA. Red dots represent assigned formulas observed in aged SOA. Adapted with permission from (Tu, P.; Hall, W. A.; Johnston, M. V. *Anal. Chem.* **2016**, *88* (8), 4495–4501). © 2016 American Chemical Society.

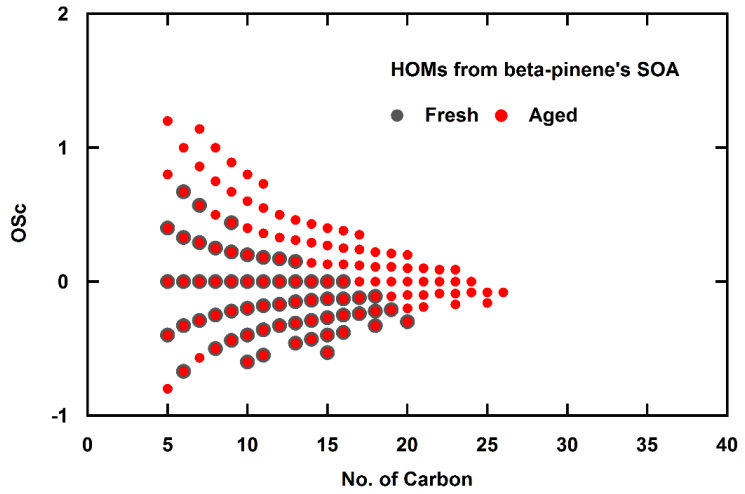

Table 2.5. Summary of highly oxidized species studied by other groups.

Highly Oxidized Species	Technique	OS_C	O/C	H/C	Formula
Ambient LV-OOA (Mexico City)[37]	HR-TOF-AMS	0.47	-	-	$C_{10}H_{12.1}O_{8.4}$ (Avg.)
Ambient LV-OOA (based on 10 sites measurements)[34]	HR-TOF-AMS	0.114	1.1	1.3	$C_{10.5}H_{13.4}O_{7.3}$ (Avg.)

Ambient LV-OOA[33]	HR-TOF-AMS	-	>0.7	-	$C_8O_{5.5}H_{10}$ (Avg.)
Ambient LV-OOA[40]	HR-TOF-AMS	0.5-0.9	-	-	N.A.
ELVOCs (Cyclohexene's Ozonolysis)[12]	CI-APi-TOF	-	-	-	$C_6O_8H_{5\text{-}9}$
ELVOCs (α-Pinene Oxidation)[8]	CI-APi-TOF	-	-	-	$C_{10}H_{14–16}O_{7–11}$, $C_{19–20}H_{28–32}O_{10–18}$
ELVOCs from Biogenic Emissions[9]	CI-APi-TOF	-	-	-	$C_{10}H_{15}O_8$, $C_{10}H_{15}O_{10}$ (endocyclic monoterpenes); $C_5H_8O_{\geq 8}$ (isoprene); C_7 and C_{10} monomers

HOMs in region 2 have similar oxygen content to most of the HOMs in region 1, but they have lower OSc, suggesting that they contain a greater fraction of more reduced functional groups (alcohols, ethers, peroxides, carbonyls), while region 1 contains a greater fraction of more oxidized functional groups (acids, carbonyls). The HOMs in region 2 are also biased toward higher molecular weight species that contain a greater number of carbon atoms. Most of the species in this region require coupling of at least two β-pinene molecules together (dimers and oligomers) to produce molecules having more than 10 carbon atoms, whereas region 1 contains a greater number of species that are able to be derived from one β- pinene molecule (monomers). The mass and intensity weighted average formula for formulas in region 2 is $C_{12.6}H_{19.6}O_{8.1}$. HOMs in this region constitute about half of the total signal intensity of all HOMs in regions 1-3. HOMs in region 3 bear little similarity to

previous studies. To the authors' knowledge, none of the assigned formulas in this region match previously reported formulas for ELVOC-like species nor have they been specifically reported in previous SOA studies. The average molecular formula of region 3 (Table 2.4) is quite different from average formulas reported in ambient studies, and the HOMs in this region account for only 10% of the total intensity in regions 1-3.

HOMs in SOA from Other Biogenic Precursors. To explore the generality of our observations for β-pinene SOA, HOMs from other biogenic precursors were also studied. Fresh and aged SOA from limonene were generated and analyzed in the same way as described above for α-pinene SOA (Unlike β-pinene, only 3 samples each rather than 5 were obtained for fresh and aged SOA from limonene.) In addition, results from our previous study[6] of fresh and aged SOA from α-pinene were re-analyzed in the manner described above. The results are shown in Table 2.4 and Figures 2.11-12. All the salient observations for β-pinene SOA were found for limonene and α-pinene SOA as well. Both number and signal intensity of HOM assigned formulas in fresh SOA from limonene and α-pinene were biased toward regions 1 and 2. Upon aging, both the number and signal intensity of HOMs in region 3 increased relative to 1 and 2, and the average number of carbon atoms in all three regions increased substantially with the greatest increase occurring in region 3 (Table 2.4). Aged SOA samples showed many new HOMs having higher carbon number than those observed in fresh SOA (Figures 2.11 and 2.12).

α-Pinene contains an endocyclic double bond while β-pinene contains an exocyclic double bond. Limonene contains both, though the endocyclic double bond is more reactive. Because of the location of the double bond, ozonolysis products of biogenic precursors containing an endocyclic double bond (e.g. α-pinene) tend to form products having greater O/C ratios and a higher incidence of carboxylic acid groups than those precursors containing an exocyclic double bond only (e.g. β-pinene).[46]

While these differences affect the specific molecular products observed in fresh and aged SOA from the different precursors, the general movement of products among the three HOM regions upon aging is the same owing to similar OH reaction pathways of the fresh SOA products.

Figure 2.11. Carbon oxidation state vs. carbon number for the HOM assigned formulas from α-pinene SOA. Adapted with permission from (Tu, P.; Hall, W. A.; Johnston, M. V. *Anal. Chem.* **2016**, *88* (8), 4495–4501). © 2016 American Chemical Society.

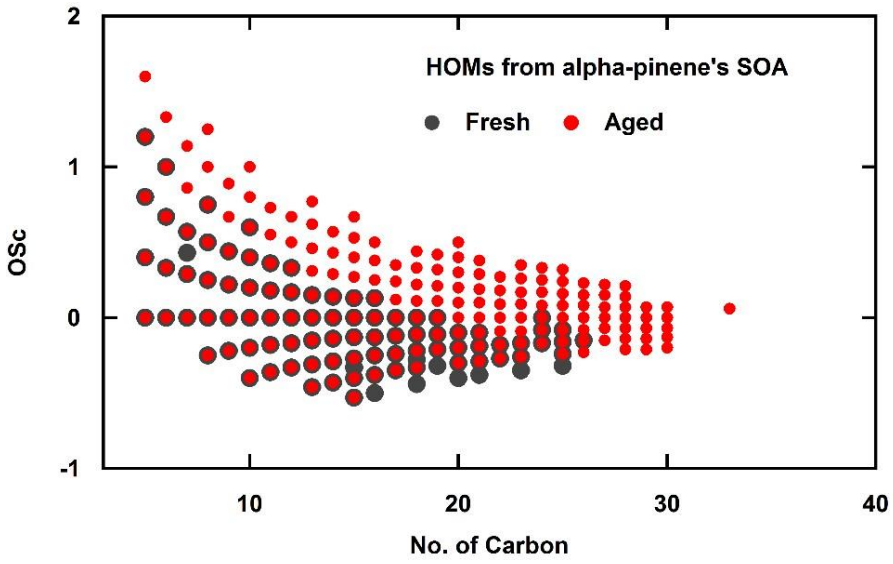

Figure 2.12. Carbon oxidation state vs. carbon number for the HOM assigned formulas from limonene SOA. Adapted with permission from (Tu, P.; Hall, W. A.; Johnston, M. V. *Anal. Chem.* **2016**, *88* (8), 4495–4501). © 2016 American Chemical Society.

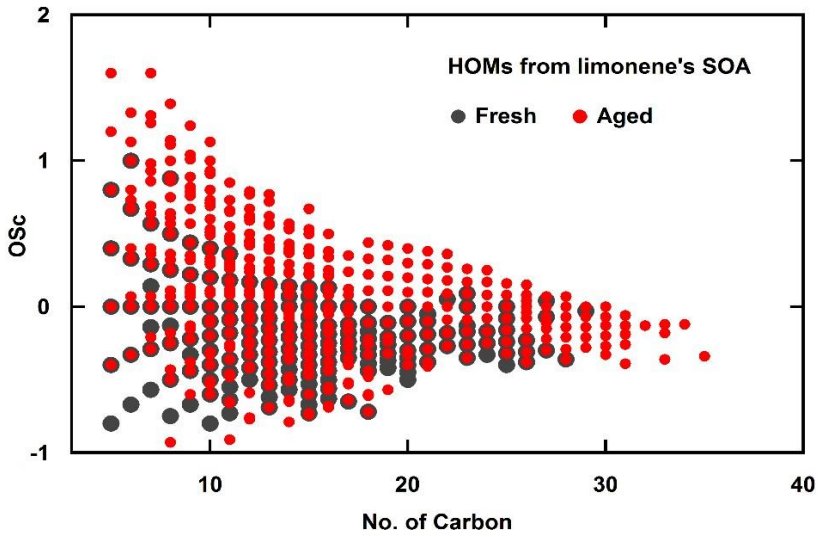

HOM formation in Fresh vs. Aged Biogenic SOA. The chemical compositions of fresh and aged SOA were discussed above. While movement toward formulas having higher O/C ratio and increasing number of HOMs is to be expected upon aging, a surprising result is the concurrent movement toward higher carbon number among the assigned HOM formulas. As shown in Table 2.4, mass and intensity weighted average formulas for aged SOA from β- pinene contain several more carbon atoms than fresh SOA. This difference is further illustrated in Figure 2.10, a plot of OSc vs. number of carbon atoms for all assigned HOM formulas from fresh vs. aged SOA. For a given number of carbon atoms, aging produced new formulas with higher OSc i.e. higher O/C and/or lower H/C. However, aging also produced many new formulas having greater numbers of carbon atoms that observed

in fresh SOA. HOMs in fresh SOA extended only up to C_{20} while HOMs aged SOA extended up to C_{26}. The overall increase in carbon number is particularly striking for region 3 where the average formula increases by more than 5 carbon atoms upon aging (Table 2.4). Region 3 also shows the greatest increase in number of formulas and signal intensity.

The characteristics of HOMs in fresh vs. aged SOA shed light on their possible formation pathways. In fresh SOA, most of the HOMs detected can be derived from one or two precursor molecules (i.e. most formulas contain fewer than 20 carbon atoms). This observation is consistent with proposed formation pathways for gas-phase ELVOCs which include auto-oxidation[47] of a single precursor molecule (inter- and intra-molecular hydrogen abstraction by OH radicals followed by rapid incorporation of oxygen atoms) as well as dimer formation between two partially oxidized monomers (e.g. coupling of oxidized precursors together). While there is some overlap between detected gas-phase ELVOCs and particle-phase HOMs in biogenic SOA, many species are unique to one phase or the other – an observation that was also made for laboratory vs. ambient SOA.[7] These differences may arise from particle phase reaction of reactive functional groups in ELVOCs e.g. peroxides and hydroperoxides.[10] Additional formation of dimers and oligomers is possible in the particle phase, but formation of higher order oligomers is unlikely in the gas phase unless the precursor concentration is extremely high. Therefore, HOMs contributing to particle formation and growth are likely to skewed toward monomers and dimers. Owing to their higher molecular mass, dimers (and higher order oligomers) need not be as highly oxidized as monomers in order to condense into the particle phase. Therefore, it is not surprising that particle phase oligomers are detected across the range from low O/C and/or OSc to high O/C and/or OSc in biogenic SOA.[1,6,48]

Aging of gas-phase species in biogenic SOA facilitates the formation of

HOMs, most of which are monomers and dimers. However, aging of particle phase oligomers may also occur, which would lead to the formation of new dimer and oligomer HOMs. This effect would be especially pronounced for formation of HOMs in region 3, since incorporation of oxidized functional groups (acids, carbonyls) into a pre-existing oligomer would both increase O/C and decrease H/C. In that regard, movement from the black region of Figure 2.8 (O/C=0.2-0.4 and H/C=1.4-1.6) along a line with a slope of -1 (as shown in a blue line) in the van Krevelen plot (corresponds to replacement of alkyl groups by acid groups[49]) would lead preferentially to formation of HOMs in region 3. Movement from the same region with a slope of -0.5 (corresponds to replacement of alkyl groups with carbonyl groups) as shown in a green line, would lead preferentially to formation of HOMs in region 1. New HOMs in region 2 can be produced only by oxidation of oligomer precursors having an O/C ratio just below 0.6.

Particle phase aging of pre-existing non-HOM oligomers in fresh SOA provides a reasonable explanation for the substantial increase in number of carbon atoms in HOMs observed for all three biogenic SOA precursors. Because the reactants and oxidation pathways are different for particle formation and aging, it is not surprising that the molecular products are also different. For all three biogenic precursors, the increase in carbon number with aging causes average molecular formula of detected HOMs to move away from the average formula reported for ambient LVOOA. For this reason, HOMs embedded within aged biogenic SOA under the conditions studied in this work are not reasonable surrogates for ambient LVOOA.

This study was designed to compare the effect of different biogenic precursors on HOM formation in fresh and aged SOA under a common set of experimental conditions. Particle formation and aging are strongly dependent on the conditions chosen. This study used relatively high precursor concentrations, which favors

bimolecular reaction products of peroxy radicals ($RO_2\cdot + RO_2\cdot$) and elevated partitioning of semi-volatile compounds into the particle phase, which may be less important under ambient conditions where lower precursor concentrations and/or high NO_x levels favor other pathways. Relative humidity can affect which products of the Criegee radical are dominant in fresh SOA produced by ozonolysis, and also the extent to which aqueous phase aging occurs.[50] No significant relative humidity dependence was observed in this study between 35 and 70%. This work employed 254 nm radiation in the PC owing to the high photochemical yield of OH. How the wavelength chosen may also influence direct photochemistry of UV-absorbing species is not well understood. While the presence of both gas and particle phase organics during the aging process does not allow particle phase vs. gas-particle reactions to be distinguished, it does more closely represent ambient conditions than, for example, removing gas phase species from the aerosol flow into the PC. Because of the impact of different experimental conditions on reaction pathways/products and the wide range of experimental conditions that can be encountered in ambient air, future work would benefit from a systematic study of particle formation and aging under a variety of conditions.

2.6 Structure Elucidation of HOMs and the Possible Formation Pathway

Tandem MS was applied for the structure elucidation of HOMs in fresh and aged SOA. CID (collision-induced dissociation) with 10 to 30 normalized collision energy (NCE) was applied aiming at various HOM ions, of which most have a relatively low abundance in the spectra. Therefore, traditional DDA (data dependent acquisition) approach[51] may not work as it always selectively fragment the most abundant ions for the subsequent activation in each precursor ion scan. In this case, a DIA (data independent acquisition) method was employed to expand the detectable

dynamic range of MS^2. An inclusion list of pre- determined m/z of the highly-oxidized species was loaded to the software. Therefore, the total range of m/z was divided into small isolation windows (1.0 m/z) that could be analyzed independently and successively. In some cases, collision energy as low as 10 NCE was still too high for some of the HOMs with extremely high oxygen content ($O \geq 10$). As a result, the fragment ions of them (almost oligomers) were hardly observed in the MS^2 spectra, which is not surprising since the highly-oxidized oligomers tends to have lower binding energy that required much lower collision energy to dissociate than monomers. 10 eV or even higher collision energy would lead to the fragment ions with $m/z < 50$ which beyond the dynamic range of the MS. As a result, MS^2 spectra of most monomers (48/48 for fresh, 63/66 for aged) and ~25% dimers could be obtained for further structure characterization. In this case, functional groups (-C(O)OOH, -C(O)OH, -OH, C=O) bearing in the formulas were determined according to the neutral molecule loss from the parent ions.

The discussion below is based on the assumptions and related studies from previous publications[31,52]: namely that formulas with carbon number ≤ 7 do not contain any ring structure whereas monomers with carbon number from 8 to 10 contain one ring. Also, the double bond could only be attributed to C=O since we assumed there was no C=C bond existing in the carbon skeleton. Hence, the number of specific functional groups was determined after considering both RDB value and the oxygen content in the formulas. MS^2 spectra of some parent ions showed multiple fragmentation pathways suggesting the occurrence of isomers. Therefore, the number of the functional groups was calculated by averaging over them. The hydroperoxyl functional group ($–CR_2OOH$) was also considered, but isn't listed here since it was only detected in a few formulas. Note that parent ions detected in both positive and negative MS^2 spectra were discussed and they were found to provide same types of

functional groups although the fragmentation pathways might be different. Based on the method and assumptions mentioned above, the number of the functional groups contained in the HOMs from fresh and aged SOA were calculated for comparison. Functional groups of peroxyl acid (–C(O)OOH) and carboxylic acid (–C(O)OH) were combined as acid groups. As a result, the amount of both –OH and acid groups were found to increase after aging due to the photo-oxidation by OH radicals. C=O groups, which did not show an increase trend, were probably consumed by reacting with OH radical to form acids.[53]

For all the HOMs detected in the spectra, oxygen content in each formula was separated as either saturated (C-O or O-O) or unsaturated (C=O). Since the double bonds in the formulas were all attributed to C=O groups, the rest of the oxygen atoms in the formulas could be assumed to be saturated. Therefore, ratios of unsaturated O vs. saturated O could be calculated. As the increased of the oxygen number in the formula, more functional groups related to saturated O (e.g. hydroxyl and hydroperoxyl) were formed or added. After aging, the number of unsaturated oxygen was increased by the twice of the saturated ones due to the formation C=O bond. In Figure 2.13, percentage of precursors that gave neutral small losses corresponding to the functional groups is shown for both fresh and aged HOMs. Molecular loss of H_2O which may attribute to either carboxylic acids or alcohols were detected in all formulas. Neutral loss related to functional groups with higher oxygen content (i.e. CH_2O_3) constituted a larger portion in the precursors that underwent further aging process. In summary, more acid groups were contained in HOMs as the increase of oxygen content. HOMs with higher degree of unsaturation contains more carboxylic acid groups and less carbonyls which may due to the reaction between aldehyde and OH radicals. It is also interesting that a large portion of HOMs presented in positive mode were found to have hydroproxide functional groups. This was also reported by a

separate study showing that organic peroxide was detected in the SOA from aqueous photo-oxidation of methylglyoxal.[54]

Figure 2.13. Average number of functional groups in the monomer region of HOMs both before and after aging.

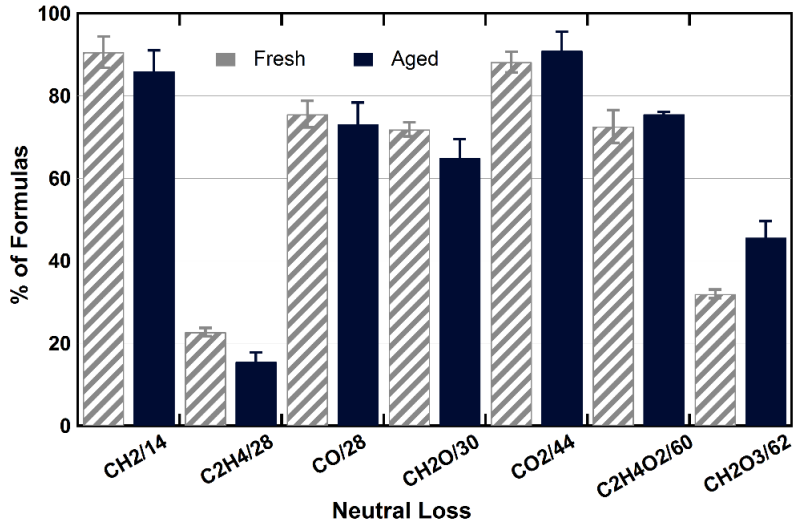

2.7 Conclusions

In this work, highly oxidized multifunctional molecules (HOMs) in fresh and aged secondary organic aerosol (SOA) derived from biogenic precursors are characterized with high resolution mass spectrometry. Fresh SOA was generated by mixing ozone with a biogenic precursor (β-pinene, limonene, α-pinene) in a flow tube reactor. Aging was performed by passing the fresh SOA through a photochemical reactor where it reacted with hydroxyl radicals. Although these aerosols were as a whole not highly oxidized, molecular analysis identified a significant number of HOMs embedded within it. HOMs in fresh SOA consisted mostly of monomers and dimers, which is consistent with condensation of extremely low-volatility organic compounds (ELVOCs) that have been detected in the gas phase in previous studies and

linked to SOA particle formation. Aging caused an increase in the average number of carbon atoms per molecule of the HOMs, which is consistent with particle phase oxidation of (less oxidized) oligomers already existing in fresh SOA. HOMs having different combinations of oxygen-to-carbon ratio, hydrogen-to-carbon ratio and average carbon oxidation state were discussed and compared to low volatility oxygenated organic aerosol (LVOOA), which has been identified in ambient aerosol based on average elemental composition but not fully understood at a molecular level. For the biogenic precursors and experimental conditions studied, HOMs in fresh biogenic SOA have molecular formulas more closely resembling LVOOA than HOMs in aged SOA, suggesting that aging of biogenic SOA is not a good surrogate for ambient LVOOA. The work and results discussed in this chapter were published at the Journal of Analytical Chemistry (2015).[16]

REFERENCES

(1) Heaton, K. J.; Sleighter, R. L.; Hatcher, P. G.; Hall IV, W. A.; Johnston, M. V. Environ. Sci. Technol. **2009**, 43 (20), 7797–7802.

(2) Ma, Y.; Marston, G. *Phys. Chem. Chem. Phys.* **2008**, *10* (40), 6115–6126.

(3) Walser, M. L.; Desyaterik, Y.; Laskin, J.; Laskin, A.; Nizkorodov, S. A. *Phys. Chem. Chem. Phys.* **2008**, *10* (7), 1009–1022.

(4) Romonosky, D. E.; Laskin, A.; Laskin, J.; Nizkorodov, S. A. *J. Phys. Chem. A* **2015**, 119, 2594−2606.

(5) Kroll, J. H.; Smith, J. D.; Che, D. L.; Kessler, S. H.; Worsnop, D. R.; Wilson, K. R. *Phys. Chem. Chem. Phys.* **2009**, *11*, 8005–8014.

(6) Hall, W. A.; Pennington, M. R.; Johnston, M. V. *Environ. Sci. Technol.* **2013**, *47* (5), 2230–2237.

(7) Mutzel, A.; Poulain, L.; Berndt, T.; Iinuma, Y.; Rodigast, M.; Böge, O.; Richters, S.; Spindler, G.; Sipilä, M.; Jokinen, T.; Kulmala, M.; Herrmann, H. *Environ. Sci. Technol.* **2015**, *49* (13), 7754–7761.

(8) Ehn, M.; Thornton, J. A.; Kleist, E.; Sipilä, M.; Junninen, H.; Pullinen, I.; Springer, M.; Rubach, F.; Tillmann, R.; Lee, B.; Lopez-Hilfiker, F.; Andres, S.; Acir, I.-H.; Rissanen, M.; Jokinen, T.; Schobesberger, S.; Kangasluoma, J.; Kontkanen, J.; Nieminen, T.; Kurtén, T.; Nielsen, L. B.; Jørgensen, S.; Kjaergaard, H. G.; Canagaratna, M.; Maso, M. D.; Berndt, T.; Petäjä, T.; Wahner, A.; Kerminen, V.-M.; Kulmala, M.; Worsnop, D. R.; Wildt, J.; Mentel, T. F. *Nature* **2014**, *506* (7489), 476–479.

(9) Jokinen, T.; Berndt, T.; Makkonen, R.; Kerminen, V.-M.; Junninen, H.; Paasonen, P.; Stratmann, F.; Herrmann, H.; Guenther, A. B.; Worsnop, D. R.; Kulmala, M.; Ehn, M.;

Sipilä, M. *Proc. Natl. Acad. Sci. U. S. A.* **2015**, *112* (23), 7123–7128.

(10) Mentel, T. F.; Springer, M.; Ehn, M.; Kleist, E.; Pullinen, I.; Kurtén, T.; Rissanen, M.; Wahner, A.; Wildt, J. *Atmos. Chem. Phys.* **2015**, *15* (12), 6745–6765.

(11) Zhang, X.; McVay, R. C.; Huang, D. D.; Dalleska, N. F.; Aumont, B.; Flagan, R. C.; Seinfeld, J. H. *Proc. Natl. Acad. Sci. U. S. A.* **2015**, *112* (46), 14168–14173.

(12) Hyttinen, N.; Kupiainen-Määttä, O.; Rissanen, M. P.; Muuronen, M.; Ehn, M.; Kurtén, T. *J. Phys. Chem. A* **2015**, *119* (24), 6339–6345.

(13) Atkinson, R.; Arey, J. *Atmos. Environ.* **2003**, *37*, 197–219.

(14) Cruz, C. N.; Dassios, K. G.; Pandis, S. N. *Atmos. Environ.* **2000**, *34* (23), 3897–3905.

(15) Cruz, C. N.; Pandis, S. N. *Environ. Sci. Technol.* **2000**, *34* (20), 4313-4319.

(16) Tu, P.; Hall, W. A.; Johnston, M. V. *Anal. Chem.* **2016**, *88* (8), 4495–4501.

(17) Johnson, D.; Marston, G. *Chem. Soc. Rev.* **2008**, *37* (4), 699–716.

(18) Hall, W. A.; Johnston, M. V. *Aerosol Sci. Technol.* **2011**, *45* (1), 37–45.

(19) Bateman, A. P.; Walser, M. L.; Desyaterik, Y.; Laskin, J.; Laskin, A.; Nizkorodov, S. A.; Bateman, A. P. *Environ. Sci. Technol.* **2008**, *42* (19), 7341–7346.

(20) Kourtchev, I.; Doussin, J.-F.; Giorio, C.; Mahon, B.; Wilson, E. M.; Maurin, N.; Pangui, E.; Venables, D. S.; Wenger, J. C.; Kalberer, M. *Atmos. Chem. Phys.* **2015**, *15* (10), 5683–5695.

(21) Hall IV, W. A.; Johnston, M. V. *J. Am. Soc. Mass Spectrom.* **2012**, *23* (6), 1097–1108.

(22) Kind, T.; Fiehn, O. *BMC Bioinformatics* **2007**, *8*, 105.

(23) Herzsprung, P.; Hertkorn, N.; von Tümpling, W.; Harir, M.; Friese, K.; Schmitt-Kopplin, P. *Anal. Bioanal. Chem.* **2014**, *406* (30), 7977–7987.

(24) Kendrick, E. *Anal. Chem.* **1963**, *35* (13), 2146–2154.

(25) Marshall, A. G.; Rodgers, R. P. *Acc. Chem. Res.* **2004**, *37* (1), 53–59.

(26) Hughey, C. A.; Hendrickson, C. L.; Rodgers, R. P.; Marshall, A. G.; Qian, K. *Anal. Chem.* **2001**, *73* (19), 4676–4681.

(27) van Krevelen, D. W. *Fuel* **1950**, *29*, 269–284.

(28) Wu, Z.; Rodgers, R. P.; Marshall, A. G. *Anal. Chem.* **2004**, *76* (9), 2511–2516.

(29) Ehn, M.; Kleist, E.; Junninen, H.; Petäjä, T.; Lönn, G.; Schobesberger, S.; Dal Maso, M.; Trimborn, A.; Kulmala, M.; Worsnop, D. R.; Wahner, A.; Wildt, J.; Mentel, T. F. *Atmos. Chem. Phys.* **2012**, *12* (11), 5113–5127.

(30) Crounse, J. D.; Nielsen, L. B.; Jørgensen, S.; Kjaergaard, H. G.; Wennberg, P. O. *J. Phys. Chem. Lett.* **2013**, *4* (20), 3513–3520.

(31) Heaton, K. J.; Dreyfus, M. A.; Wang, S.; Johnston, M. V. *Environ. Sci. Technol.* **2007**, *41* (17), 6129–6136.

(32) Pankow, J. F. *Atmos. Environ.* **2003**, *37* (24), 3323–3333.

(33) Jimenez, J. L.; Canagaratna, M. R.; Donahue, N. M.; Prevot, a. S. H.; Zhang, Q.; Kroll, J. H.; DeCarlo, P. F.; Allan, J. D.; Coe, H.; Ng, N. L.; Aiken, A. C.; Docherty, K. S.; Ulbrich, I. M.; Grieshop, A. P.; Robinson, a. L.; Duplissy, J.; Smith, J. D.; Wilson, K. R.; Lanz, V. a.; Hueglin, C.; Sun, Y. L.; Tian, J.; Laaksonen, A.; Raatikainen, T.; Rautiainen, J.; Vaattovaara, P.; Ehn, M.; Kulmala, M.; Tomlinson, J. M.; Collins, D. R.; Cubison, M. J.; Dunlea, J.; Huffman, J. A.; Onasch, T. B.; Alfarra, M. R.; Williams, P. I.; Bower, K.; Kondo, Y.; Schneider, J.; Drewnick, F.; Borrmann, S.; Weimer, S.; Demerjian, K.; Salcedo, D.; Cottrell, L.; Griffin, R.; Takami, a.; Miyoshi, T.; Hatakeyama, S.; Shimono, A.; Sun, J. Y.; Zhang, Y. M.; Dzepina, K.; Kimmel, J. R.; Sueper, D.; Jayne, J. T.; Herndon, S. C.; Trimborn, a. M.; Williams, L. R.; Wood, E. C.; Middlebrook, A. M.; Kolb, C. E.; Baltensperger, U.; Worsnop, D. R. *Science*. **2009**, *326* (5959), 1525–1529.

(34) Daumit, K. E.; Kessler, S. H.; Kroll, J. H. *Faraday Discuss.* **2013**, *165* (0), 181–202.

(35) Ng, N. L.; Canagaratna, M. R.; Jimenez, J. L.; Chhabra, P. S.; Seinfeld, J. H.; Worsnop, D. R. *Atmos. Chem. Phys.* **2011**, *11* (13), 6465–6474.

(36) Aiken, A. C.; Decarlo, P. F.; Kroll, J. H.; Worsnop, D. R.; Huffman, J. A.; Docherty, K. S.; Ulbrich, I. M.; Mohr, C.; Kimmel, J. R.; Sueper, D.; Sun, Y.; Zhang, Q.; Trimborn, A.; Northway, M.; Ziemann, P. J.; Canagaratna, M. R.; Onasch, T. B.; Alfarra, M. R.; Prevot, A. S.

H.; Dommen, J.; Duplissy, J.; Metzger, A.; Baltensperger, U.; Jimenez, J. L. *Environ. Sci. Technol.* **2008**, *42* (12), 4478–4485.

(37) Decarlo, P. F.; Ulbrich, I. M.; Crounse, J.; De Foy, B.; Dunlea, E. J.; Aiken, A. C.; Knapp, D.; Weinheimer, A. J.; Campos, T.; Wennberg, P. O.; Jimenez, J. L. *Atmos. Chem. Phys.* **2010**, *10* (12), 5257–5280.

(38) Crippa, M.; El Haddad, I.; Slowik, J. G.; Decarlo, P. F.; Mohr, C.; Heringa, M. F.; Chirico, R.; Marchand, N.; Sciare, J.; Baltensperger, U.; Prévôt, A. S. H. *J. Geophys. Res. Atmos.* **2013**, *118* (4), 1950–1963.

(39) Docherty, K. S.; Aiken, A. C.; Huffman, J. A.; Ulbrich, I. M.; Decarlo, P. F.; Sueper, D.; Worsnop, D. R.; Snyder, D. C.; Peltier, R. E.; Weber, R. J.; Grover, B. D.; Eatough, D. J.; Williams, B. J.; Goldstein, A. H.; Ziemann, P. J.; Jimenez, J. L. *Atmos. Chem. Phys.* **2011**, *11* (23), 12387–12420.

(40) Kroll, J. H.; Donahue, N. M.; Jimenez, J. L.; Kessler, S. H.; Canagaratna, M. R.; Wilson, K. R.; Altieri, K. E.; Mazzoleni, L. R.; Wozniak, A. S.; Bluhm, H.; Mysak, E. R.; Smith, J. D.; Kolb, C. E.; Worsnop, D. R. *Nat. Chem.* **2011**, *3* (2), 133–139.

(41) Yu, L.; Smith, J.; Laskin, A.; Anastasio, C.; Laskin, J.; Zhang, Q. *Atmos. Chem. Phys.* **2014**, *14* (24), 13801–13816.

(42) Rissanen, M. P.; Kurtén, T.; Sipilä, M.; Thornton, J. A.; Kangasluoma, J.; Sarnela, N.; Junninen, H.; Jørgensen, S.; Schallhart, S.; Kajos, M. K.; Taipale, R.; Springer, M.; Mentel, T. F.; Ruuskanen, T.; Petäjä, T.; Worsnop, D. R.; Kjaergaard, H. G.; Ehn, M. *J. Am. Chem. Soc.* **2014**, *136* (44), 15596–15606.

(43) Canagaratna, M. R.; Jimenez, J. L.; Kroll, J. H.; Chen, Q.; Kessler, S. H.; Massoli, P.; Hildebrandt Ruiz, L.; Fortner, E.; Williams, L. R.; Wilson, K. R.; Surratt, J. D.; Donahue, N. M.; Jayne, J. T.; Worsnop, D. R. *Atmos. Chem. Phys.* **2015**, *15* (1), 253–272.

(44) Schobesberger, S.; Junninen, H.; Bianchi, F.; Lönn, G.; Ehn, M.; Lehtipalo, K.; Dommen, J.; Ehrhart, S.; Ortega, I. K.; Franchin, A.; Nieminen, T.; Riccobono, F.;

Hutterli, M.; Duplissy, J.; Almeida, J.; Amorim, A.; Breitenlechner, M.; Downard, A. J.; Dunne, E. M.; Flagan, R. C.; Kajos, M.; Keskinen, H.; Kirkby, J.; Kupc, A.; Kürten, A.; Kurtén, T.; Laaksonen, A.; Mathot, S.; Onnela, A.; Praplan, A. P.; Rondo, L.; Santos, F. D.; Schallhart, S.; Schnitzhofer, R.; Sipilä, M.; Tomé, A.; Tsagkogeorgas, G.; Vehkamäki, H.; Wimmer, D.; Baltensperger, U.; Carslaw, K. S.; Curtius, J.; Hansel, A.; Petäjä, T.; Kulmala, M.; Donahue, N. M.; Worsnop, D. R. *Proc. Natl. Acad. Sci. U. S. A.* **2013**, *110* (43), 17223–17228.

(45) Nguyen, T. B.; Roach, P. J.; Laskin, J.; Laskin, A.; Nizkorodov, S. A. *Atmos. Chem. Phys.* **2011**, *11* (14), 6931–6944.

(46) Canagaratna, M. R.; Jimenez, J. L.; Kroll, J. H.; Chen, Q.; Kessler, S. H.; Massoli, P.; Hildebrandt Ruiz, L.; Fortner, E.; Williams, L. R.; Wilson, K. R.; Surratt, J. D.; Donahue, N. M.; Jayne, J. T.; Worsnop, D. R. *Atmos. Chem. Phys.* **2015**, *15* (1), 253–272.

(47) Emanuelsson, E. U.; Watne, Ågot K.; Lutz, A.; Ljungström, E.; Hallquist, M. *J. Phys. Chem. A* **2013**, *117* (40), 10346–10358.

(48) Crounse, J. D.; Nielsen, L. B.; Jørgensen, S.; Kjaergaard, H. G.; Wennberg, P. O. *J. Phys. Chem. Lett.* **2013**, *4* (20), 3513–3520.

(49) Reinhardt, A.; Emmenegger, C.; Gerrits, B.; Panse, C.; Dommen, J.; Baltensperger, U.; Zenobi, R.; Kalberer, M. *Anal. Chem.* **2007**, *79* (11), 4074–4082.

(50) Kroll, J. H.; Lim, C. Y.; Kessler, S. H.; Wilson, K. R. *J. Phys. Chem. A* **2015**, *119* (44), 10767–10783.

(51) Aljawhary, D.; Lee, A. K. Y.; Abbatt, J. P. D. *Atmos. Meas. Tech.* **2013**, *6* (11), 3211–3224.

(52) Chapman, J. D.; Goodlett, D. R.; Masselon, C. D. *Mass Spectrom. Rev.* **2014**, *33* (6), 452–470.

(53) George, C.; Ammann, M.; D'Anna, B.; Donaldson, D. J.; Nizkorodov, S. A. *Chem. Rev.* **2015**, *115* (10), 4218–4258.

(54) Chacon-Madrid, H. J.; Henry, K. M.; Donahue, N. M. *Atmos. Chem. Phys.* **2013**, *13* (6), 3227–3236.

(55) Lim, Y. B.; Turpin, B. J. *Atmos. Chem. Phys.* **2015**, *15* (22), 12867–12877.

Chapter 3

ON- AND OFF-LINE ANALYSIS OF SIZE SELECTED SOA PARTICLES WITH VARIOUS MASS SPECTROMETRY TECHNIQUES

3.1 The Formation and Growth of Ultrafine Particles in the Atmosphere

Ultrafine particles, defined here as smaller than 100 nm in diameter, constitute the largest number of particles in the atmosphere and are of interest owing to their disproportionate influence on climate and human health[1,2]. Particularly important is their role in formation of CCN and their corresponding impact on radiative forcing[3]. For ultrafine particles to grow to a climatically-relevant size, the particle growth rate must exceed the loss rate. The greatest uncertainty associated with particle growth and its impact on radiative forcing is the contribution of secondary organic matter[4], which is formed by oxidation of volatile compounds in the gas phase followed by subsequent migration of the products to the particle phase.

The ultrafine particles that are suspended in ambient air are significant fraction of the total atmospheric aerosol, of which the source could be both organic and inorganic. On a global scale, organic aerosol particles constitute a substantial fraction of the total aerosol mass in the atmosphere[5–7] and most of them are secondary [6,8]. On a molecular level, atmospheric organic aerosol is very complex, encompassing hundreds to thousands of individual compounds[5,9–12]. Laboratory SOA is similarly complex and a variety of oxidation and degradation pathways have been proposed to explain the product distributions[5,13–15]. Part of this complexity arises from the formation of high molecular weight (MW) oligomeric species from two or more precursor molecules[16,17]. Oligomers can constitute almost half of the SOA mass in laboratory experiments[18,19].

The distribution of organic molecules between gas and particle phase is described by absorptive partitioning theory[20]. When precursor molecules are oxidized in the gas phase, the products partition to the particle phase causing particle growth. Non-volatile molecules have a negligible evaporation rate once they partition to the particle phase. These molecules cause particle growth at a rate given by their condensation rate from the gas phase. Comparatively, semi-volatile molecules have a substantial evaporation rate and therefore cause particle growth at a rate much slower than their condensation rate. For simplicity, in this chapter I use the terms "condensation" and "condensational growth" to describe the process by which non-volatile molecules in the gas phase undergo partitioning to cause particle growth at the condensation rate. The recent detection and characterization of extremely low-volatility organic compounds (ELVOCs) in the gas phase has uncovered a previously underappreciated pathway for condensational growth[21,22]. For monoterpene oxidation, the range of ELVOC species includes both highly functionalized monomers and oligomers.

The dependence of chemical composition on particle size can provide insight into particle growth mechanisms. Processes limited by the amount of available surface area, such as condensation, are favored in smaller particles where the surface-to-volume ratio is high. Processes limited by the amount of available volume, such as partitioning, are favored in larger particles where the surface-to-volume ratio is low. Superimposed on these dependencies is the radius-of-curvature (Kelvin) effect[23] on molecular volatility, which also favors the incorporation of lower volatility species into smaller diameter particles. Winkler et al. [24] have reported size-resolved composition of particles between 10 and 40 nm in diameter that were produced by α-pinene ozonolysis. Based on signal intensities of species detected by thermal desorption chemical ionization mass spectrometry (TDCIMS), 10-20 nm particles

contained a greater fraction of lower volatility species, while 30-40 nm particles contained a greater fraction of higher volatility species. In this experiment, species volatility was qualitatively assessed by the loss of signal intensity due to sample evaporation over time. In second study of SOA from α-pinene ozonolysis, Zhao et al.[25] used measurements of gas phase molecular species by chemical ionization mass spectrometry to show a positive correlation of higher MW (and presumably less volatile) species with the number concentration of 10-20 nm particles, whereas lower MW (and presumably more volatile) species were positively correlated with the number concentration of 30-40 nm particles. In a third study of SOA from α-pinene ozonolysis, Kidd et al.[26] showed that particles in the 250- 500 nm range contained a greater fraction of oligomers while particles greater than 500 nm contained a greater fraction of monomers. Molecular composition measurements by Zhao et al.[27] of size-selected particles produced by trans-3-hexene ozonolysis showed that particles smaller than 100 nm contained a greater fraction of high MW oligomers than particles larger than 100 nm. With the exception of Kidd et al. which focused on much larger particle sizes than the rest, the above experiments are consistent with the concept that higher MW, lower volatility species formed in the gas phase are more strongly represented in smaller diameter particles, as would be expected from a condensation-driven process.

Particle phase chemistry, specifically accretion reactions in the particle phase that form higher MW lower volatility oligomers from higher volatility lower MW monomers[28], have been proposed as an additional pathway for SOA formation. Accretion chemistry, which produces non-volatile molecules directly in the particle phase, and ELVOC condensation represent two separate sources for oligomers that are detected in the particle phase. It has been noted that relatively few ELVOC molecular formulas obtained from gas phase measurements match those of oligomers detected in particle phase measurements[29,30]. This dissimilarity could arise from subsequent

reaction of ELVOCs after they enter the particle phase, or by the formation of completely new oligomers in the particle phase through accretion chemistry. In principle, these two sources can be distinguished through the size dependence of particle composition, since molecular species derived from condensation (surface area limited) should be more strongly represented in smaller particles while those derived from accretion chemistry (volume limited) should be more strongly represented in larger particles. A particle size dependent molecular composition arising from particle phase reaction was suggested in a modelling study of SOA produced from dodecane photooxidation, though experimental measurements in that work were confined to particle size distributions as a function of reaction time[31].

3.2 Size-Resolved SOA Particles Generated in the Lab

In my research, particle size-dependent chemical composition of SOA produced by β- pinene ozonolysis was studied. Figure 3.1 shows the experimental setup used in this work. All gas flows were generated from zero air (model 737, Aadco Instruments Inc., Miami, FL, USA) to minimize contamination. SOA was generated in a flow tube reactor (FTR) (section A of Figure 3.1) as described previously[30,32]. In most experiments, the concentrations of β- pinene and ozone after mixing in the reactor were 1 ppmv and 10 ppmv respectively, giving an SOA mass loading of about 2300 $\mu g/m^3$ at the reactor exit. In a separate set of experiments, the SOA mass loading was varied in the 5-2300 $\mu g/m^3$ (the size distribution and concentration are shown in Figure 3.2) range by varying the β-pinene concentration between 0.03 and 1 ppmv. Blank samples were obtained by flowing zero air into FTR to mix withozone in the absence of β-pinene. All FTR experiments were performed at a low relative humidity (8%) since very little difference were found in the molecular composition of SOA from β-pinene ozonolysis that was generated with 35-70% RH vs.

conditions used in the current work[30]. Understanding how relative humidity (as well as other experimental conditions) might quantitatively impact oligomer formation is important to consider in future studies.

Figure 3.1. Schematic of the experimental workflow. SOA is produced either directly from the flow tube reactor (A) or re-aerosolization from an atomizer (B). Analysis is performed on-line by NAMS (C) or off-line by HR-MS after sample collection with NAS-s (D). Adapted from [Tu, P.; Johnston, M. V. *Atmos. Chem. Phys.* **2017**, 17, 7593-7603]. © Peijun Tu and Murray V. Johnston 2017.

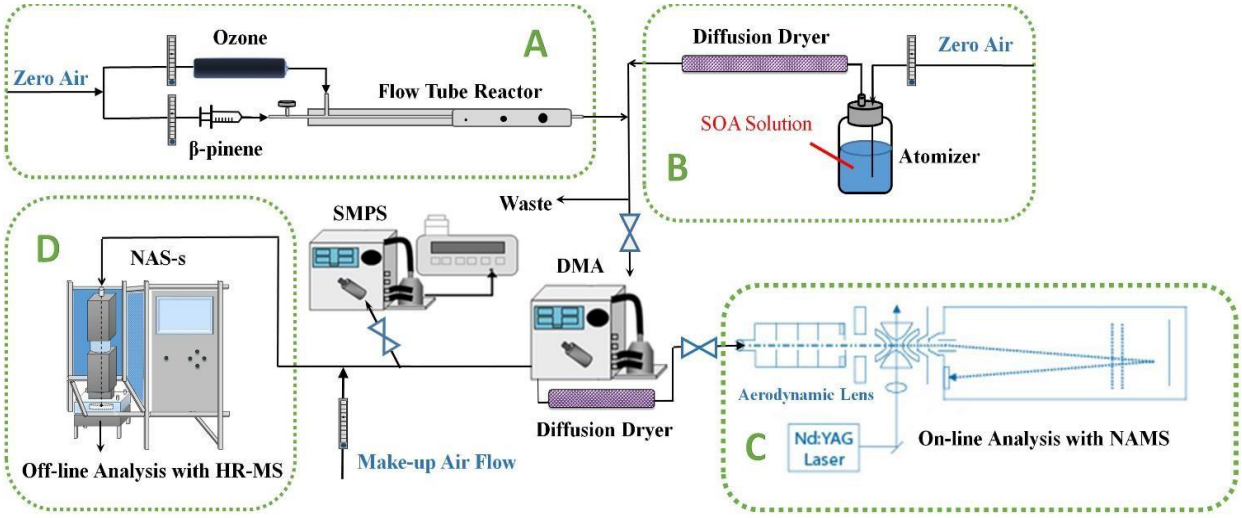

Figure 3.2. Size distributions of polydisperse SOA samples produced from the flow tube reactor (a, b, c) monitored with SMPS. The mass concentration of polydisperse SOA sample (c) was multiplied by a factor of 20 to fit on this scale. Adapted from [Tu, P.; Johnston, M. V. *Atmos. Chem. Phys.* **2017**, 17, 7593-7603]. © Peijun Tu and Murray V. Johnston 2017.

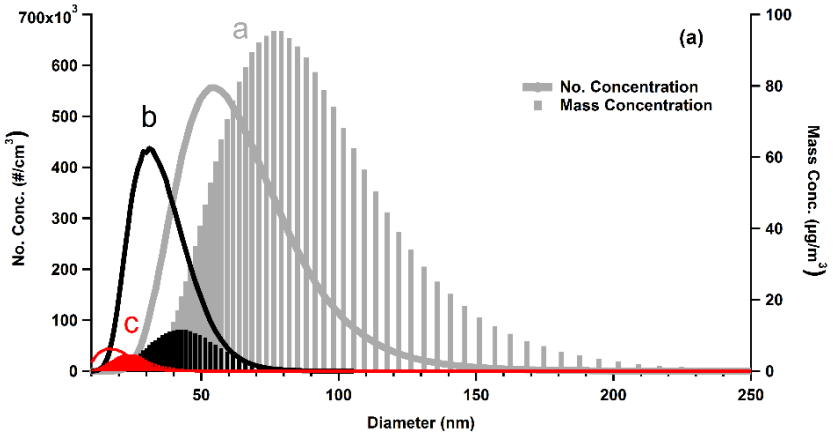

In a control experiment, polydisperse SOA from the FTR (2300 µg/m^3) that had been previously collected onto a filter was extracted into 50/50 acetonitrile/water and atomized (ATM 226, TOPAS, Dresden, Germany) to produce a control aerosol. Section B of Figure 3.1 shows the apparatus, which included a diffusion dryer to reduce the amount of water vapour in the aerosol flow. The goal of this experiment was to generate SOA-like aerosol that did not have a particle size dependent chemical composition associated with it, though the composition of this aerosol was not expected to be precisely the same as the original collected SOA because of possible chemical reactions prior to and/or during atomization. This experiment also provided the opportunity to assess possible artifact due to sample collection and analysis after

size selection (see section 3.3). The particle size distribution of the control aerosol was fine tuned by varying the gas flow conditions into the atomizer and the concentration of extracted SOA in the solution used for atomization[33], so that a sufficient aerosol mass concentration was obtained at each mobility diameter of interest (35, 60, 85, 110 nm) to permit chemical analysis. Sample blanks for the control experiment were obtained by atomizing pure solvent[34].

Particle size distributions were monitored with a Scanning Mobility Particle Sizer (SMPS, TSI Incorporated, St. Paul, Minnesota, USA). Specific particle sizes within the size distribution were selected with a separate Differential Mobility Analyzer (DMA, model 3081, TSI Incorporated, St. Paul, Minnesota, USA). In this setup, particles were electrically charged with the advanced Aerosol Neutralizer (Model 3088, TSI Incorporated, St. Paul, Minnesota, USA) which is a non-radioactive, soft x-ray bipolar diffusion charger. The (singly) charged particles that entered DMA were separated based on their electrical mobility in the DMA cylindrical capacitor that has inner/outer electrodes. The particle mobility diameters studied in this work were 35, 60, 85, 110 nm and their size distributions are shown in Figure 3.3. Mass concentrations are given in Table 3.1. Because of the low mass concentrations after size selection, zero-air was sent through the entire experimental apparatus for 12 h after each experiment to remove contamination. The size selection efficiency of DMA was examined by performing long-term scan on each size particles with SMPS. Figure 3.4 shows the average concentration and selected diameter averaging over ~100 scans in approximately 9 hr. The calculated standard deviation suggested that the smaller particles especially the 30 nm ones suffered more from the interference from the background and were less stable. This explains the necessity of SMPS monitoring of mass concentrations to get a precise sample mass loading and multiple replicates collected for each size samples. In this project, polydisperse SOA samples

having similar volume to surface area ratios to the size-selected samples were also investigated.

Figure 3.3. Size distributions of polydisperse SOA samples produced from the flow tube reactor monitored with SMPS. Size distributions of monodisperse SOA obtained from polydisperse sample are also shown. The mass concentration of the 35 nm monodisperse sample in the inset was multiplied by a factor of 40. Adapted from [Tu, P.; Johnston, M. V. *Atmos. Chem. Phys.* **2017**, 17, 7593-7603]. © Peijun Tu and Murray V. Johnston 2017.

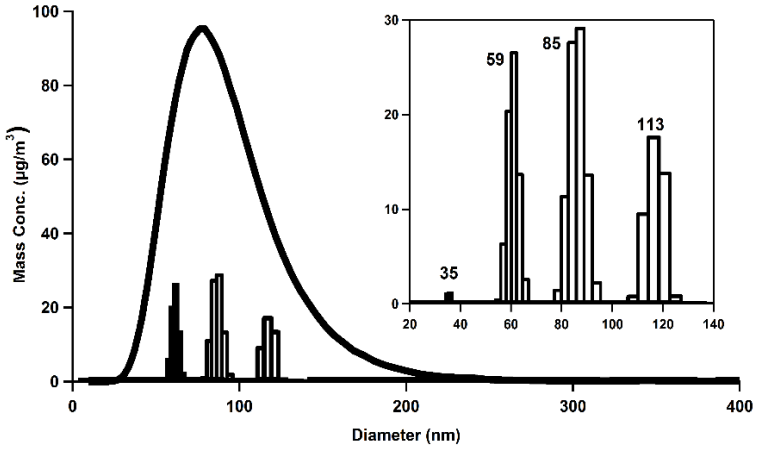

Figure 3.4. Average number and mass concentration for monodisperse particles selected at different diameters over ~100 scans using SMPS.

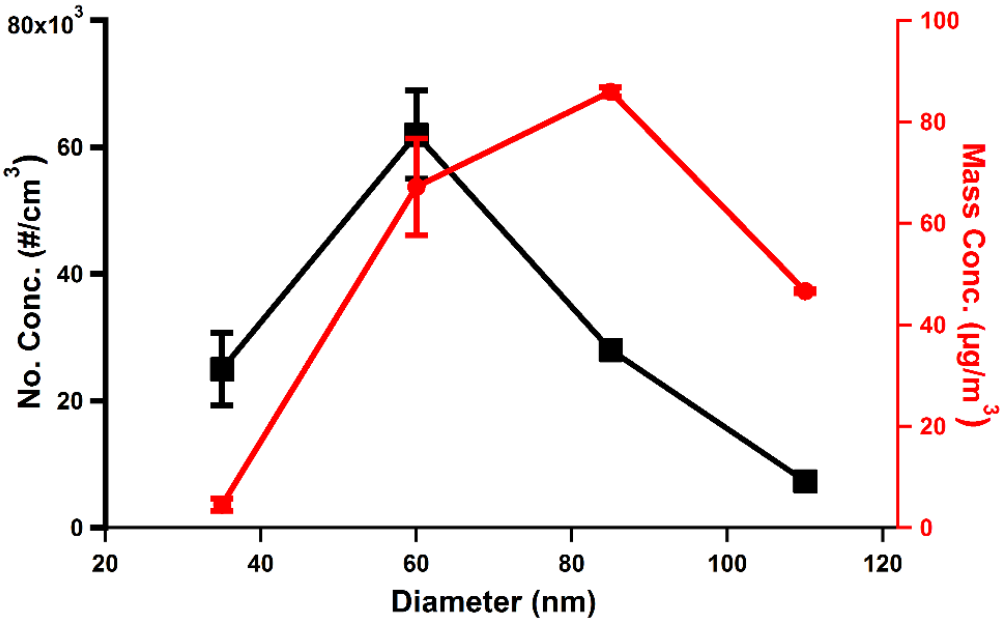

Table 3.1. SOA Samples (poly- and mono-disperse particles) investigated with SMPS.

Sample Type	SOA Generation	Avg. Mode Diameter (nm)	Surface-to-Volume Ratio (nm^{-1})	Avg. Mass. Concentration ($\mu g/m^3$)	Time Required for 10µg sample to be Collected (hr)
Poly-a	Flow Tube Reactor	76	0.08	2300	0.07
35 nm		35	0.17	5	34
60 nm		59	0.10	66	2.5
85 nm		85	0.07	87	1.9
110 nm		113	0.05	48	3.5
Poly-b		43	0.14	240	0.69
Poly-c		23	0.26	5	33
Poly-d	Atomizer	240	N/A	510	0.33
35 nm		35	0.17	2	93
60 nm		62	0.10	23	7.3
110 nm		112	0.05	20	8.3

3.3 Sample Collection with Nano-Aerosol Sampler (NAS)

Particles were collected with a Nano Aerosol Sampler operating in the spot collection mode (NAS-s; Section D in Figure 3.1). The sampler was custom designed and built by Aerosol Dynamics, Inc. (Berkeley, California, USA). This device uses a water-based condensation method[35] to either sample particles into a small spot in a

collection well or to concentrate them into an outlet flow aerosol flow. When used in spot mode, particles deposited in the collection well were able be dissolved in a minimum amount of solvent for subsequent offline analysis. In this device, aerosol with a flowrate of ~1000 cpm first passed through a "conditioner" region at 5˚C, followed by a heated "initiator" region at 35 ˚C where the aerosol became saturated with water vapor. The aerosol then entered a cooled "moderator" region at 10 ˚C where the temperature decrease created a supersaturated vapor. In this region, water condensed on the particles to produce droplets, which were subsequently focused to a ~1 mm spot in a collection well. Since the SOA deposits onto the well as liquid droplets, rebounce of the nanoparticles is not likely to occur. The well was then heated to 35 ˚C to evaporate the condensed water (dry deposition mode) from collected particles. After a sufficient amount of sample was collected (~10 µg in these experiments), acetonitrile/deionized water (1:1) solvent was added to the well to dissolve the collected particles to a concentration of 0.1 mg/mL for offline analysis. Depending on aerosol mass concentration, <1 to ~34 hours were required to collect a sufficient amount of sample, though one specific control sample required 93 hours (see Table 3.1).

In this work, SOA samples generated under the exact same experimental conditions were collected onto filter as well. As shown in Figure 3.5, molecular formula distribution of polydisperse SOA were similar for samples collected with NAS-c at 35˚C vs. a standard filter at room temperature. Formulas that represent >98% of the signal intensity are the same for NAS and filter. The difference is the detection of several very low intensity oligomers in the filter sample. The reason of this difference remains unclear that whether these higher order oligomers undergo decomposition in the NAS or an artifact of filter collection are formed by accretion reaction during sample preparation of the filter sample. NAS-s had the advantage over

filter collection of being able to work with smaller sample sizes with a much lower mass loading collected. Therefore, shorter collection times could be achieved. Filter collection, comparatively, requires much longer collection time especially for the smaller particles. Additionally, sample collected on the filter is easily to be interfered by the background impurities brought in by the sample exaction process which results in some noise peaks that need to be get rid of during spectra analysis.

Figure 3.5. OSc vs. No. of Carbon Atoms in SOA samples collected via NAS-s and glass fiber filter in the positive ion mode.

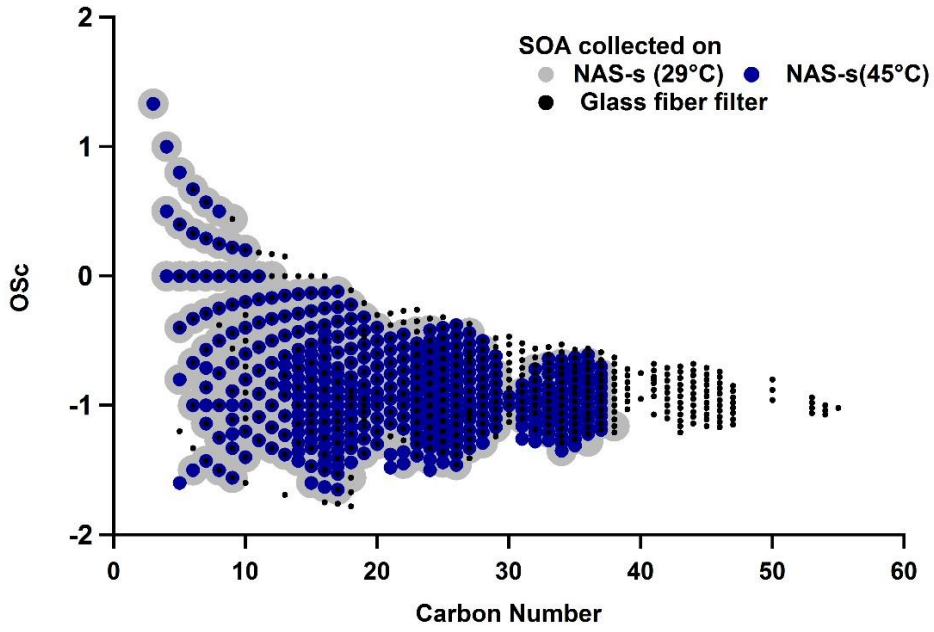

3.4 On- and Off- line Mass Spectrometry Analysis

As mentioned in Chapter 2, offline molecular characterization was performed by high resolution mass spectrometry (HR-MS) with a Q Exactive™ Hybrid Quadrupole-Orbitrap Mass Spectrometer (Thermo Scientific, Waltham, Massachusetts, USA) coupled to a heated- electrospray ionization (HESI) probe. For these measurements, the sample flow rate was 3 µL/min with an injection volume of 10 µL. Other operating parameters included: spray voltage, 2.5-3.5 kV; capillary temperature, 250-275˚C. The possibility of producing artifacts of non-covalently bound clusters was ruled out using the approach discussed elsewhere[30,32]. Full MS scans were acquired over the range 100−1000 m/z with a mass resolving power of 70 000. Each spectrum was obtained by averaging ∼130 scans over a period of approximately 1.0 min and then processed with Xcalibur™ Software.

In this work, five replicate samples were analyzed for each experiment, and molecular formulas had to be positively detected and assigned in all five replicates in order to be considered further. Blank sample subtraction was performed for each sample prior to the data analysis. Data analysis was performed as described previously targeting closed-shell molecular formulas[30]. I also performed Kendrick Mass Defect plots and RDB-O[36,37] value (the maximum RDB-O distribution resides in -10 and 10 for hydrophobic CHO species[36]) as the updated criteria to help filtering the unreasonable assigned formulas. After removing background peaks, unreasonable formulas and redundancies due to isotopic substitution, hundreds of unique molecular formulas remained for each sample. The number of common molecular formulas detected and assigned in all five replicates for each experiment are given in Table 3.2 along with the mass and intensity weighted average O/C ratios of these formulas. This table also highlights the inherent variability among replicates that arises from low

intensity peaks near the detection limit. The reproducibility of the size selection experiments is also demonstrated in Figure 3.6. In this figure, X-axis shows the SI Variance% of a particular ion in a single run. It was calculated as the equation below:

$$\text{SI Variance\% of a Particular Ion} = 100*(SI_i - SI_{avg})/SI_{avg}$$

Y-axis in the plot gives the number of ions (in a single spectrum) with SI variance% that lie within a certain range. Top and bottom arrows represent the percentage of formulas within 30% and 10% variance from its average SI. It is clear that most of the ions with SI variance% less than 30%. The average RSD% of SI of formulas in each sample was also listed in Table S2 to demonstrate the reproducibility.

Figure 3.6. No. of molecular formulas detected in the positive mode spectra that lies within a certain range of variance% from its average signal intensity (SI).

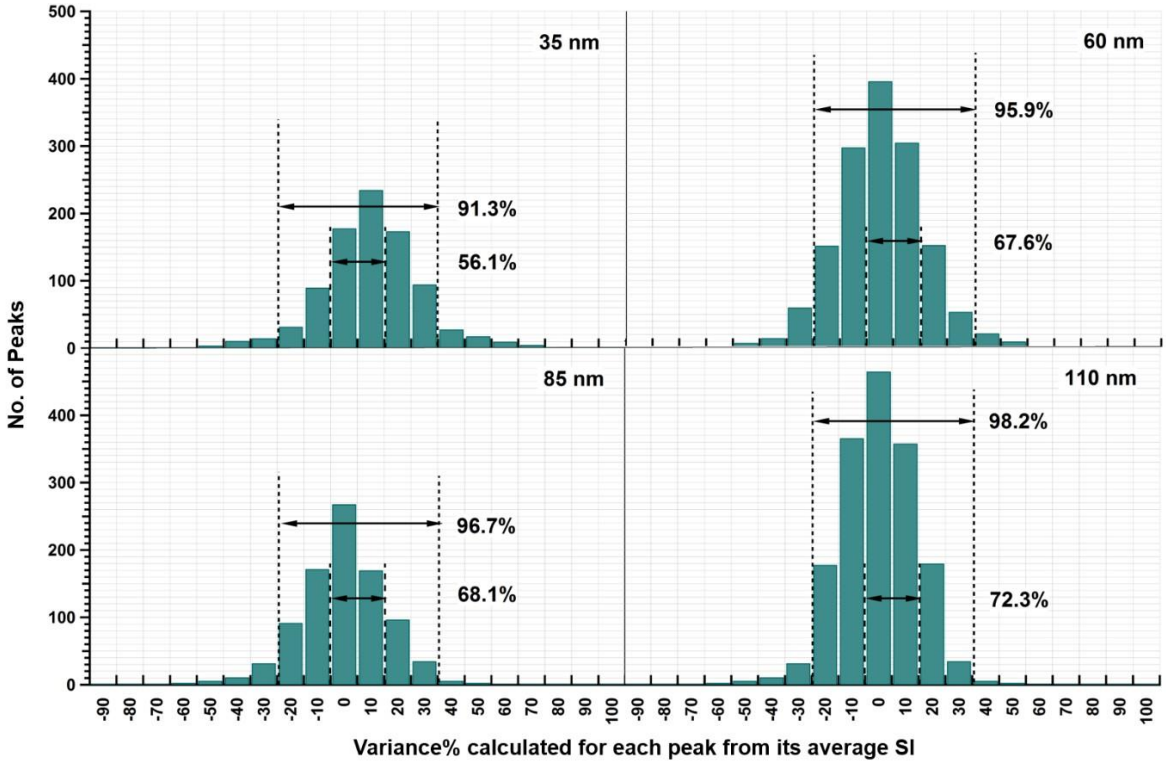

Table 3.2. Summary of Off-Line Composition Measurements with HR-MS.

Sample	Ion	Unique Molecular	Avg. SI	Avg. RSD%	Avg. O/C
Poly-a	(+)	1203 ± 108	5.8E+06	6.8	0.28 ± 0.01
	(-)	1035 ± 89	7.9E+06	3.3	0.41 ± 0.004
35 nm[a]	(+)	897 ± 82	3.6E+06	5.1	0.36 ± 0.01
	(-)	459 ± 78	3.1E+06	9.8	0.51 ± 0.01
60 nm[a]	(+)	1179 ± 111	8.3E+06	6.0	0.32 ± 0.02
	(-)	405 ± 52	8.5E+06	13	0.48 ± 0.01
85 nm[a]	(+)	1097 ± 152	8.9E+06	7.8	0.31 ± 0.02
	(-)	420 ± 38	5.0E+06	13	0.46 ± 0.01
110 nm[a]	(+)	1644 ± 191	5.2E+06	7.1	0.23 ± 0.01
	(-)	587 ± 54	6.0E+06	9.8	0.44 ± 0.01
Poly-b	(+)	1115 ± 156	3.4E+06	7.5	0.31 ± 0.02
	(-)	847 ± 45	6.5E+06	4.2	0.42 ± 0.01
Poly-c	(+)	1047 ± 103	2.5E+06	11	0.34 ± 0.01
	(-)	743 ± 55	8.3E+06	5.6	0.47 ± 0.02
Poly-d	(+)	1029 ± 83	5.9E+06	3.8	0.31 ± 0.02
	(-)	896 ± 77	7.8E+06	10	0.51 ± 0.01
35 nm[b]	(+)	430 ± 33	1.9E+06	6.7	0.37 ± 0.01
	(-)	226 ± 28	8.6E+06	2.7	0.47 ± 0.01
85 nm[b]	(+)	914 ± 86	7.1E+05	5.4	0.35 ± 0.01
	(-)	552 ± 46	3.9E+05	2.8	0.45 ± 0.01
110 nm[b]	(+)	873 ± 51	6.3E+05	2.6	0.36 ± 0.01
	(-)	439 ± 25	4.3E+05	7.7	0.45 ± 0.01

[a]Monodisperse samples were classified from polydisperse SOA sample (a).
[b]Monodisperse samples were classified from polydisperse SOA sample (d).

As a complimentary technique, online single particle analysis was performed with a modified Nano Aerosol Mass Spectrometer (NAMS) of which the configuration is shown in section C of Figure 3.1. Due to the almost real-time analysis, the background contaminations and unexpected reactions during the sample preparation and storage for offline analysis can be eliminated. The previously reported NAMS configuration for analysis of 10-30 nm diameter particles[38–40] was modified to enable analysis of particles between 40 and 110 nm in diameter. Particles entered the mass spectrometer through an aerodynamic lens assembly that focused particles into a tight beam in the ion source region. A focused, high energy pulsed laser beam (532 nm, 5 Hz, 230 mJ/pulse focused to an effective spot size of about 0.1 mm dia.) intercepted the particle beam. When a particle was in the beam path when the laser fired, a plasma was formed that quantitatively disintegrated the particle into multiply charged atomic ions, whose relative signal intensities gave the elemental composition of the particle[41,42]. A simple deconvolution model was conducted for the isobaric ions signals (e.g. O^{4+} and $C^{3+)}$ based on the assumption that the charge state distribution of a given element is independent of the chemical form of that element in the particles[39,42]. Similar to the Aerosol Mass Spectrometer (AMS), NAMS was able to perform a bulk measurement of nanoparticles and provide elemental information that could be compared with those obtained by the off-line analysis. Aerosol mass spectra were obtained by averaging ~200 individual particle spectra, and the process of obtaining an average mass spectrum was repeated three times over the course of each experiment, which provided confirmation that particle composition did not change during an experiment. Figure 3.7 gives an example mass spectrum of size selected 60 nm SOA

particles. Table 3.3 summarizes the elemental composition data from the various experiments.

Figure 3.7. Average NAMS spectrum of 150 single particle spectra from polydisperse SOA sample (a). Figure (b) was adapted from [Tu, P.; Johnston, M. V. *Atmos. Chem. Phys.* **2017**, 17, 7593-7603]. © Peijun Tu and Murray V. Johnston 2017.

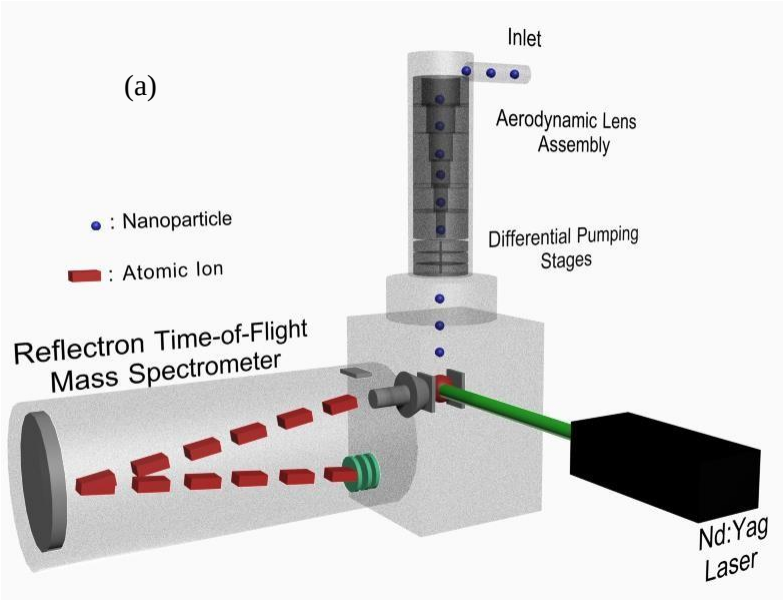

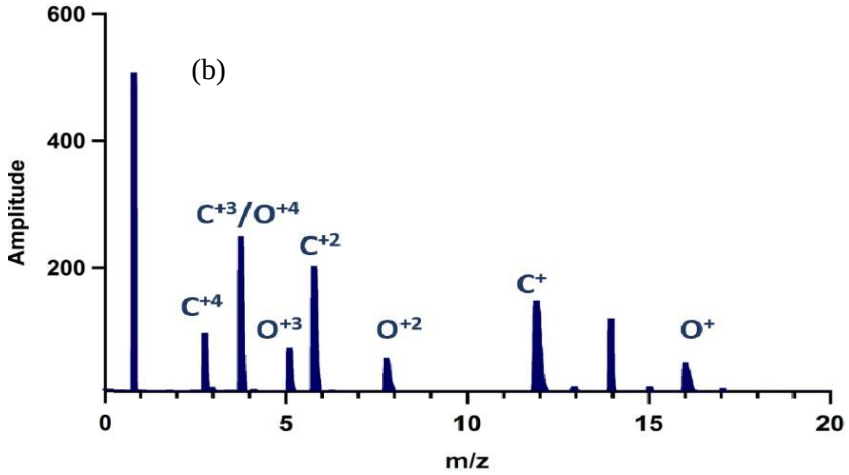

Table 3.3. Summary of On-Line Measurements with NAMS.

Sample Type	Poly/Mono	Avg. O/C	Std. dev$_{O/C}$
Poly SOA a	poly	0.35	9.8E-03
Poly SOA b	poly	0.40	1.5E-02
Poly SOA (atomizer)	poly	0.45	8.6E-03
60 nm	Mono	0.42	1.4E-02
85 nm	Mono	0.35	1.3E-02
110 nm	Mono	0.33	5.5E-03
85 nm (atomizer)	Mono	0.45	1.9E-03
110nm (atomizer)	Mono	0.46	3.6E-03

3.5 Results and Discussions

Elemental Composition of Size-Selected SOA. NAMS measurements provided the opportunity to determine the bulk elemental composition of size-selected SOA, specifically the oxygen-to-carbon (O/C) ratio. O/C ratios as a function of particle size are summarized in Table 3.3 and shown in Figure 3.8. The trend of decreasing O/C ratio with increasing particle size is consistent with the expectation that lower volatility (and more highly functionalized) molecules are preferentially found in small particles where the high surface-to-volume ratio favours condensation of non-volatile molecules over partitioning of semi-volatile molecules, while higher volatility (and less functionalized) molecules are preferentially found in large particles where the lower surface-to-volume ratio favours partitioning of semi-volatile molecules to a greater degree. This same general trend was found for molecular analysis, as shown in Figure 3.8a by the mass and intensity weighted O/C ratios[32]

averaged over all assigned molecular formulas. For both positive and negative molecular ions, the average O/C ratio was also found to decrease with increasing particle size. The average O/C ratios obtained from negative ions were much greater than those from positive ions, which reflects the bias of negative ion detection toward molecules containing acid groups whereas positive ion detection is biased toward detection of molecules containing carbonyls only[32]. The O/C ratios obtained from NAMS lie between the positive and negative mode O/C ratios obtained from HR-MS, which is reasonable since the NAMS measurements represent all molecular species in the sample.

Figure 3.8. Average O/C ratio vs. particle diameter for SOA (a) generated from the flow tube reactor and (b) re-aerosolized from the atomizer. Dashed lines in the plots give the O/C ratios of the corresponding polydisperse SOA samples. Error bars represent one standard deviation for the 5 replicate experiments. Adapted from [Tu, P.; Johnston, M. V. *Atmos. Chem. Phys.* **2017**, 17, 7593-7603]. © Peijun Tu and Murray V. Johnston 2017.

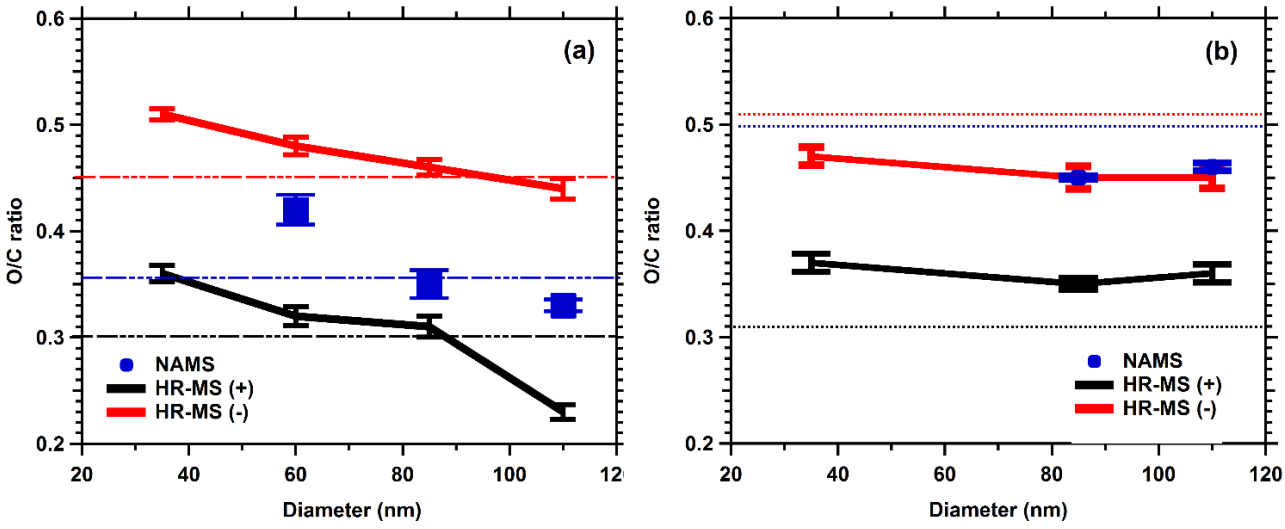

The similarity of the NAMS and HR-MS data in Figure 3.8 suggests that these size dependencies are not artefacts of the respective measurement methods. To provide further confirmation, the control aerosol was analysed by the same procedure. The results are shown in Figure 3.8b. As expected, no particle size dependence is observed in either the NAMS or HR-MS data. Furthermore, the (particle size independent) O/C ratio for negative ion mode of the control aerosol in Figure 3.8b matches the average O/C ratio of the polydisperse sample (shown as a line in Figure 3.8a). This similarity is expected since the negative ion mode preferentially detects highly oxidized molecules that have low volatility and are likely to be retained through the extraction and atomization steps used to generate the control aerosol. The O/C ratio for positive ion mode of the control aerosol in Figure 3.8b is somewhat higher than the average O/C ratio for polydisperse aerosol in Figure 3.8a. This difference suggests that lower O/C ratio (and presumably higher volatility) molecules are lost during the extraction and atomization process. Loss of these molecules is consistent with the NAMS O/C ratio for the control aerosol in Figure in 3.8b, which is higher than the NAMS O/C ratio for polydisperse aerosol in Figure 3.8a and matches the O/C ratio for the negative ion mode.

Molecular Composition of Size-Selected SOA. To provide context for the particle size-dependent changes in molecular composition discussed below, it is helpful to consider the gas-phase products of β-pinene ozonolysis and their relevance to chemical processes that drive particle growth. Gas-phase products were not measured in this study, but have been the subject of several previous investigations. Aerosol yields for β-pinene ozonolysis under conditions similar to the experiments performed here have been reported to be on the order of 30%, with products spanning a wide range of volatilities[43]. First and foremost with regard to particle formation in an unseeded experiment is the production of ELVOCs, which for monoterpene

ozonolysis[22] include molecular formulas spanning monomers (for the purpose of this study defined as molecules having fewer than 9 carbon atoms since β-pinene ozonolysis results in the loss of a carbon atom) and dimers (defined here as molecules having between 10 and 18 carbon atoms). Monomer ELVOCs necessarily are highly oxidized since this is needed to achieve very low volatility, whereas dimers can be somewhat less oxidized owing to their larger molecular size. ELVOCs corresponding to higher order oligomers (defined here as molecules having greater than 18 carbon atoms) are exceedingly rare, which is not surprising since the probability of gas phase reaction decreases quickly with increasing number of precursor molecules. ELVOCs are inefficiently produced from β-pinene ozonolysis owing to its exocyclic double bond, with an estimated yield less than 0.1%[22]. Most products of β-pinene ozonolysis are volatile or semi-volatile monomers partition between the gas and particle phases[44].

Molecular level changes in particle composition are summarized in Figure 3.9 which compare the mass spectra and corresponding molecular products, respectively, for both positive and negative ion mass analysis of size-selected SOA at 35 nm and 110 nm. These changes are interpreted on the basis of monomers (which encompass both ELVOCs that condense and semi-volatile products that partition), dimers (which encompass both ELVOCs that condense and products of accretion chemistry that are produced directly in the particle phase), and higher order oligomers (produced almost exclusively by accretion chemistry in the particle phase).

Figure 3.9 Positive (+) and negative (-) ion mass spectra of 35 nm (red) and 110 nm (blue) monodisperse SOA samples averaged over the five replicate experiments. Adapted from [Tu, P.; Johnston, M. V. *Atmos. Chem. Phys.* **2017**, 17, 7593-7603]. © Peijun Tu and Murray V. Johnston 2017.

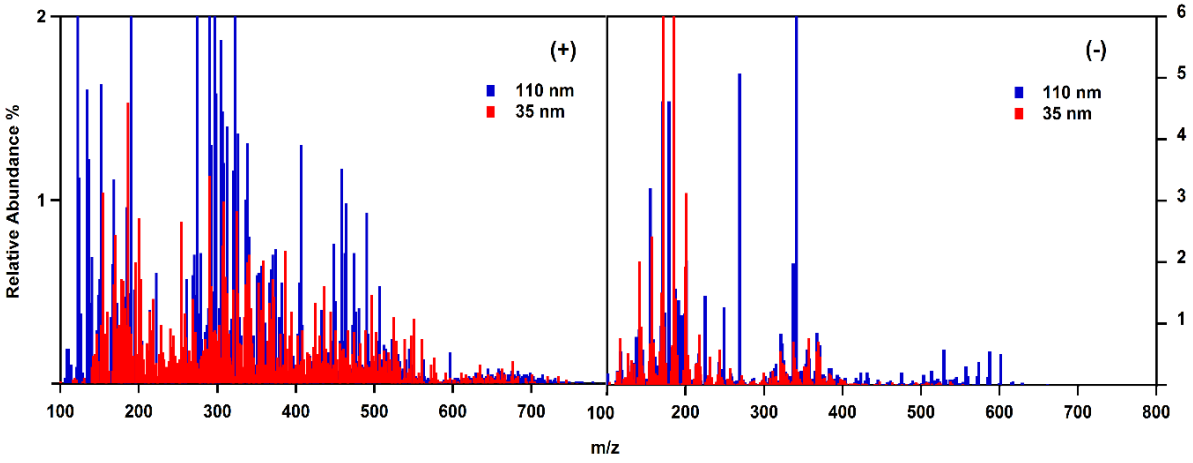

Figure 3.10 shows plots of average carbon oxidation state (OSc) vs. number of carbon atoms for all assigned molecular formulas, colour coded to indicate formulas that are unique to 35 nm particles, unique to 110 particles, and common to both particle sizes. Two general trends are observed in Figure 3.10 for both ion polarities. First, the unique formulas in 35 nm particles tend to have higher OSc than the common formulas, while the unique formulas in 110 nm particles tend to have lower OSc than the common formulas. Second, 110 nm particles tend to have a greater number of unique oligomer formulas with greater than 18 carbon atoms than 35 nm particles, and this disparity increases with increasing number of carbon atoms. Both differences are consistent with the elemental composition changes in Figure 3.10. Higher OSc formulas tend to have higher O/C elemental ratios, which favor higher O/C in smaller

particles. Formulas of higher order oligomers tend to have lower OSc than monomers and dimers, which favour lower O/C in larger particles.

Figure 3.10. Carbon oxidation state (OSc) vs. number of carbon atoms for assigned molecular formulas from the positive (+) and negative (-) ion mass spectra of 35 and 110 nm monodisperse SOA samples. Unique formulas in the 35 nm samples are shown in red. Unique formulas in the 110 nm samples are shown in blue. Formulas common to both samples are shown in black. Adapted from [Tu, P.; Johnston, M. V. *Atmos. Chem. Phys.* **2017**, 17, 7593-7603]. © Peijun Tu and Murray V. Johnston 2017.

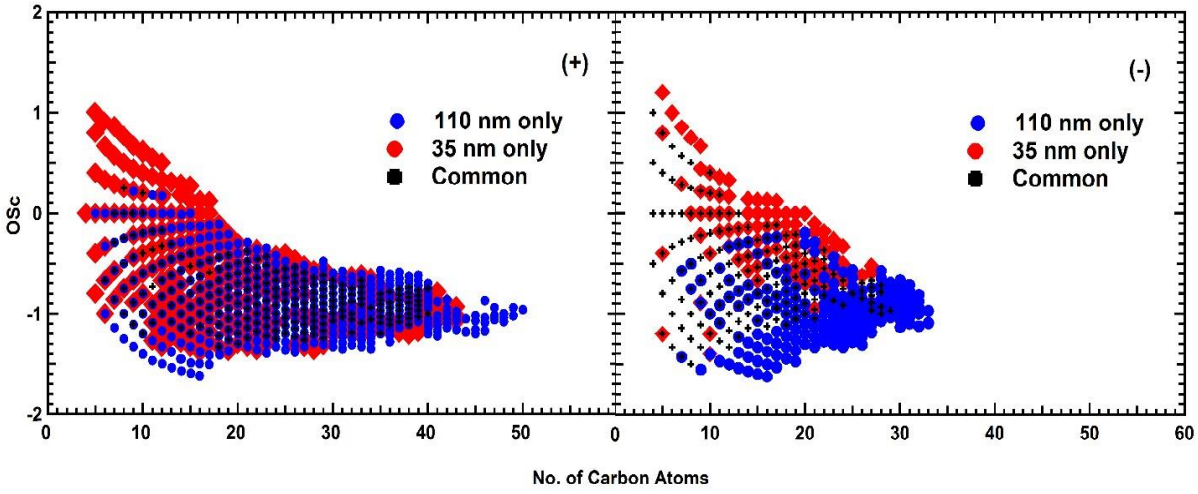

Further insight can be gained from the ion signal intensities of each assigned molecular formula. Figure 3.11 shows the fraction of the total signal intensity due to higher order oligomers (defined here as formulas with greater than 18 carbon atoms) as a function of particle size. These oligomers are produced almost exclusively by accretion chemistry in the particle phase[28,45]. In Figure 3.11, both ion polarities show an approximate linear increase of oligomer intensity with increasing particle diameter. A linear increase is expected for a volume-limited process such as accretion chemistry

relative to a surface-limited process such as condensation. Here, "volume-limited" means that the particle volume available for reaction increases linearly with increasing particle volume i.e. the cube of the particle diameter. It does not preclude the possibility that processes such as phase separation or hindered diffusion within the particle causes a portion of the total particle volume to be inaccessible to this chemistry, though we note that phase separation is unlikely in such small particles [46]. Oligomerization has been considered for many years to be a significant contributor to SOA formation [16,17,19,47,48], and Figure 3.11 shows through chemical measurement that this contribution strongly depends on particle size.

Figure 3.11. Percentage of total signal intensity (SI %) in positive (+) and negative (-) ion mass spectra from higher order oligomers (molecular formulas having greater than 18 carbon atoms) vs. particle diameter. Error bars represent one standard deviation for the five replicate experiments. Adapted from [Tu, P.; Johnston, M. V. *Atmos. Chem. Phys.* **2017**, 17, 7593-7603]. © Peijun Tu and Murray V. Johnston 2017.

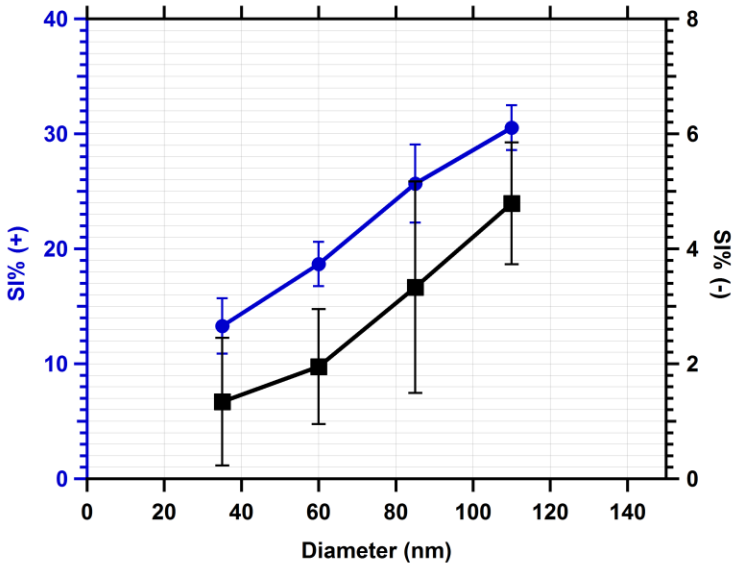

The particle size dependence of oligomers reported here for β-pinene SOA is opposite that reported previously in the ultrafine size range for two other precursors, α-cedrene and trans-3-hexene [25,27]. This difference is related most likely to the origin of the species involved (gas phase vs. particle phase). The molecular structure of α-cedrene is much more conducive to the production of ELVOCs in the gas phase than β-pinene, making condensational growth more likely. In contrast, the analysis of β-pinene SOA in Figure 3.11 focuses on accretion chemistry and does not include "dimer" (C_{10-17}) products of β- pinene ozonolysis, which may contribute to growth by a combination of condensation from the gas phase and accretion chemistry in the particle phase. The dimer products of β-pinene ozonolysis in this work show a roughly constant relative signal intensity with increasing particle size, which likely reflects the multiple sources of these species. High molecular weight oligomers observed in the trans-3-hexene ozonolysis experiment were suggested to be formed in the gas phase by reaction of a peroxy radical with the stable Criegee intermediate, which is unlikely for either α-cedrene or β-pinene[27].

Figure 3.12 shows the intensity-weighted, average OSc of all monomer formulas (carbon number < 10) as a function of particle size. The average OSc for species detected in negative ion mode is essentially independent of particle diameter, suggesting very little change in composition among these species. This dependence is suggested by the OSc (-) vs. carbon number plot in Figure 3.10, where most monomer species are found to be common to both particle sizes. The lack of a composition dependence probably arises from the fact that negative ion mode is biased toward detection of more highly oxidized species, as reported in the past by our group and others[30,32,49]. These highly oxygenated/oxidized species are suggested to have very low volatilities so their rates of condensation relative to each other arenot expected to be size dependent - all of them will condense with similar probability when striking the

particle surface.

Figure 3.12. Average OSc vs. particle diameter for monomer species (less than 10 carbon atoms in the assigned formula) detected in positive (+) and negative (-) ion mass spectra. Error bars represent one standard deviation for 5 replicate experiments. Adapted from [Tu, P.; Johnston, M. V. *Atmos. Chem. Phys.* **2017**, 17, 7593-7603]. © Peijun Tu and Murray V. Johnston 2017.

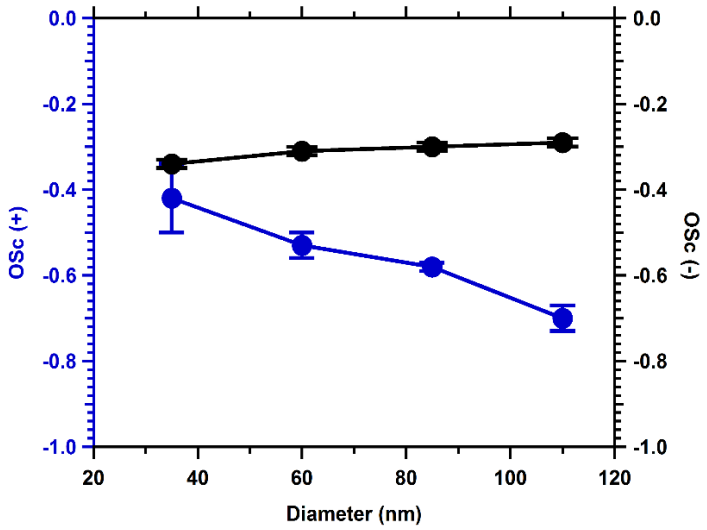

More interesting is the plot in Figure 3.12 for positive ion mode, which shows a substantial decrease of monomer OSc with increasing particle diameter. This dependence is suggested by the OSc (+) vs. carbon number plot in Figure 3.10 for positive ion mode, where fewer molecular formulas are common between the two particle sizes and the unique formulas in 35 nm particles have higher OSc than the unique formulas in 110 nm particles. While it is tempting to interpret these data as enhanced partitioning of higher volatility species into larger particles, this explanation is problematic. The particle sizes investigated in this work are too large for the Kelvin

effect to influence molecular volatility. To the extent that partitioning reaches equilibrium, there should be no difference in the particle phase concentrations of partitioned species since the equilibrium state does not depend explicitly on particle size. Partitioning does depend on the relative volumes of the gas and particle phases for the entire system, but these volumes are fixed in the current experiments since the selection of different particle sizes was performed at the same time point in the SOA formation process.

Particle phase reactions such as accretion chemistry have the ability to increase SOA mass by transforming semi-volatile monomers into non-volatile oligomers. Molecular partitioning from the gas phase to the particle phase provides a continuous source of reactant molecules to feed the reaction as it proceeds. The decreasing OSc(+) of monomers with increasing particle size suggests that oligomerization is partially reversible. Larger particles have greater oligomer content relative to the total particle mass (Figure 3.11), so they also have greater potential to yield decomposition products. Oligomer decomposition could be an artifact of the sample preparation and analysis steps after particle collection, or it could be an intrinsic aspect of accretion chemistry that occurs prior to particle collection and analysis. If reversibility is an intrinsic aspect of accretion chemistry, then the higher amounts of low OSc monomers in large particles suggests that diffusion within the particle phase is hindered [50–53] and/or phase separation has occurred [54–57], effectively trapping the released monomers within the particle making them unable to re-equilibrate with the gas phase. Reversibility of the oligomerization process provides a reasonable explanation why β-pinene SOA yields are so strongly dependent on temperature and relative humidity [58].

Elemental and Molecular Composition of Polydisperse SOA. Additional experiments were performed to study the change in composition of polydisperse SOA samples with volume to surface area ratios between 3.8 and 12.5 nm, and compare the results to those discussed above for size-selected particles having a similar range of volume to surface area ratios. For the aerosol generation method used in this work, the polydisperse aerosol mode diameters and volume to surface area ratios increased monotonically with increasing mass loading (Table 3.1). Three mass loadings were investigated: 5 $\mu g/m^3$, 240 $\mu g/m^3$ and 2300 $\mu g/m^3$ (which was also the mass loading used to study the particle size dependencies above). The results are included in Tables 3.1-3.3. Mass spectra and plots of OSc vs. carbon number are given in Figure 3.13 and Figure 3.14. The mass loading trends mirror those of particle size. For both NAMS and HR-MS, the average O/C ratio decreases with increasing mass loading. Unique molecular formulas in the low mass loading spectra generally have high OSc values, while unique molecular formulas in the high mass loading spectra generally have low OSc values. Oligomer ions increase in relative signal intensity with increasing mass loading. Because of the particle volume dependence of accretion reactions, high mass loadings (and their correspondingly high volume to surface area ratios) also have a higher percentage of oligomer products. A similar volume to surface area ratio dependence was reported for accretion reaction products associated with polydisperse secondary aerosol produced from OH oxidation of cyclic siloxanes by another member of my research group [59].

A decrease in average O/C ratio with increasing SOA mass loading has been reported previously for elemental analysis of laboratory SOA produced from related biogenic precursors [60,61]. The results presented here utilizing both elemental and molecular composition measurements provide a mechanistic explanation for this general observation: accretion chemistry increases in importance relative to

condensation and partitioning as the particle size increase

Figure 3.13. Positive (+) and negative (-) ion mass spectra of high (red; polydisperse sample a) and low (red; polydisperse sample c) mass loading SOA averaged over 5 replicate measurements. Adapted from [Tu, P.; Johnston, M. V. *Atmos. Chem. Phys.* **2017**, 17, 7593-7603]. © Peijun Tu and Murray V. Johnston 2017.

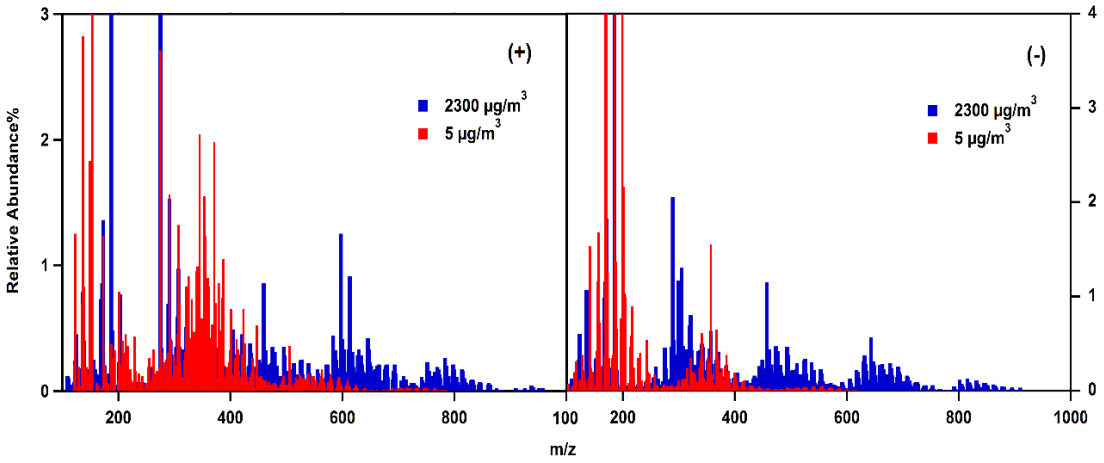

Figure 3.14. Molecular compositions of polydisperse SOA a (high mass loading of 2300 μg/m^3) and c (low mass loading of 5 μg/m^3) in positive (+) and negative (-) ion mode averaged over five replicate measurements. Adapted from [Tu, P.; Johnston, M. V. *Atmos. Chem. Phys.* **2017**, 17, 7593-7603]. © Peijun Tu and Murray V. Johnston 2017.

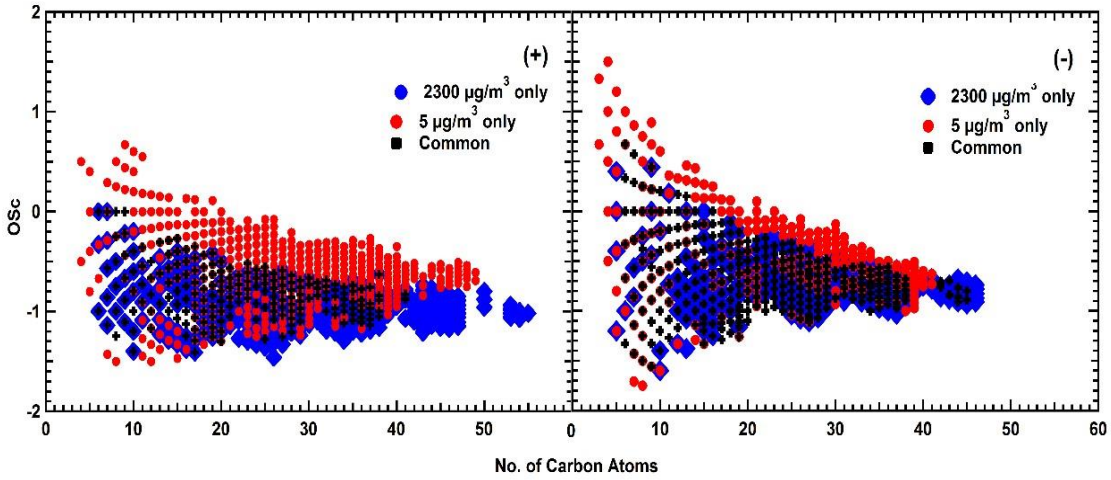

3.6 Conclusions

In this chapter, elemental and molecular analysis of size-selected biogenic SOA particles between 35 nm and 110 nm diameter is reported. These results provide clear evidence for oligomer formation via accretion chemistry in the particle phase and show that the impact of accretion chemistry (a particle volume-limited process) on molecular composition increases with increasing particle size. As depicted in Figure 3.15, since accretion reactions provide the opportunity to transform semi-volatile monomers into non- volatile oligomers, they represent a chemical pathway to increase the aerosol yield and also potentially to increase the growth rate of ultrafine particles. The particles of interest, 30-110 nm in diameter, are size-selected from a polydisperse aerosol and are large enough that the radius-of-curvature effect of molecular volatility is negligible. Therefore, size-dependent changes in composition

reflect the relative importance of surface area vs. volume limited processes. In addition, the particles are small enough that phase separation within the particles is unlikely to occur[46].

Since the ELVOC yield from α-pinene ozonolysis is much smaller than that from other biogenic SOA precursors, it is possible that accretion chemistry plays a larger role in formation of α-pinene SOA than in formation of SOA from other precursors where the likelihood of ELVOC condensation is greater. As noted in a previous study, oligomer formation in α-pinene SOA is strongly dependent on reaction conditions[43]. The impact of accretion chemistry for may be greater for the laboratory SOA studied here than ambient SOA owing to different reaction conditions. In this regard, elemental analysis shows that ambient SOA is generally more highly oxidized than laboratory SOA[62]. Also, molecular analysis of ambient samples show that oligomer ions tend to have very low signal intensities[29], though higher oligomer signal intensities appear to be strongly correlated with CCN activity[63]. The results we present here illustrate the potential impact that particle phase chemistry can have on SOA formation and the particle size range where this chemistry becomes important.

Figure 3.15. Condensation and partition during the growth of SOA particles.

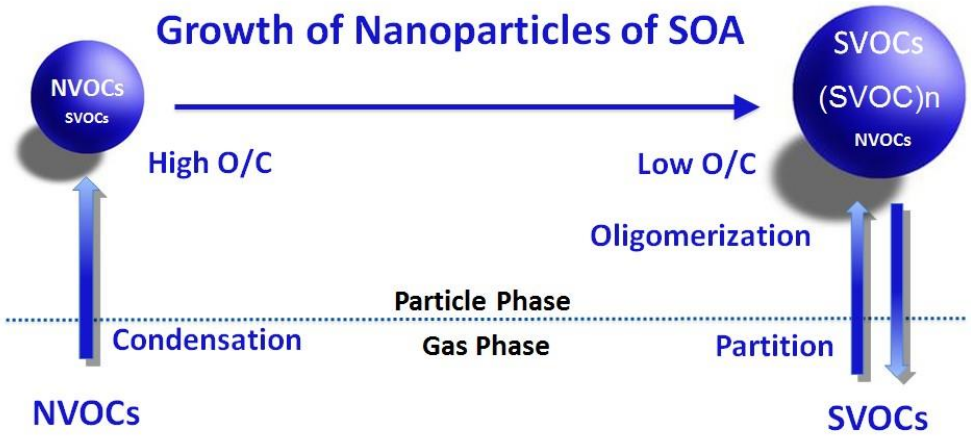

REFERENCES

(1) Zhang, R.; Khalizov, A.; Wang, L.; Hu, M.; Xu, W. *Chem. Rev.* **2012**, *112* (3), 1957–2011.

(2) Bzdek, B. R.; Pennington, M. R.; Johnston, M. V. *Journal of Aerosol Science*. **2012**, 109–120.

(3) Myhre, G.; Shindell, D.; Bréon, F.-M.; Collins, W.; Fuglestvedt, J.; Huang, J.; Koch, D.; Lamarque, J.-F.; Lee, D.; Mendoza, B.; Nakajima, T.; Robock, A.; Stephens, G.; Takemura, T.; Zhang, H. *Clim. Chang. Phys. Sci. Basis. Contrib. Work. Gr. I to Fifth Assess. Rep. Intergov. Panel Clim. Chang.* **2013**, 659–740.

(4) Carslaw, K. S.; Lee, L. a; Reddington, C. L.; Mann, G. W.; Pringle, K. J. *Faraday Discuss.* **2013**, *165*, 495–512.

(5) Hallquist, M.; Wenger, J. C.; Baltensperger, U.; Rudich, Y.; Simpson, D.; Claeys, M.; Dommen, J.; Donahue, N. M.; George, C.; Goldstein, A. H.; Hamilton, J. F. *Atmos. Chem. Phys. Atmos. Chem. Phys.* **2009**, *9*, 5155–5236.

(6) Jimenez, J. L.; Canagaratna, M. R.; Donahue, N. M.; Prevot, a. S. H.; Zhang, Q.; Kroll, J. H.; DeCarlo, P. F.; Allan, J. D.; Coe, H.; Ng, N. L.; Aiken, a. C.; Docherty, K. S.; Ulbrich, I. M.; Grieshop, A. P.; Robinson, a. L.; Duplissy, J.; Smith, J. D.; Wilson, K. R.; Lanz, V. a.; Hueglin, C.; Sun, Y. L.; Tian, J.; Laaksonen, A.; Raatikainen, T.; Rautiainen, J.; Vaattovaara, P.; Ehn, M.; Kulmala, M.; Tomlinson, J. M.; Collins, D. R.; Cubison, M. J.; Dunlea, J.; Huffman, J. A.; Onasch, T. B.; Alfarra, M. R.; Williams, P. I.; Bower, K.; Kondo, Y.; Schneider, J.; Drewnick, F.; Borrmann, S.; Weimer, S.; Demerjian, K.; Salcedo, D.; Cottrell, L.; Griffin, R.; Takami, a.; Miyoshi, T.; Hatakeyama, S.; Shimono, A.; Sun, J. Y.; Zhang, Y. M.; Dzepina, K.; Kimmel, J. R.; Sueper, D.; Jayne, J. T.; Herndon, S. C.; Trimborn, a. M.; Williams, L. R.; Wood, E. C.; Middlebrook, A. M.; Kolb, C. E.; Baltensperger, U.; Worsnop, D. R. *Science.* **2009**, *326* (5959), 1525–1529.

(7) Kanakidou, M.; Seinfeld, J. H.; Pandis, S. N.; Barnes, I.; Dentener, F. J.; Facchini, M.

C.; Van Dingenen, R.; Ervens, B.; Nenes, A.; Nielsen, C. J.; Swietlicki, E.; Putaud, J. P.; Balkanski, Y.; Fuzzi, S.; Horth, J.; Moortgat, G. K.; Winterhalter, R.; Myhre, C. E. L.; Tsigaridis, K.; Vignati, E.; Stephanou, E. G.; Wilson, J. *Atmos. Chem. Phys.* **2005**, *5*, 1053–1123.

(8) Ng, N. L.; Canagaratna, M. R.; Zhang, Q.; Jimenez, J. L.; Tian, J.; Ulbrich, I. M.; Kroll, J. H.; Docherty, K. S.; Chhabra, P. S.; Bahreini, R.; Murphy, S. M.; Seinfeld, J. H.; Hildebrandt, L.; Donahue, N. M.; Decarlo, P. F.; Lanz, V. A.; Prévôt, A. S. H.; Dinar, E.; Rudich, Y.; Worsnop, D. R. *Atmos. Chem. Phys.* **2010**, *10* (10), 4625–4641.

(9) Chan, A. W. H.; Isaacman, G.; Wilson, K. R.; Worton, D. R.; Ruehl, C. R.; Nah, T.; Gentner, D. R.; Dallmann, T. R.; Kirchstetter, T. W.; Harley, R. A.; Gilman, J. B.; Kuster, W. C.; De Gouw, J. A.; Offenberg, J. H.; Kleindienst, T. E.; Lin, Y. H.; Rubitschun, C. L.; Surratt, J. D.; Hayes, P. L.; Jimenez, J. L.; Goldstein, A. H. *J. Geophys. Res. Atmos.* **2013**, *118* (12), 6783–6796.

(10) Goldstein, A. H.; Galbally, I. E. *Environ. Sci. Technol.* **2007**, *41* (5), 1514–1521.

(11) Mutzel, A.; Poulain, L.; Berndt, T.; Iinuma, Y.; Rodigast, M.; Böge, O.; Richters, S.; Spindler, G.; Sipilä, M.; Jokinen, T.; Kulmala, M.; Herrmann, H. *Environ. Sci. Technol.* **2015**, *49* (13), 7754–7761.

(12) Putman, A. L.; Offenberg, J. H.; Fisseha, R.; Kundu, S.; Rahn, T. A.; Mazzoleni, L. R. *Atmos. Environ.* **2012**, *46*, 164–172.

(13) Daumit, K. E.; Kessler, S. H.; Kroll, J. H. *Faraday Discuss.* **2013**, *165* (0), 181–202.

(14) Hall IV, W. A.; Johnston, M. V. *J. Am. Soc. Mass Spectrom.* **2012**, *23* (6), 1097–1108.

(15) Perraud, V.; Bruns, E. a; Ezell, M. J.; Johnson, S. N.; Yu, Y.; Alexander, M. L.; Zelenyuk, A.; Imre, D.; Chang, W. L.; Dabdub, D.; Pankow, J. F.; Finlayson-Pitts, B. J. *Proc. Natl. Acad. Sci. U. S. A.* **2012**, *109* (8), 2836–2841.

(16) Kalberer, M.; Paulsen, D.; Sax, M.; Steinbacher, M.; Dommen, J.; Prevot, a S. H.; Fisseha, R.; Weingartner, E.; Frankevich, V.; Zenobi, R.; Baltensperger, U. *Science.* **2004**, *303* (5664), 1659–1662.

(17) Tolocka, M. P.; Jang, M.; Ginter, J. M.; Cox, F. J.; Kamens, R. M.; Johnston, M. V. *Environ. Sci. Technol.* **2004**, *38* (5), 1428–1434.

(18) Gao, S.; Ng, N. L.; Keywood, M.; Varutbangkul, V.; Bahreini, R.; Nenes, A.; He, J.; Yoo, K. Y.; Beauchamp, J. L.; Hodyss, R. P.; Flagan, R. C.; Seinfeld, J. H. *Environ. Sci. Technol.* **2004**, *38* (24), 6582–6589.

(19) Hall, W. A.; Johnston, M. V. *Aerosol Sci. Technol.* **2011**, *45* (1), 37–45.

(20) Pankow, J. F. *Atmos. Environ.* **1994**, *28* (2), 185–188.

(21) Bianchi, F. et al. *Science.* **2016**, *352* (6289), 1109–1112.

(22) Ehn, M.; Thornton, J. A.; Kleist, E.; Sipilä, M.; Junninen, H.; Pullinen, I.; Springer, M.; Rubach, F.; Tillmann, R.; Lee, B.; Lopez-Hilfiker, F.; Andres, S.; Acir, I.-H.; Rissanen, M.; Jokinen, T.; Schobesberger, S.; Kangasluoma, J.; Kontkanen, J.; Nieminen, T.; Kurtén, T.; Nielsen, L. B.; Jørgensen, S.; Kjaergaard, H. G.; Canagaratna, M.; Maso, M. D.; Berndt, T.; Petäjä, T.; Wahner, A.; Kerminen, V.-M.; Kulmala, M.; Worsnop, D. R.; Wildt, J.; Mentel, T. F. *Nature* **2014**, *506* (7489), 476–479.

(23) Thomson, W. *Proc. R. Soc. Edinburgh* **1872**, *7*, 63–68.

(24) Winkler, P. M.; Ortega, J.; Karl, T.; Cappellin, L.; Friedli, H. R.; Barsanti, K.; McMurry, P. H.; Smith, J. N. *Geophys. Res. Lett.* **2012**, *39* (20), 1–6.

(25) Zhao, J.; Ortega, J.; Chen, M.; McMurry, P. H.; Smith, J. N. *Atmos. Chem. Phys.* **2013**, *13* (15), 7631–7644.

(26) Kidd, C.; Perraud, V.; Finlayson-Pitts, B. J. *Phys. Chem. Chem. Phys.* **2014**, *16*, 22706–22716.

(27) Zhao, Y.; Wingen, L. M.; Perraud, V.; Greaves, J.; Finlayson-Pitts, B. J. *Phys. Chem. Chem. Phys.* **2015**, *17* (19), 12500–12514.

(28) Barsanti, K. C.; Pankow, J. F. *Atmos. Environ.* **2005**, *39* (35), 6597–6607.

(29) Mentel, T. F.; Springer, M.; Ehn, M.; Kleist, E.; Pullinen, I.; Kurtén, T.; Rissanen, M.; Wahner, A.; Wildt, J. *Atmos. Chem. Phys.* **2015**, *15* (12), 6745–6765.

(30) Tu, P.; Hall, W. A.; Johnston, M. V. *Anal. Chem.* **2016**, *88* (8), 4495–4501.

(31) Shiraiwa, M.; Yee, L. D.; Schilling, K. A.; Loza, C. L.; Craven, J. S.; Zuend, A.; Ziemann, P. J.; Seinfeld, J. H. *Proc. Natl. Acad. Sci. U. S. A.* **2013**, *110* (29), 11746–11750.

(32) Hall, W. A.; Pennington, M. R.; Johnston, M. V. *Environ. Sci. Technol.* **2013**, *47* (5), 2230–2237.

(33) Stabile, L.; Trassierra, C. V.; Dell'Agli, G.; Buonanno, G. *Aerosol Air Qual. Res.* **2013**, *13* (6), 1667–1677.

(34) Park, J. Y.; McMurry, P. H.; Park, K. *Aerosol Sci. Technol.* **2012**, *46* (3), 354–360.

(35) Hering, S. V.; Stolzenburg, M. R. *Aerosol Sci. Technol.* **2005**, *39*, 428–436.

(36) Herzsprung, P.; Hertkorn, N.; von Tümpling, W.; Harir, M.; Friese, K.; Schmitt-Kopplin, P. *Anal. Bioanal. Chem.* **2014**, *406* (30), 7977–7987.

(37) Phungsai, P.; Kurisu, F.; Kasuga, I.; Furumai, H. *Water Res.* **2016**.

(38) Ross Pennington, M.; Johnston, M. V. *Int. J. Mass Spectrom.* **2012**, *311*, 64–71.

(39) Wang, S.; Zordan, C. A.; Johnston, M. V. *Anal. Chem.* **2006**, *78* (6), 1750–1754.

(40) Wang, S.; Johnston, M. V. *Int. J. Mass Spectrom.* **2006**, *258* (1–3), 50–57.

(41) Klems, J. P.; Johnston, M. V. *Anal. Bioanal. Chem.* **2013**, *405* (22), 6995–7003.

(42) Zordan, C. A.; Pennington, M. R.; Johnston, M. V. *Anal. Chem.* **2010**, *82* (19), 8034–8038.

(43) Von Hessberg, C.; Von Hessberg, P.; Pöschl, U.; Bilde, M.; Nielsen, O. J.; Moortgat, G. K. *Atmos. Chem. Phys. Atmos. Chem. Phys.* **2009**, *9*, 3583–3599.

(44) Jaoui, M.; Kamens, R. M. *J. Atmos. Chem.* **2003**, *43*, 101–141.

(45) Barsanti, K. C.; Pankow, J. F. *Atmos. Environ.* **2006**, *40* (34), 6676–6686.

(46) Veghte, D. P.; Altaf, M. B.; Freedman, M. A. *J. Am. Chem. Soc.* **2013**, *135* (43), 16046–16049.

(47) Kroll, J. H.; Seinfeld, J. H. *Atmos. Environ.* **2008**, *42* (16), 3593–3624.

(48) Trump, E. R.; Donahue, N. M. *Atmos. Chem. Phys.* **2014**, *14*, 3691–3701.

(49) Mutzel, A.; Poulain, L.; Berndt, T.; Iinuma, Y.; Rodigast, M.; Böge, O.; Richters, S.; Spindler, G.; Sipilä, M.; Jokinen, T.; Kulmala, M.; Herrmann, H. *Environ. Sci. Technol.* **2015**, *49* (13), 7754–7761.

(50) Grayson, J. W.; Zhang, Y.; Mutzel, A.; Renbaum-Wolff, L.; Böge, O.; Kamal, S.; Herrmann, H.; Martin, S. T.; Bertram, A. K. *Atmos. Chem. Phys. Discuss.* **2015**, *15* (22), 32967–33002.

(51) Faulhaber, A. E.; Thomas, B. M.; Jimenez, J. L.; Jayne, J. T.; Worsnop, D. R.; Ziemann, P. J. *Atmos. Meas. Tech.* **2009**, *2* (1), 15–31.

(52) Renbaum-Wolff, L.; Grayson, J. W.; Bateman, A. P.; Kuwata, M.; Sellier, M.; Murray, B. J.; Shilling, J. E.; Martin, S. T.; Bertram, A. K. *Proc. Natl. Acad. Sci. U. S. A.* **2013**, *110* (20), 8014–8019.

(53) Koop, T.; Bookhold, J.; Shiraiwa, M.; Pöschl, U. *Phys. Chem. Chem. Phys.* **2011**, *13*, 19238.

(54) Werner, J.; Dalirian, M.; Walz, M.-M.; Ekholm, V.; Wideqvist, U.; Lowe, S. J.; Öhrwall, G.; Persson, I.; Riipinen, I.; Bjorneholm, O. **2016**, *50* (14), 7434-7442.

(55) Virtanen, A.; Kannosto, J.; Kuuluvainen, H.; Arffman, A.; Joutsensaari, J.; Saukko, E.; Hao, L.; Yli-Pirilä, P.; Tiitta, P.; Holopainen, J. K.; Keskinen, J.; Worsnop, D. R.; Smith, J. N.; Laaksonen, A. *Atmos. Chem. Phys.* **2011**, *11* (16), 8759–8766.

(56) Laskina, O.; Morris, H. S.; Grandquist, J. R.; Qin, Z.; Stone, E. A.; Tivanski, A. V.; Grassian, V. H. *J. Phys. Chem. A* **2015**, *119* (19), 4489–4497.

(57) Veghte, D. P.; Altaf, M. B.; Freedman, M. a. *J Am Chem Soc* **2013**, *135*, 16046–16049.

(58) von Hessberg, C.; von Hessberg, P.; Pöschl, U.; Bilde, M.; Nielsen, O. J.; Moortgat, G. K. *Atmos. Chem. Phys.* **2009**, *9* (11), 3583–3599.

(59) Wu, Y.; Johnston, M. V. *Environ. Sci. Technol.* **2017**, *51*, 4445−4451.

(60) Chhabra, P. S.; Flagan, R. C.; Seinfeld, J. H. *Atmos. Chem. Phys.* **2010**, *10* (9), 4111–

4131.

(61) Shilling, J. E.; Chen, Q.; King, S. M.; Rosenoern, T.; Kroll, J. H.; Worsnop, D. R.; Decarlo, P. F.; Aiken, A. C.; Sueper, D.; Jimenez, J. L.; Martin, S. T. *Atmos. Chem. Phys.* **2009**, *9* (3), 771–782.

(62) Aiken, A. C.; Decarlo, P. F.; Kroll, J. H.; Worsnop, D. R.; Huffman, J. A.; Docherty, K. S.; Ulbrich, I. M.; Mohr, C.; Kimmel, J. R.; Sueper, D.; Sun, Y.; Zhang, Q.; Trimborn, A.; Northway, M.; Ziemann, P. J.; Canagaratna, M. R.; Onasch, T. B.; Alfarra, M. R.; Prevot, A. S. H.; Dommen, J.; Duplissy, J.; Metzger, A.; Baltensperger, U.; Jimenez, J. L. *Environ. Sci. Technol.* **2008**, *42* (12), 4478–4485.

(63) Kourtchev, I.; Giorio, C.; Manninen, A.; Wilson, E.; Mahon, B.; Aalto, J.; Kajos, M.; Venables, D.; Ruuskanen, T.; Levula, J.; Loponen, M.; Connors, S.; Harris, N.; Zhao, D.; Kiendler-Scharr, A.; Mentel, T.; Rudich, Y.; Hallquist, M.; Doussin, J.-F.; Maenhaut, W.; Bäck, J.; Petäjä, T.; Wenger, J.; Kulmala, M.; Kalberer, M. *Sci. Rep.* **2016**, *6*, 35038.

Chapter 4

MOLECULAR SEPARATION OF SOA WITH VARIOUS ANALYTICAL TECHNIQUES

4.1 Introduction

Molecular Composition of Secondary Organic Aerosol. As mentioned in previous chapters, the chemical composition of both ambient and lab-generated SOA is very complex, encompassing hundreds to thousands of individual compounds[1–3]. Both number and types of their components change with the identity of the VOC precursor and the manner and extent to which oxidation occurs.[3–7] The monomeric components formed during the formation of SOA were investigated and found to have multifunctional groups bearing in them.[8–11] For example, carbonyls generally possess relatively high vapor pressures, which means that they might not reach supersaturation to nucleate homogeneously or condense directly.[12] Comparatively, carboxylic acids, which are more polar and have lower vapor pressures than the corresponding carbonyls, play an important role in the formation of SOA in the particle phase.[7] Some research also demonstrated the significance of hydroperoxides and peroxy acids by synthesizing peroxy acid standards with C_8-C_{10} backbone. Among these, the highly-oxidized components such as acids, hydroperoxides have received attention due to their low volatility and important role in particle phase chemistry of SOA.[13] Due to the complexity, the high-resolution of MS is essential and allows the identification/distinguishing of multiple species within one nominal mass unit. Off-line analysis with various analytical techniques were applied to study the chemical

composition, oxidation/ degradation pathways and their formation mechanism and product distributions.[1,14-16].

Monomers derived from unimolecular decomposition /isomerization[16] and bimolecular reactions (e.g. oligomerization) of Stabilized Criegee Intermediates (SCIs) make the situation complicated by producing a great variety of isomeric species. Both isobaric (different formulas that share the same nominal mass) and isomeric (same formulas with different chemical structures) components of SOA derived from various precursors are also proved to exist.[11,18-20] However, the molecular level analysis of these is difficult to obtain by high- resolution MS without a prior separation step (e.g. gas or liquid chromatography). Both laboratory and ambient work have been performed to study the terpenoic acid fraction in aerosol using GC-MS, CIMS and LC/(-)-ESI-MS[19]. Liquid Chromatography (LC), which utilized the combination of aqueous/organic solvents as the mobile phase and packed porous particles as stationary phase, separates chemicals based on their polarities and distribution between the two phases. With the authentic standards as reference, a series of acids were selectively and sensitively separated and detected. Organosulfates and organic nitrates from both laboratory generated and ambient aerosol were also investigated in the similar way with HPLC-MS.[19,21] Additionally, the aging (OH-oxidized) process of fresh SOA was investigated with HPLC and both known and novel tracers were tentatively identified.[20] Separation with inclusion of one or more chemical derivatization steps was performed with GC-MS for the relatively volatile analytes to improve the separation efficiency.[22]

In some cases, subsequent structure elucidation was successfully performed in ion-trap MS due to its capability to perform MS^n.[19,23] Some monomeric and dimeric species yield slightly different MS^2 spectra (e.g. same fragment ions with different relative abundance) that are hardly distinguished. A better distinction between the two

isomers is achieved through MS^3 fragment ion spectra, which is able to show the fragmentation via different routes. For instance, Winterhalter et al. reported use of HPLC coupled with LCQ ion–trap MS to investigate SOA which allows the multiple CID process applied in the ion trap.[24]

The ESI(-)-MS analysis of isomeric/isobaric species derived from the oxidation of α-pinene, β-pinene, limonene and 3-carene have been reported.[19] In some recent work, a series of terpenoic acids (which contain one or more carboxylic acid groups) were selectively and sensitively detected[25–28]. Combining the further analysis with Tandem Mass Spectrometry (MS^n), tentative molecular structures are proposed and in some selected cases, the authentic standard is needed to characterize the novel tracers such as the lactone-containing terpenylic acid, an α-pinene SOA tracer[27] and the tricarboxylic acid, 3-methyl-1,2,3-butanetricarboxylic acid, a terpene SOA tracer.[19,28]

In this chapter, multifunctional monomers (e.g. carboxylic acid, peroxy acid) of SOA were separated and tentatively identified based on the carboxylic/peroxy functional groups bearing in them. Isomeric species of the acids were detected in some of them confirmed with MS^2 spectra and isotopic labeling experiment, and their relative abundances were tracked during the formation/growth of SOA derived from various biogenic precursors. The highly oxidized carboxylic/peroxy acids, some of which were identified as HOMs (i.e. Highly Oxidized Multifunctional species), significantly affect the chemical composition/volatility of SOA after condensing into particle phase. Therefore, investigating the development of the highly oxidized acidic component of SOA helps us to gain insight into the fate of SOA in the atmosphere.

42 Ion-Mobility Spectrometry (IMS) of SOA Derived from Various BVOCs

Separation of complicated SOA samples based on their ion mobility can be achieved using Ion Mobility Spectrometry coupled with MS. Generally, IMS separates the ions based on the ion mobility, K, which is sensitive to molecular structure such as size and shape. The ions entering the ion mobility drift cell interact with a buffer gas such as He and N_2. Larger ions undergo longer drift time with smaller ion mobility than the smaller ions. Therefore, ions are separated based on the gas- phase mobility in the cell, which will not be limited by the stationary-phase constraints as in the case of GC/LC separation. Both ambient and lab-generated aerosols were analyzed with ion mobility spectrometry MS. The capability to separate the components of aerosol have been shown to an extent. Iinuma et al. demonstrated the capability of IMS-MS to separate the structural isomers of water soluble organosulfates based on their ion mobility[29]. Renard et al. reported the analysis/separation of multiply charged ions of natural organic matter using IMS coupled with FTICR-MS.[30] My research aims at investigating the components of SOA derived from different BVOCs (i.e. α-pinene, β-pinene, limonene and 3-carene).

Laboratory generated SOA samples from various BVOCs were analyzed with an ESI coupled IMS–TOF Mass Spectrometry (Synapt G2-S, Waters). SOA samples were dissolved in HPLC grade solvents (H_2O: ACN=1:1) with a final concentration of 0.5 µg/ml and 30 µl injection volume. For each sample, Naphthalene, which was non-reactive with SOA components, was used as internal standard and lock mass as well to improve the accuracy. The TOF mass analyzer was set to 'high resolution' mode under which the resolution could reach ~ 35000 to help distinguish isobaric ions. The optimized ESI condition was set as followed: 100 ˚C source temperature, 250 ˚C desolvation temperature, 3.2 kV capillary voltage, 60 ˚C source offset temperature, 100 ˚C sampling cone temperature, 600 L/Hr desolvation gas flow and 6 bar nebulizer gas

flow. The parameters of the IMS cell were set as follows: Helium gas flow 185 ml/min, IMS gas (N_2) flow 120 ml/min, trap gas flow 2 ml/min. The trap and transfer collision gas flow were set as zero. And the travel wave velocity and height were set at 300m s^{-1} and 10 v respectively. Data acquisition and offline analysis of the mass spectra were performed with Masslynx Mass Spectrometry Software (v.4.1, Waters).

The spectra and data associated with ion mobility separation were processed with the Driftscope software (v.2.1, Waters), which provides information of ions with the corresponding drift time and 2D IMS-MS spectra as shown in Figure 4.1 (a). The data processing using Driftscope started from setting up the selected peak detection parameters for the target ions in the spectra: 0.05 ms peak width, 0-10 ms drift time range, the minimum intensity threshold was set to 0.1% intensity of the base peak in each spectrum, which was similar to the data processing method used for Orbitrap data discussed in previous chapters. The purpose here is to also get rid of the peaks with extremely low SI or do not belong to the component of SOA. As a result, in Figure 4.1a, the blue markers represent all the ions detected in one SOA sample. The red markers represent the target ions after applying the detection peak parameters mentioned above. It is clear that more than 60% peaks with relatively low SI are removed that might be from background interference. A linear correlation between the drift time and m/z was exhibited. The blue dots with relatively low m/z at the bottom of the plot, which was circled by the red oval, gives the distribution of doubly charged ions of SOA components. Similar to the singly charged ions with significant abundance shown in red, their drift time/ion mobility in the drift cell also correlated linearly to their molecular mass but with a significantly lower slope. This was also observed and reported from literature.[30-32] The negative ion mode was found to yield much less multiply charged ions that the positive ion mode. The doubly charged ions detected in the spectra, due to their low abundance, are not discussed in this dissertation. In Figure 4.1b, the blue line displays the distribution of RA of the peak

detected at a specific drift time (bins). The red vertical line represents each peak detected. Some isobaric/isomeric species that share the same nominal mass went through the drift cell together which means that the relative abundance (RA) represented by the blue line might be the summation of multiple peaks at one specific drift time. It is interesting that the distribution of the detected peaks as a function of their drift time (blue line) looks similar to their mass spectrum. And these three peaks of blue line happen to represent the distribution of SOA components which are monomers, dimers and trimers. This suggests the linear correlation between the drift time and the mass to charge ratio of the peaks, which was also shown in the 3-D graph in Plot c of Figure 4.1.

Figure 4.1. A typical example of IMS-MS data of b-pinene derived SOA sample (-). a) The 2-D plot of m/z ratio vs. drift time; b) The total ion mobility spectrum (blue line) for the entire m/z range (red line); c) 3-D plot of m/z ratio vs. drift time, *z*-axis shows the relative abundance of each detected ion. The red oval in figure a) circled the doubly charged ions detected in the spectra.

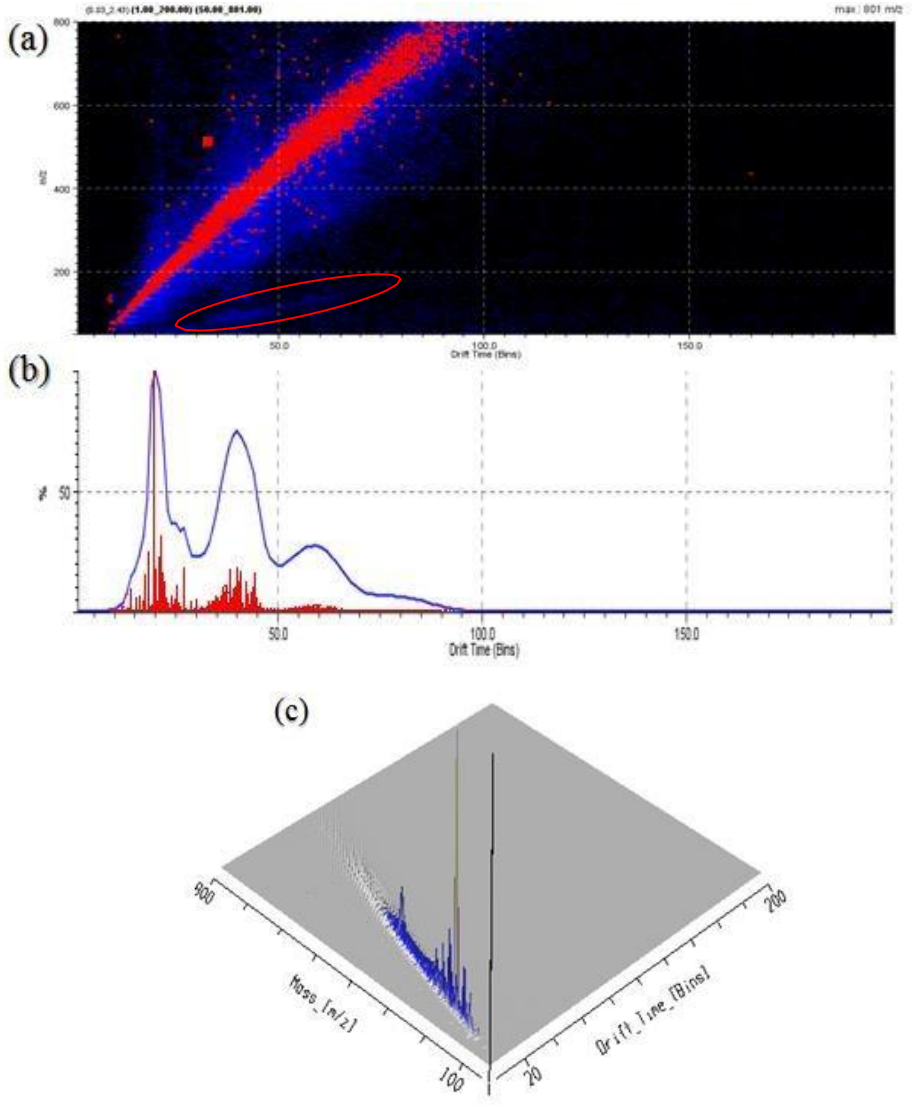

The molecular ion list of each SOA sample was exported into an Excel spreadsheet as well along with their relative abundance, drift time (DT), assigned molecular formula. Note that the absolute value of drift time was not explicitly calibrated with an IMS standard and the transit times outside the drift cell was not considered in this work. Therefore, I report it as 'apparent drift time' in units of milliseconds. The assigned molecular formula list was processed with the same method mentioned previously to remove isotope redundancy. As a result, more than 92% formulas were commonly observed in both IMS-MS and orbitrap MS detected spectra for β-pinene derived SOA demonstrating the capability of IMS-MS to detect the complex SOA sample. DT of the BVOC as the precursors, their deriving monomer (pinic acid as an example) and corresponding dimer (di(α-hydroxy) ether as an example) were measured and plotted in Figure 4.2a. Each value was obtained averaging over three replicate experiments and the standard deviation was calculated as well. As seen in Figure 4.2a, it is not surprising that the β-pinene derived SOA was separated into monomers, dimers and higher order oligomers based on their MW. The ozonolysis of β-pinene resulting in the addition of three oxygen atoms only increased the DT from ~1.5 to ~2.2 ms. Oligomerization between pinic acid ($C_9H_{14}O_4$) and another -OH containing species produces the di(α- hydroxy) ether ($C_{18}H_{32}O_7$) gave a much higher increase of DT (~4.1 ms). The great difference in the DT allows the monomers and oligomers to be separated based on their size and structure. Unfortunately, the isobaric and isomeric components SOA were not separated in the drift cell based on their ion mobility and the reason will be discussed in detail.

When I looked into the DT distribution of the monomer region, the separation results were not satisfying. The DT of each detected ion was plotted as a function of its m/z and the linear correlation was same as the snapshot from Driftscope Software as shown in Figure 4.1a. And the expanded spectrum (+) which focused on the small m/z range within monomer region (160-220 m/z) was shown in Figure 4.2b. Both

protonated and sodiated molecules were displayed. It is obvious that increase in the number of carbon, hydrogen and oxygen atoms would change the DT of the formula they bear in. Among these, based on their atomic mass, same number of oxygen atoms resulted in the greatest increase than the other two. For instance, the increase in DT of $C_9H_{17}O_3^+$ to $C_9H_{19}O_3^+$ is less than that of $C_{10}H_{15}O_3^+$ to $C_{10}H_{15}O_5^+$. In this case, the smallest increase which can be resolved in the spectra is the increase of one H atom. This illustrates why the isomeric/isobaric components with a much smaller mass different than that of one H atom cannot be separated. SOA derived from other BVOCs (α-pinene, d-limonene, 3- carene) were also studied using IMS-MS with the same method mentioned above. The results were similar in that IMS could not separate molecular structures, even though they were derived from different biogenic precursors.

In summary, with the use of ion mobility spectrometry MS, biogenic precursor derived SOA were separated into monomers, dimers and high orders of oligomers based on their size and molecular weight. To separate the isomeric/isobaric components and perform further structure elucidation, other separation techniques such as gas/liquid chromatography techniques which separated analytes based on their polarities are necessary.

Figure 4.2. Drift time vs. m/z (+) of ions detected in β-pinene derived SOA as an example. (a) Measured DT of β-pinene, monomer (pinic acid) and its corresponded dimers based on three replicated experiments; (b) expanded ion mobility spectrum of β-pinene derived SOA. Both protonated (blue) and sodiated (red) ions are displayed.

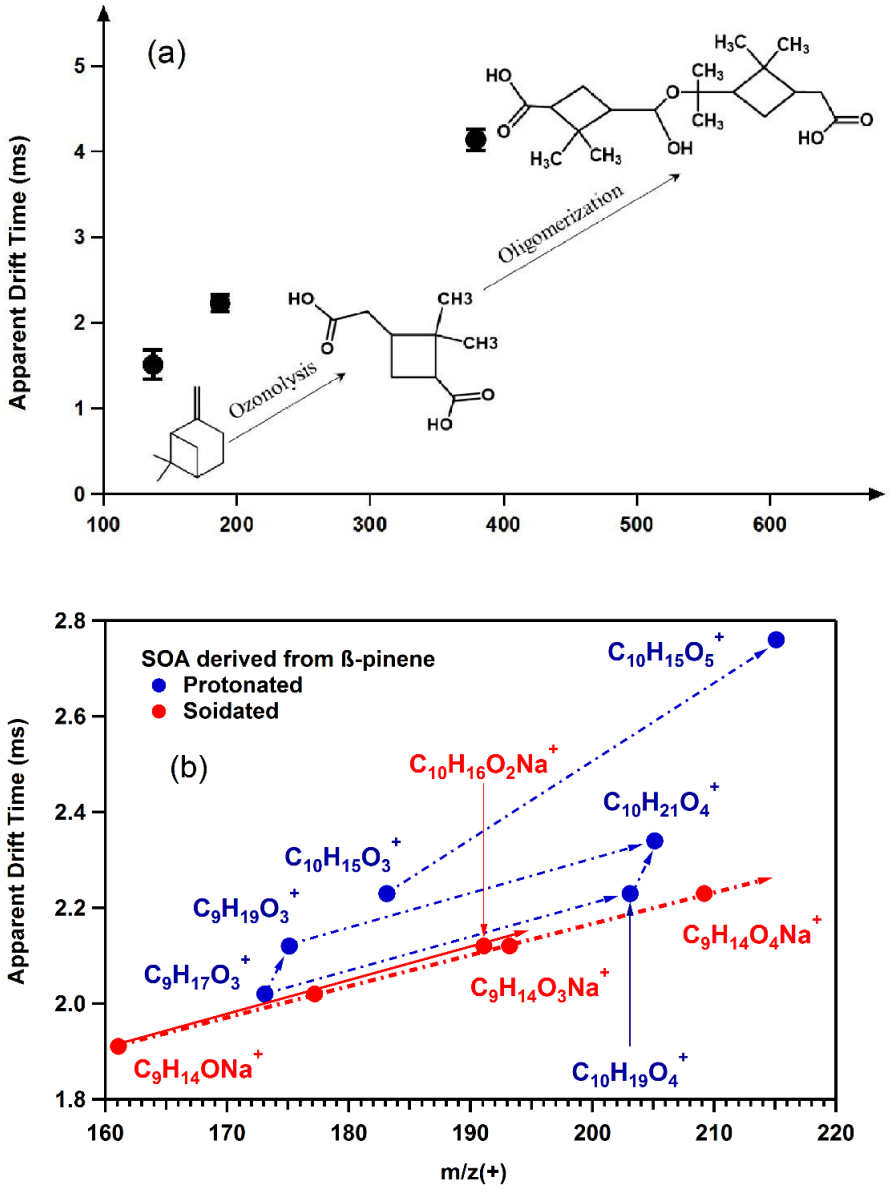

43 Gas/ Liquid Chromatography Separation of Multifunctional Monomers of SOA

Due to the complexity of the mass spectra, separation is essential for the identification of molecular structures. Apart from IMS-MS, separation of the isomeric/isobaric species based on their polarity and distribution between mobile and stationary phase using gas/liquid chromatography is also employed during aerosol studies. For instance, both laboratory and ambient work have been performed to study the terpenoic acid fraction in aerosol using GC- MS, CIMS and LC/(-)-ESI-MS[19]. With the authentic standard as reference, a series of acids were selectively and sensitively separated and detected. Winterhalter et al. reported the use of HPLC coupled with LCQ ion–trap MS to investigate SOA which allows the multiple CID process applied in the ion trap.[24] The structure elucidation with Tandem mass spectrometry was aided by the fragmentation pattern of the authentic standards as the reference. To my knowledge, most of the research of GC/LC analysis of aerosols was performed with the help of reference standards/marker compounds either obtained from chemical synthesis or bought directly from the chemical company.

GC-MS separation of volatile organic components of SOA. Gas Chromatography coupled with MS or other detector (e.g. UV-Vis spectrometer) has been used in previous analysis of SOA and is particularly helpful to detect/separate species with relatively high vapor pressure. The formation of SOA includes the oxidation of volatile organic compounds (VOCs) in the gas phase followed by the subsequent partition/condensation of semi- and nonvolatile species into the particle phase. During this process, the semi-volatile species build up an equilibrium state between the two phases. Further aging (with OH or NOx) process accompanied by functionalization (cleavage of the chemical bond such as carbon- carbon bond) might lower the vapor pressure of the components that eventually evaporate to the gas phase. These species, detected in the gas phase, have been reported by various studies aiming

at the relatively volatile components of SOA using Gas Chromatography coupled with mass spectrometer.[33,34]

In my research, both mixture of monomeric standards and freshly formed SOA (dissolved in methanol) were analyzed with GC-EI-MS (Agilent 5973). Fragment ions detected provide information of the molecular formula and chemical structure of the species. Then temperature of the oven reaches as high as 280 ℃ during the separation and volatile species are separated based on their interaction with the stationary phase. The TIC of the standard mixture obtained showed the separation and detection of a few semi-volatile compounds (e.g. pinonic acid, nopinone). However, the use of GC-MS does not give a detailed characterization of β-pinene SOA due to the inability to detect non-/low volatililty species, especially the higher order oligomers (e.g. trimers), which are produced by accretion reactions in the particle phase. A prior derivatization (e.g. silylation of carbonyls[35]) step to convert the less volatile species into volatile derivatives allows the detection with GC but alters the chemical composition of the analytes. In summary, application of Liquid Chromatography is essential to have a better understanding of the products and reaction mechanism of β-pinene derived SOA and help to bridge the gap among different studies.

Separation of isobaric and isomeric monomers with LC-MS. Apart from a few somewhat volatile organic species contained in an SOA sample, most of the components are favorably detected by LC, which utilized the combination of aqueous/organic solvents as the mobile phase and packed porous particles as stationary phase to separate chemicals based on their polarities and distribution between the two phases. Compounds that are temperature- sensitive are especially suitable for the detection of LC. In my research, reverse phase column of non-polar packing of C_{18} as the stationary phase was applied. Compounds were tentatively identified using ESI-HR-MS (Q-Exactive Orbitrap) as introduced in Chapter 2. Laboratory generated SOA samples (as described in Chapter 2 and 3) were collected and dissolved in water

(HPLC Grade, Sigma-Aldrich) to a final concentration of 0.1 mg/ml. This study utilized an injection flow rate of 3 μL/min with a 33min mobile phase gradient consisting of 0.1% acetate acid in both water and methanol. The gradient was as follows: 0% methanol for 4 min, followed by an increase to 75% methanol in 20 min and held for 2 min before the gradient was decreased to 0% methanol at 27 min and then held for 15 min before next injection. Note that the separation was optimized by adjusting the gradient method (e.g. solvents and their ratio in the mobile phase, pH of the mobile solvents, oven temperature and the flow rate). The settings of ESI-HR-MS were same as those described in Chapter 3.

As mentioned above, the use of an authentic standard compound is essential especially for the characterization of samples with complex matrices. In this work, seven standard samples were obtained from Sigma-Aldrich as follows: pinic acid (>98%, Sigma- Aldrich), pinonic acid (>98%, Sigma-Aldrich), ketopinic acid (>99%, Sigma-Aldrich), pinanediol (>99%, Sigma-Aldrich), nopinone (>98%, Sigma-Aldrich), T-butyl-3- oxocyclobutanecarboxylate (>97%, Alfa Aesar) and Diethyl 1,2-cyclobutanedicarboxylate (<98%, Sigma-Aldrich). All of them are attributable to $C_{9-10}H_xO_y$ formulas that are found in SOA samples. Some of them were shown in previous studies to exist in α- and β-pinene derived SOA and the rest have closed structures and represent reasonable components within the SOA. The purpose of utilizing standard samples is to help the identification of the similar species by comparing their retention time. The product ions in MS^2 spectra of the standards would also shed light upon other SOA species with similar structures by detecting similar product ions in their MS^2 spectra. Due to the complexity of SOA samples and large number of formulas detected, the focus of this study is the monomeric (~150-220 m/z) multifunctional species detected in the negative ion mode. It is also the range that many of the highly-oxidized molecules (e.g. HOMs) are found. The fact that negative ion mode tends to detect the relatively highly oxidized species might help the

identification of the HOMs in SOA samples that will allow a better understanding of their role/fate during different SOA formation stages. The sample preparation and final concentration of the standards were mentioned above.

The top left panel in the Figure 4.3 gives the Total Ion Chromatogram (TIC) of freshly formed SOA derived from ozonolysis of β-pinene (negative ion mode). The mass spectrum extracted from the TIC diagram, which corresponds to the molecular ions/species that elute at a specific retention time (RT), were analyzed through the method (i.e. formula assignment and unreasonable redundancies remove with Xcalibur and Excel) described previously. The resulting formulas were compared with those directly entering ESI source without the prior separation step. Typically 98% of the formulas found in direct infusion ESI are also found in LC-MS with the elution time up to 23 min. The rest formulas, mostly high orders oligomers with extremely low intensity, were not detected with LC-MS. Therefore, the TIC diagram was cut at 23 min in Figure 4.3 for discussion. The SOA components are found to be separated as groups (i.e. monomers, dimers and other oligomers). Monomers elute faster than others due to their relatively higher polarities. Intense monomer peaks between ~2 and 13 min are easily observed in the TIC due to their high abundance in SOA. Dimers and trimers elute between ~13 and 20 min, and some of them coelute due to the large number of components detected. Note that the coelution of a few monomers within 2-13 min RT range is observed as well probably due to the fact that the number of formulas present in each SOA formulas exceeds the sample capacity of the column. The left panels a-d in Figure 4.3 show the ion chromatograms at specific m/z (-). With the aid of monomer standards, these panels identify pinanediol ($C_{10}H_{17}O_2^-$), pinic acid ($C_9H_{13}O_4^-$), pinonic acid ($C_{10}H_{15}O_3^-$) and ketopinic acid ($C_{10}H_{13}O_3^-$) in the sample. The three acids (pinic, pinonic and ketopinic acid) were reported previously and found to play important roles in the formation of α- and β-pinene derived SOA.[11,19,34] And they were found to be highly abundant (SI >$1x10^7$) as shown in Figure 4.3. Their

structure information was given in the right top panel as well as their MS^2 spectra, which will be discussed later. Note that pinic acid, which is a dicarboxylic acid, tends to have a different neutral loss (e.g. CH_2O_3) from pinonic acid (monocarboxylic acid) during the fragmentation process. Among these, no isomeric species were detected at m/z 183.102 and 185.082 as confirmed by comparison with the corresponding standards. Isomers were observed at m/z 181.086, which gives two peaks at 9.91 and 10.74 min. The formula eluting at 9.91 min was proved to be ketopinic acid by comparison with the authentic standard, while the weaker one at 10.74 is found to be a component with different functional groups according to its MS^2 spectrum. The ion at m/z 169.122 yields several peaks (pinanediol was identified at RT= 14.08 min), which elutes more slowly than the acids mentioned above. This can be explained by the acid groups being more hydrophilic than the carbonyl groups[19]. Additionally, the ions with carbonyl groups are not preferably detected in the negative ion mode, which explain the low intensity of pinanediol (RT=14.08 min) in this mass spectrum. Due to its low abundance in the spectrum, it was not selected by the traditional Data Dependent Acquisition[36] (DDA)-MS^2 for structure elucidation as it tends to select the relatively intense ions for subsequent activation in each precursor ion scan. Therefore, the corresponding fragmentation pattern of pinanediol is not discussed here, nor are the other peaks of m/z 169.122 that might be attributed to the impurities or the isomeric species of pinanediol. The possibility of the solvent-analyte clusters cannot be excluded as well. For these reasons, the peaks of m/z 169.112 remain unknown due to the lack of suitable structure information. The standard sample of nopinone ($C_9H_{14}O$) was found to elute with a much lower RT than other monomers in the positive ion mode, but was hardly detected in negative mode. Standard samples of t-Butyl-3-oxocyclobutanecarboxylate and Diethyl 1,2-cyclobutanedicarboxylate, of which the structures resemble those of monomers in SOA, are not detected in the spectrum. Their fragmentation patterns will be discussed later.

Usually, three isobaric formulas were detected within one nominal mass in the high- resolution mass spectrum of monoterpene derived SOA. For example, three formulas at m/z 171 elute as the following sequence: $C_7H_7O_5^-$, $C_8H_{11}O_4^-$, $C_9H_{15}O_3^-$. As shown in Figure 4.4, $C_8H_{11}O_4^-$ with more oxygen atoms (more hydrophilic) than its isobaric formula of $C_9H_{15}O_3^-$ (the signal intensity was shown on the right axis with a different scale) elutes at a lower RT. $C_7H_7O_5^-$ elutes at ~7 min, is barely observed in the figure due to its low abundance. It turns out that the RT of SOA components were mostly affected by the number of oxygen atoms, which was consistent with the observation that $C_8H_{11}O_6^-$ elutes faster than $C_8H_{11}O_4^-$ in the figure. Multiple peaks of $C_8H_{11}O_4^-$ eluted at different RT demonstrate the existence of isomeric components and exhibit the separation efficiency of the gradient method developed. Among these peaks, the compound eluting at 9.86 min is found to be dicarboxylic acid and attributed to norpinic acid while the one eluting at 8.95 min gives a different MS^2 spectrum and might be attributed to terpenylic acid. Note that the TIC shown in Figure 3 and the separation results discussed here are based on the employment of optimized separation method. Due to the complexity of SOA samples, the numerous species were partially separated. Further improvement on the separation efficiency might need to consider the prior derivatization step or the employment of the column with higher capacity. Since the focus of this work is on the multifunctional monomeric species detected in the negative ion mode, the TIC diagram of the species in this range exhibit enough separation ability to distinguish the isomeric/isobaric species. The identification of them requires the combination of Tandem Mass Spectrometry for the structure elucidation.

Figure 4.3. Total Ion Chromatograph (TIC) of four monomers that are prevalent in monoterpene derived SOA and their corresponding MS^2 spectra.

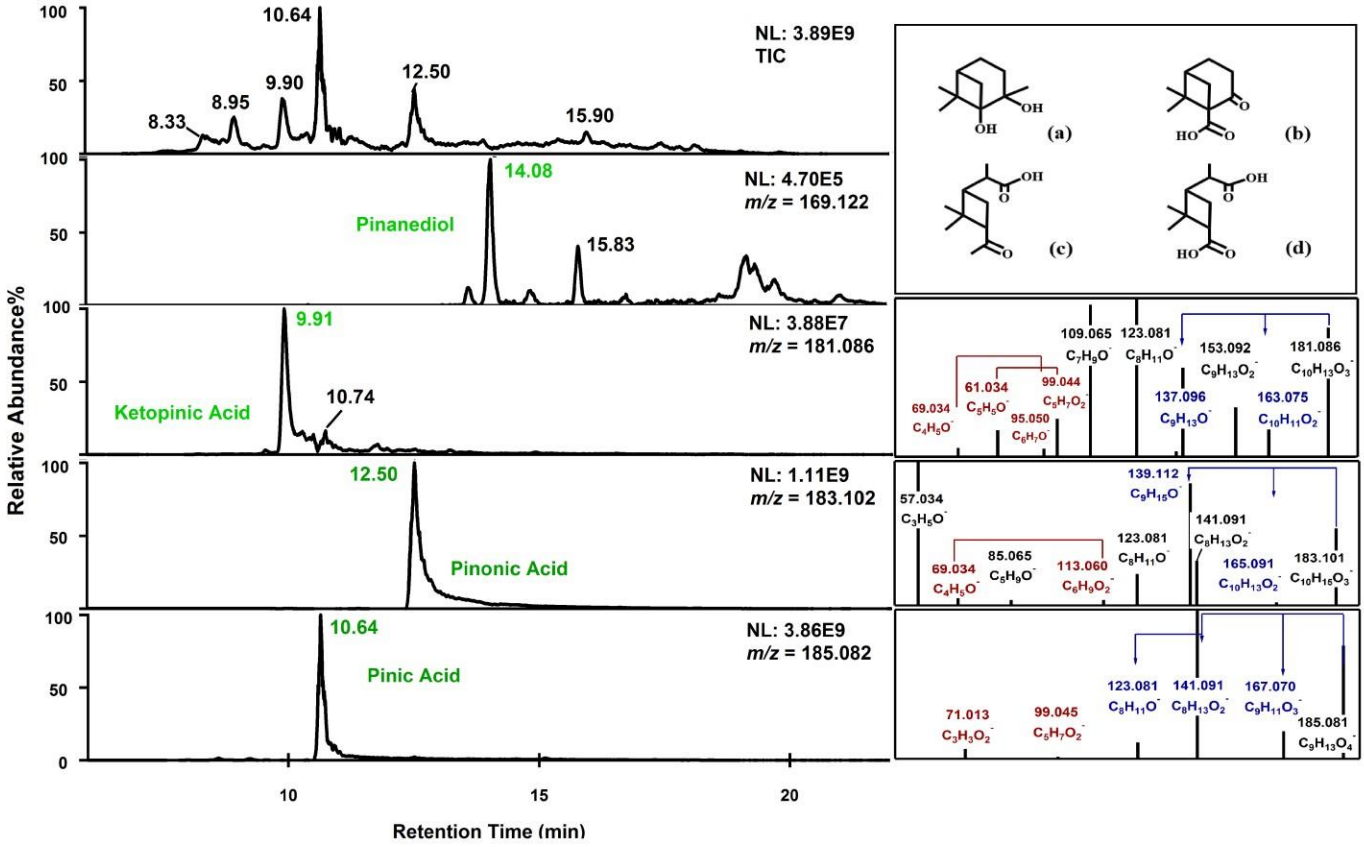

Figure 4.4. Expanded TIC diagram of isomeric/isobaric monomers detected in β-pinene derived SOA. Note that peaks of m/z 171.102 (pink) and 203.155 (green) are scaled with Y- axis on the right to compare with the other two.

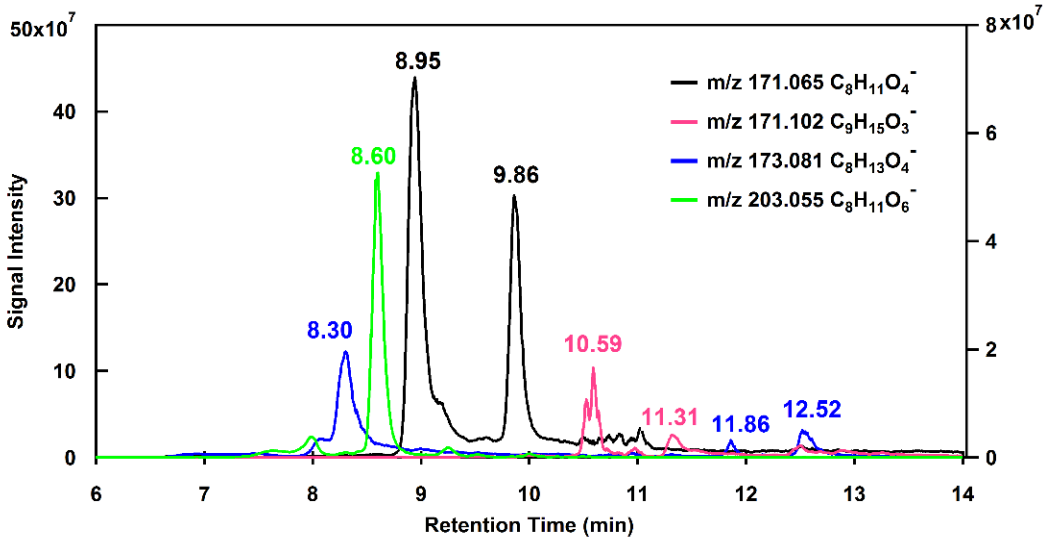

4.4 Structure Elucidation with Tandem Mass Spectrometry and Identification of Isomeric/isobaric Components

As discussed in Chapters 2 and 3, molecular level analysis of SOA samples provides information on how the chemical composition of SOA changes at different formation stages in atmosphere, and thus helps us to gain insight into the fate of SOA and the biogeochemical cycle it is involved with in the atmosphere. Tandem Mass Spectrometry was also applied to give structure information of HOM components in both fresh and aged SOA. The analysis of SOA did not stop at this and further investigation of their structure information is performed. According to previous analysis by other environmental analysis groups, a large amount of isomers are found

to exist in SOA sample[19,20,24,25,33]. Also, β-pinene and α-pinene tend to yield different types of products due to their different location of double bonds. Ozonolysis of α-pinene tends to provide monomers of C_{10} and oligomers derived from them. Comparatively, most of monomers generated from β-pinene are C_9 products result from the release of a formaldehyde from the SCI. Further isomerization is also reported previously to explain the large number of monomers produced. In most SOA studies, structure elucidation was successfully performed in Ion-trap MS due to its capability to perform MS^n.[19,23] Some monomeric and dimeric species yield slightly different MS^2 spectra (e.g. same fragment ions with different relative abundance) that are hardly distinguished. With the help of further CID of MS^3 or even MS^4, structure elucidation and isomer identification are achieved. A better distinction between the two isomers is achieved through MS^3 fragment ion spectra, which is able to show the fragmentation via different routes.

In this portion of my work, the discovery of the isomeric/isobaric components of SOA through LC separation requires further confirmation to get rid of the possibilities that multiple TIC peaks are from impurities or the tailing effect of the column. To each separated SOA sample, a second trial coupled with CID (35 normalized collision energy) was performed. This was also applied to the standard samples, and the MS^2 spectra are shown in Figure 4.3 on the right panels. The fragment ions obtained from MS^2 spectra are separated into small neutral loss and ring-opening ions with further neutral loss. As shown in the MS^2 spectra in Figure 4.3, the blue line/arrow helps the identification of the small neutral loss and the red line/arrow gives the fragment ions produced during the ring-opening process. Cleavage of the ring structure is a common route that yields two fragment ions containing oxygen atom(s). A series of fragment ions that undergo ring-opening fragmentation were commonly observed in almost all MS^2 spectra of monomers of SOA sample. This is probably due to the fact they are derived from the common precursor and the

similarities in their structure. Further identification and distinguishing of their structures (e.g. the position of carbon skeleton that functional groups attached) rely on CID of these commonly observed fragment ions in MS^3 and/or MS^4. This method was employed and reported previously.[19] In my study, due to the type of mass spectrometry and mass analyzer (Orbitrap) applied, multiple tandem mass spectrometry is not achievable for further structure elucidation. Instead, the method I developed here uses the typical neutral loss that suggests the existence of different functional groups (i.e.-COOH, -CHO, -C(O)OOH) to partially identify the isomeric differences and/or to confirm the suggested tentative structure. As summarized in Table 4.1, some small neutral molecules lost during the CID process can be used as indicators to specific types of functional groups embedded in the compounds either confirmed using the authentic standard samples in my work or reported previously in separated studies. For example, monocarboxylic acids like pinonic acid and ketopinic acid, though with different ring structures, exhibit same loss of H_2O and CO_2 from the parent ion (Figure 4.3).[15,20,22,37] In some cases, loss of $C_2H_4O_2$ (CH_3-COOH) was observed as well.[15] Comparatively, dicarboxylic acids such as pinonic acid undergo further loss of H_2O after losing CO_2 (CO_2+H_2O or CH_2O_3).[9,37] Loss of CH_2O_3 was also reported previously to be an indicator of the existence of dicarboxylic functional groups in the parent ion.[8] The possibility of peroxy acid to yield CH_2O_3 was also excluded by other studies. Instead, study of both synthesized peroxy acid standards and the SOA components that contains peroxyl groups reported the typical fragment ion of CH_2O_2 which was commonly observed in all peroxy acids. Neutral loss of CH_4O_4, $C_2H_4O_5$ and H_2O_2 were reported during the detection of diperoxydicarboxylic acid as well. Additionally, the MS^2 spectra of the standard samples exhibit typical neutral loss, which indicates the existence of carbonyl and hydroxyl groups.

Table 4.1. Typical neutral loss from MS^2 spectra as indicators to the specific functional groups in the molecular formulas detected in the negative ion mode.

Typical Neutral Fragment from MS^2 (-) (with the reference cited)	**Functional Group**	**Confirmed in This Work[a]**
(H_2O_2, CHO_3, CH_2O_2, CH_2O_3, CH_4O_4, $C_2H_4O_5$)[8,9]	(di)Peroxyl	N
(H_2O, CO_2, CH_2O_3, $C_2H_4O_2$)[15,20,22,37]	(di)Carboxyl	Y
CH_2O[15,20], C_2H_4O, C_3H_6O	Carbonyl	Y
H_2O[15,20], CH_2O[20] C_3H_8O	Hydroxyl	Y

[a] The authentic standard samples were used to confirm the typical neutral fragments and their corresponding functional groups.

Figure 4.5 shows two fragmentation conditions regarding to the isomeric species in SOA sample. $C_{10}H_{17}O_5^-$ of m/z 217.11 elutes at 9.2 and 11.6 min with their fragmentation patterns are given in Figure 4.5a. Both neutral loss and small fragment ions that undergo ring- cleavage process are labeled. Two distinct fragmentation patterns are observed: the formula eluting at 9.2 min yields neutral small loss of H_2O and CH_2O_2 which suggest the existence peroxyl groups in the negative mode. The observation of $C_3H_8O_2$ loss indicates the existence of two unsaturated oxygen atoms. Considering the RDB value of $C_{10}H_{18}O_5$, a ring is included in the chemical structure. In contrast, neutral loss of CH_2O_3 and $2CO_2$ in the MS^2 spectrum of the species eluting at 11.6 min suggest that dicarboxylic acid groups are embedded in the species. Therefore, the existence of isomeric components of $C_{10}H_{17}O_5^-$ eluting at different RT are confirmed and the potential chemical structure are proposed as well. Another example given in Figure 4.5b shows the two peaks of $C_9H_{13}O_7^-$ at 7.3 and 9.4 min, exhibiting same types of fragmentation ions but with different RA. Similar type of

fragmentations was reported before to indicate the existence of isomers. Small neutral loss (i.e. H_2O, C_3H_6O, CH_2O_3) from the MS^2 spectrum suggests the existence of dicarboxylic acid group and carbonyl/hydroxyl group. The chemical structure of the same molecular formula was proposed in SOA from limonene ozonolysis[38] and a linear multifunctional hydrocarbon derivatives was proposed. In my study, $C_9H_{14}O_7$ may be derived from $C_9H_{14}O_3$ following the auto-oxidation reaction mechanism discussed earlier in my dissertation. Therefore, it might undergo the ring-opening reaction as well allowing the addition of O_2 and the chemical structure differs from that derived from limonene. A candidate structure was given based on the information obtained from the MS^2 spectrum. However, due to the lack of further MS^3 information, other possibilities could not be excluded. Additionally, a series of fragment ions produced from ring-opening process yield are commonly observed in some monomers which might suggest that their similarity of the structure especially their ring structure. Further investigation of higher orders of MS^n is essential to test the results.

Figure 4.5. MS^2 spectra of isomers that bear in the monomeric components detected in β- pinene derived SOA.

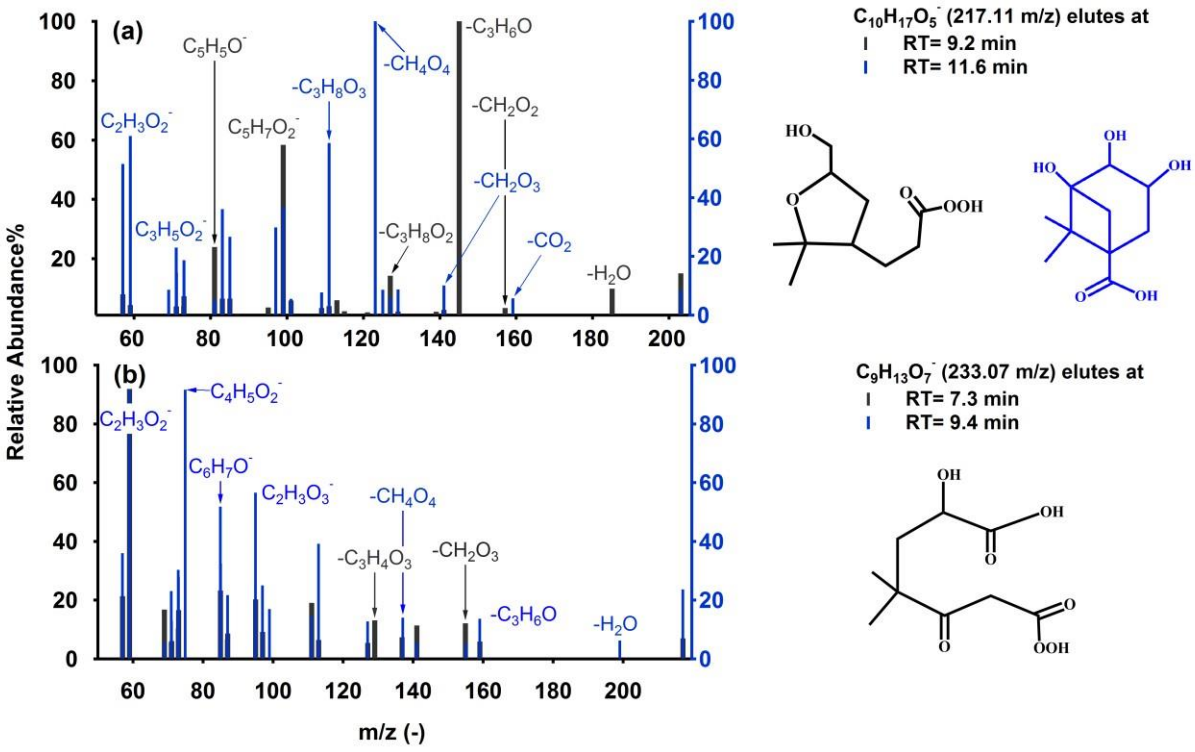

Table 4.2 summarizes the monomeric components of SOA (derived from β-pinene ozonolysis) of which the structure information is obtained from their MS^2 spectra. Thirty molecular formulas were tentatively identified using the approach mentioned above and 14 of them are found to have isomers confirmed with different RT/fragmentation patterns. The identification of isomers of some formulas cannot be performed in two conditions: 1) same fragmentation ions with different RA are detected in MS^2 spectra of species at different RT or 2) intensity of some eluted peaks are too low to be selected for CID thus lack of MS^2 information. Formulas are identified as unique structure without isomers if same fragmentation types with

consistent RA observed. Note that some formulas such as $C_{10}H_{19}O_3^-$ at m/z 187 was not listed in the table due to their low abundance and were not selected for CID. In this table, the names of the species with the same fragmentation patterns reported previously are listed. Typical neutral fragments detected in MS^2 spectra suggest the types of oxygen-contained functional groups based on the summary in Table 4.1.; H_2O_2 was also detected as neutral loss of a few species suggesting the existence of hydroperoxides. These species detected in negative ion mode are highly oxidized and eleven of them are HOMs of which the identification and definition were described in a separate study. Previous studies have discussed the identification and categorization of highly oxidized species (e.g. peroxy acid, hydroperoxide, carboxylic acid) and their evolvement in the atmosphere.[9,11,13,19,34] They have been shown to play an important role in the particle phase chemistry of SOA due to their high extent of oxidation and low vapor pressure. To my knowledge, it is the first time that a prior separation step coupled with MS^2 was performed allow the characterization of a series of HOM component and their isomeric compounds as well.

Table 4.2. List of SOA components that analyzed in LC separation and further MS^2.

m/z (-)	Formula	Candidate Species	RT(min)	Neutral Loss from MS^2	Th Shift by H/D Exchange[d]
159.065	$C_7H_{11}O_4^-$	Dicarboxylic acid	3.8	C_3H_6O, CH_2O_3	2
		Peroxy acid	10	CO_2, H_2O, CH_2O_2	1
159.102	$C_8H_{15}O_3^-$	Peroxy acid	11.4	H_2O, CH_2O_2	1
169.122	$C_{10}H_{17}O_2^-$	Pinanediol[b]	14.1, 15.8, 19.2	N.A.	0
171.065	$C_8H_{11}O_4^-$	Terpenylic Acid[a]	8.9	$C_2H_4O_2$, H_2O, CO_2	1
		Norpinic Acid[a]	9.9	CH_2O_3, H_2O, CO_2	2
173.044	$C_7H_9O_5^-$	Diacid	2.5	CO_2, CH_2O_2, $C_2H_4O_2$	2
173.081	$C_8H_{13}O_4^-$	Monoacid	8.3	H_2O, CO_2, CH_2O_2, C_3H_6O	1
		Suberic Acid[a]	11.8	CH_2O_3, H_2O, CO_2	1
181.086	$C_{10}H_{13}O_3^-$	Ketopinic Acid[b]	9.9	H_2O, CO_2	1
183.065	$C_9H_{11}O_4^-$	Monoacid	10.4	CO, H_2O, CO_2, C_2H_4O, CH_2O	1
183.102	$C_{10}H_{15}O_3^-$	Pinonic Acid[b]	12.5	CO_2, H_2O, C_3H_6O, $C_2H_4O_2$	1
185.082	$C_9H_{13}O_4^-$	Pinic Acid[b]	10.6	CO_2, H_2O, CH_2O_3	2
187.060	$C_8H_{11}O_5^-$	N.A.[c]	3.7	CO_2, H_2O, CH_2O_3, C_3H_6O	1
		Diacid	6	CO_2, H_2O, CH_2O_3, $C_2H_4O_2$	2
		Diacid	8.1	$2CO_2$, H_2O, $C_2H_4O_2$	2
187.096	$C_9H_{15}O_4^-$	Monoperoxy acid	5.5	C_2H_4O, CH_2O_2	1
		2-Hydroxyterpenylic acid	12.9	CH_4O_4, CO_2, H_2O, C_3H_6O	1
189.076	$C_8H_{13}O_5^-$	Diacid	3	CO_2, H_2O, C_3H_6O, CH_2O_3	2
		Monoperoxysuberic acid[a]	8.4	CO_2, H_2O, CH_2O_2, CH_4O_4	2

197.081	$C_{10}H_{13}O_4^-$	N.A.	8.6, 10.2	CH_2O_3, $C_2H_4O_2$, H_2O, CO_2	1
		N.A.	17.7	C_3H_6O, CH_2O_2	2
199.060	$C_9H_{11}O_5^-$	N.A.	7.3	CO_2, H_2O, CH_2O_2, CH_4O_4	2
199.096	$C_{10}H_{15}O_4^-$	Monoperoxy acid	9.9	2 H_2O, CO_2, CH_2O_2	1
201.039	$C_8\dot{H}_9O_6$	Diacid	3.6	2 CO_2, H_2O, CH_2O_3	2
201.076	$C_9H_{13}O_5^-$	Diacid	8.5, 9.9	CH_2O_3, CO_2, H_2O	2
201.112	$C_{10}H_{17}O_4^-$	Monoperoxy acid	8.5, 9.8, 10.3	CO_2, H_2O, CH_2O_2, C_2H_4O	1
203.055	$C_8H_{11}O_6^-$	MBTCA[a]	2.5	2 CO_2, H_2O, C_3H_6O, CH_2O_3	2
		N.A.	7.6	CH_2O_3, H_2O, CO_2	1
203.091	$C_9H_{15}O_5^-$	Diacid	5.3	CH_2O_3, H_2O, C_3H_6O	2
		Diacid	10.1	2 CO_2, CH_2O_3, H_2O, CH_4O	2
		Monoperoxyazelaic acid[a]	11.7	CO_2, CH_2O_2, CH_4O_4	1
205.07	$C_8H_{13}O_6^-$	Diperoxysuberic acid[a]	7.6	CH_4O, CH_4O_4, H_2O, H_2O_2, $C_2H_4O_5$	2
215.06	$C_9H_{11}O_6^-$	Diacid	6.8, 8.8	2 CO_2, CH_2O_3	2
215.09	$C_{10}H_{15}O_5^-$	Diacid	9.0	CO_2, H_2O, CH_2O_2, CH_2O_3	2
		Monoperoxycamphoric acid[a]	13.8	H_2O, C_3H_6O, CH_4O_4, CH_2O_2, $C_2H_5O_3$	1
217.07	$C_9H_{13}O_6^-$	Diacid	7.3	2 CO_2, H_2O, $C_3H_4O_3$, $C_2H_2O_4$	2
		Monoperoxy acid	9.5	CH_2O_2, CO_2, H_2O, CH_4O_4	1
217.107	$C_{10}H_{17}O_5^-$	N.A.	9.2	H_2O, C_2H_4O, $C_3H_4O_3$	1
		Monoperoxysebacic acid[a]	11.6	H_2O, C_3H_6O, CH_2O_3, CH_4O_4	1
219.086	$C_9H_{15}O_6^-$	Diperoxyazelaic acid[a]	2.3, 9.6	H_2O_2, CH_2O_3, CH_2O_2, $C_2H_4O_5$, CH_4O_4	2
219.123	$C_{10}H_{19}O_5^-$	N.A.	2.3, 2.9	H_2O, CH_2O_2, CH_2O, CH_2O_3	1
		Monoperoxy acid	8	H_2O_2, C_3H_8O	1
233.065	$C_9H_{13}O_7^-$	Monoperoxy acid	7.3	CO_2, CH_2O_2, CH_4O_4	1

		Diperoxy acid	9.4	2 H_2O, CH_2O_2, CH_4O_4, $C_2H_4O_5$	2
233.102	$C_{10}H_{17}O_6^-$	Diperoxysebacic acid[a]	9.6	$C_2H_4O_5$	1
			10	$2H_2O$, CH_2O_2, CH_2O_3, CH_4O_4, $C_2H_4O_5$	2

[a] The species was reported by literature before.
[b] The detection (RT and fragmentation pattern) of these species was confirmed by using the same authentic standard bought from commercial company.
[c] The shift observed in H/D exchange experiment was inconsistent with the number of acidic functional groups suggested in MS^2 spectra.
[d] The m/z shift in this column refers to that of the precursor ions in MS^2 spectra.

Isotopic labelling of SOA samples. In this portion of my work, an isotopic labeling method with H/D exchange combined with Tandem Mass Spectrometry was employed as a complimentary method for the structure elucidation through the screening of neutral loss in MS^2 spectra. The general method of isotopic labeling has been applied before for molecular analysis of SOA by other researchers. Ehn et. al. used isotopically labeled $^{18}O_3$ to initiate the ozonolysis of α-pinene comparing with those react with 'normal' ozone ($^{16}O_3$).[39] In another study, HOMs generated from ozonolysis and OH oxidation of unsubstituted ($C_{10}H_{16}$) and deuterated ($C_{10}H_{13}D_3$) α-pinene were investigated with IMS-MS.[40] In Richters et al. (2016) work, acidic H atoms were exchanged by D atoms in the presence of D_2O, which allowed for the study of hydroperoxide groups in the spectrum suggested by the signal shift by the number of acidic H atoms. In my work, SOA formed and collected at different stages as mentioned above was stored in the refrigerator near dryness and then reconstituted with D_2O. 0.1% Acetic acid dissolved in D_2O was added to facilitate the H/D exchange. pH, temperature and reaction time are all important factors to affect the exchange efficiency. Seven standard samples were used to test the exchange efficiency first by varying the experiment conditions such as pH, temperature and reaction time.

Therefore, SOA sample was reconstituted in pure D_2O and slightly heated to 40 ℃ for 1 hour to achieve the best exchange efficiency. Monomers of which the -CH_3 groups are partially exchanged are found to have extremely low RA (<0.76%) thus was negligible. Figure 4.6 gives an example of authentic standard sample (pinic acid) that undergoes the H/D exchange experiment. The shift in 2 Th after H/D exchange as shown in the spectrum is consistent with the existence of dicarboxylic groups embedded in the structure. Comparatively, Figure 4.7 shows an expanded mass spectrum (165-235 m/z) of deuterium exchanged SOA sample comparing with its original spectrum. It is evident that most species were found to give a 1 Th (black arrow) shift after the exchange and some of them (red arrow) exhibit 2 Th. This is not surprising since monomers detected in negative mode tend to be more highly oxidized with more acidic functional groups. The occurrence of 2 Th shift in the spectrum, confirmed with the MS^2 spectra of Deuterium-labelled pinic acid ($C_9H_{14}O_3$), indicates that these species might be attributed to dicarboxylic acid due to the multiple acidic H atoms bearing in them (Figure 4.6).

Comparatively, H/D exchange spectrum of pinonic acid ($C_{10}H_{16}O_3$) exhibits 1 Th shift in the m/z of parent ion which is consistent with the fact that one carboxylic acid group is embedded in the compound. The possibility that H atom in hydroxyl group is exchanged with D atom is excluded since the pinanediol (with two -OH groups) did not exhibit any shift during the H/D exchange. In my work, the peroxy acid is assumed to work in the similar manner to carboxylic acid in the H/D exchange experiment due to the lack of standard peroxy acid sample. The results obtained from the authentic standard samples helps the identification of the functional groups embedded in the SOA component by studying the mass spectra of deuterium-labelled SOA sample. Theoretically, the fragment ions with/without D labelled would suggest the number of acidic H (i.e. acidic functional groups) bearing in it and type of functional group lost as the neutral molecule. However, due to the low intensity of

some highly-oxidized species and the interference by H/D exchange take place on alkyl group, some formulas were hardly analyzed with the H/D exchange method (labelled as N.A. in the Table 4.2 column 'H/D exchange'). A few of the rest are found to yield different functional group information from that obtained from neutral loss. As a result, ~60% species with the acid groups (mostly dicarboxylic acids) were tentatively identified using H/D exchange method and shown to be consistent with results obtained from neutral small loss in MS^2 spectra. These species were tracked during different formation stages of SOA and the results were discussed next section.

Figure 4.6. Spectra of deuterium-labelled authentic standard of pinic acid detected in the negative mode**.**

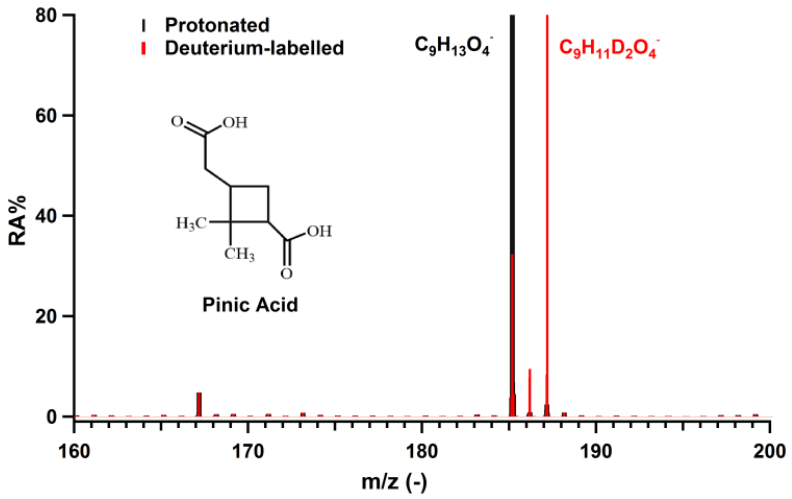

Figure 4.7. Spectra of deuterium-labelled SOA sample detected in the negative mode.

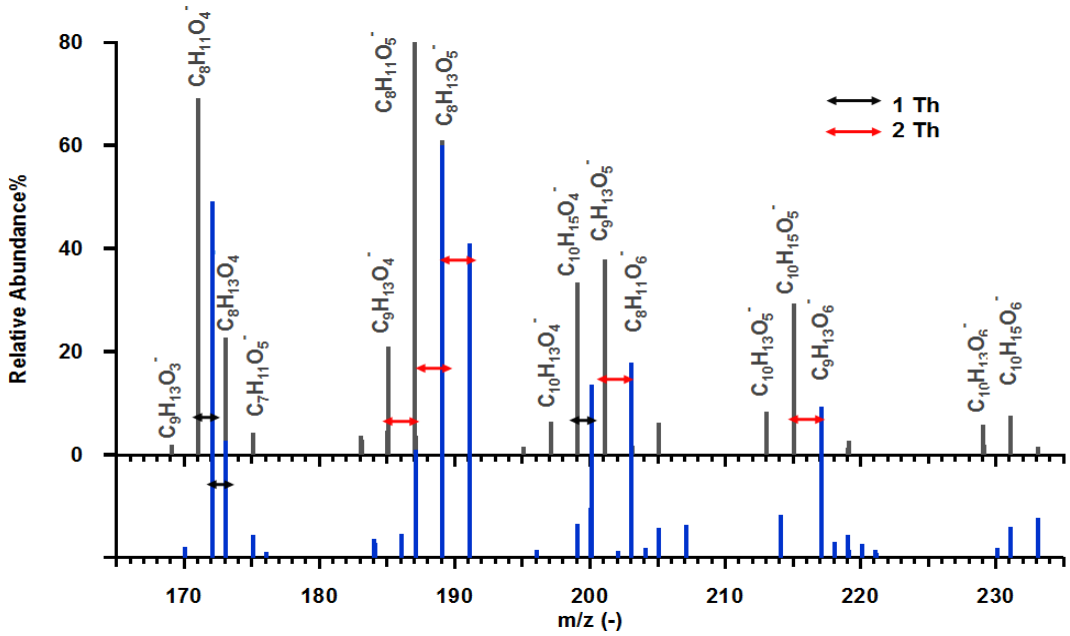

45 Highly oxidized Acid components of SOA at different formation stages

Highly oxidized acid components of fresh/aged SOA. The freshly formed RO_2 radicals that undergo successive H shifts followed by O_2 additions will increase the extent of oxygenation if additional acidic hydrogen atoms are present[40,41] thus form the highly-oxidized species in the particle phase (i.e. HOMs). Once entering the particle phase these HOM species will condense onto the pre-existing nanoparticles and facilitate the growth process. In the meantime, molecular species in the freshly formed particle phase are exposed to the UV light during the daytime and might undergo further photo-oxidation (aging) with oxidants such as OH radicals. The aging process alters the chemical composition of SOA by increasing the extent of oxidation of the species (as discussed in Chapter 2). In general, highly oxidized components especially the (di)carboxylic/peroxy acids plays an important role during the formation

of SOA and can be served as an indicator of the oxidation degree of SOA at different formation stages.

Figure 4.8 presents the fraction of the highly-oxidized species in fresh/aged SOA. Note that some formulas are listed multiple times suggesting the existence of isomers that are found to have different acid groups. And formulas of ketopinic acid ($C_{10}H_{13}O_3^-$) and pinonic acid ($C_{10}H_{15}O_3^-$) were found to give a relatively constant fraction after aging so were not displayed in the figure. The existence of the isomeric components of some species remain uncertain (labelled as 'N.A.' in column 'isomer' in Table 2) due to the lack of further MS^3 information, but H/D exchange experiment allows the partial structure elucidation of their functional groups therefore they are still included in the discussion of this section. As shown in the figure, both (di)carboxylic and (di) peroxy acids are investigated and separated by the red line in the figure. The relative abundance and its standard deviation of the species are calculated based on two trials for each sample with three samples generated for fresh/aged SOA. It is not surprising that formulas detected to have peroxyl groups, with relatively low RA though, are found to be constitute a larger fraction after aging. RA of dicarboxylic acid such as $C_8H_9O_6^-$ and $C_9H_{11}O_6^-$ are increased as aging proceeds as well. Comparatively, most monocarboxylic acids (e.g. ketopinic acid, pinonic acid) were found to be either constant or exhibit the opposite trend. Part of them was consumed by OH radicals to produce the species with higher extent of oxidation (functionalization) such as peroxy acids. Note that 1,2,3- butanetricarboxylic acid (MBTCA, $C_8H_{12}O_6$) was suggested to be a product of OH radical initiated oxidation of pinonic acid[19] ($C_{10}H_{16}O_3$) which was found to be consumed during aging process. However, it is also reported as an important photo-oxidation product during aging process.[42] As a result, the fraction of MBTCA was found to increase (as shown in Figure 4.8) while that of pinonic acid remain almost the same. All of these observations can be explained by the reaction between fresh SOA and OH radicals

which was described previously as auto-oxidation process.[43] The reaction is initiated with the H abstraction by OH radicals to produce RO_2 radicals. The subsequent H rearrangement taken place on the radicals allows further O_2 addition onto the carbon skeleton to increase the extent of oxidation. This process allows the progression from carboxylic acid to dicarboxylic acid and (di)peroxy acids as well. In previous studies by other groups, hydroperoxy acids were also found to be important products of photo-oxidation of SOA, but it is not included in my discussion here due to the lack of proper authentic standard sample.

Figure 4.8. Relative abundance of acids identified in the monomer region of fresh and aged SOA (negative ion mode) from β-pinene ozonolysis.

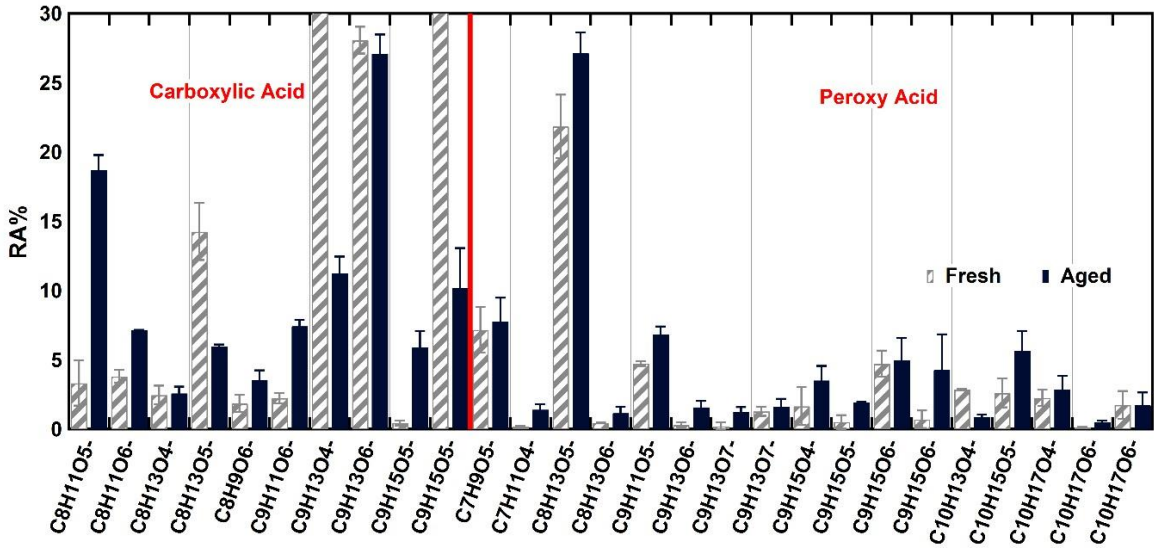

Highly oxidized acid components of size selected SOA particles. As mentioned in Chapter 2, smaller nanoparticles tend to have higher O/C ratios and the formation of these particles was predominantly by the condensation of highly oxidized, low volatility species from the gas phase. The specific chemical species that dominate this process remain unknown. In this portion of the research, the (di)carboxylic acid and (di)peroxy acids tentatively identified above were tracked during the growth of SOA particles from 30 to 110 nm. Size selected SOA particles collected as mentioned in Chapter 3 were analyzed with LC- MS coupled with MS^2. Species (with their isomers) that were identified with MS^2 spectra and confirmed with H/D exchange are listed in Figure 4.9. Similar as Figure 4.8, carboxylic acid and peroxy acid are separated for comparison. It is evident that most peroxy acids have their highest abundances in 35 nm particles and their lowest abundances in 110 nm particles. This particle size dependence suggests that they are formed primarily in the gas phase and then condense (based on their low volatility) irreversibly into the particle phase. After they enter the particle phase, they may undergo decomposition and/or accretion reaction to form carboxylic acids as the particles grow. A few of them (e.g. $C_{10}H_{17}O_6^-$) remain do not change in RA during this process. Comparatively, most (di)carboxylic acids have their highest abundances in 110 nm particles and lowest abundances in 35 nm particles. This dependence suggests that they are play a less important role during the formation and initial growth of small particles, but become more abundant as the particle size increases because of chemical reactions inside the particle. Reactions of this type have been reported in both organic synthesis[44] and aerosol[8] studies. In my work, it was observed on the basis of negative ion spectra rather than positive ion spectra. This conversion increases the average extent of oxidation for SOA particles, which is consistent with the results obtained from previous size- selection experiment.[45]

Figure 4.9. Relative abundance of acids identified in the monomer region of size-segregated SOA particles (negative ion mode) from β-pinene ozonolysis. The y-axis was cut at RA% of 3 for a better comparison of the species with relatively low RA.

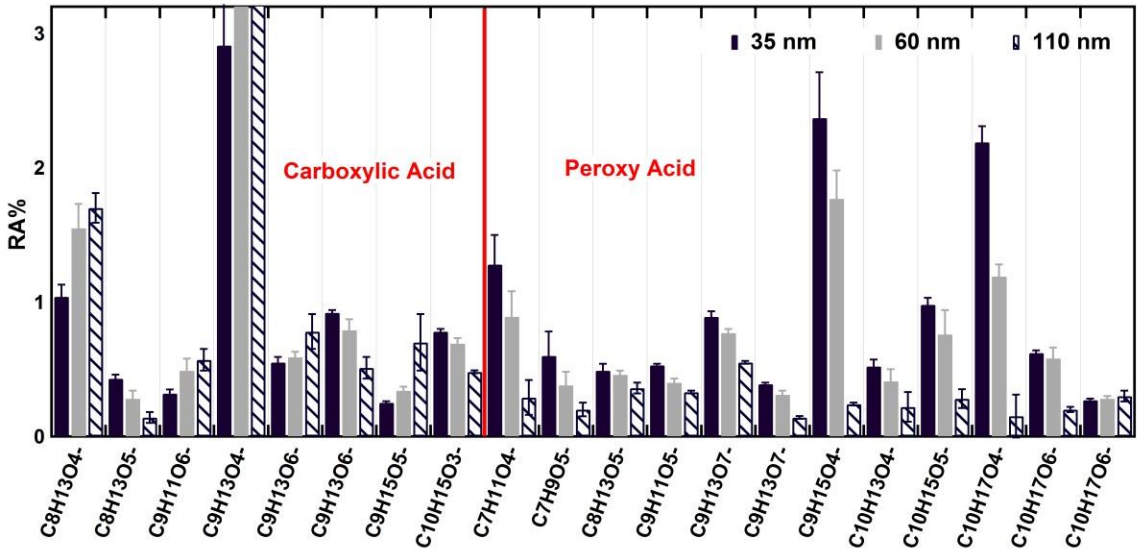

Highly oxidized acid components of SOA derived from various BVOCs. As mentioned above, 30 formulas with the isomeric species detected in 12 of them were tentatively identified and some of them were reported in previous studies. The isomeric species are mostly derived from SCIs of β-pinene followed by subsequent stabilization and isomerization. And the employment of liquid chromatography was shown to separate them based on their difference in polarity and hydrophobicity. In this portion of my research, SOA derived from various biogenic precursors were separated and analyzed. S OA derived from mixtures of biogenic precursors was studied in lab and field measurement previously.[19,34,46] MS analysis of isomeric/isobaric species derived from the oxidation of α-pinene, β-pinene, limonene and 3-carene (isomeric species of $C_{10}H_{16}$ and their chemical structure was displayed in

Figure 4.10) are discussed here. These isomeric species are mostly derived from SCIs (stabilized Criegee intermediates) of the precursors followed by subsequent stabilization and isomerization. The structure of α-pinene, β-pinene and 3-carene differs in the endo-/exo-cyclic double bond bearing in it while d-limonene has both of them which result in the larger number/type of isomeric components.

A series of isomeric/isobaric species derived from BVOCs were detected. Ion chromatograms in Figure 4.10 give some examples. Ions assigned as $C_7H_9O_5^-$ which derived from β-pinene yields neutral fragment of CH_2O_2 and $C_2H_2O_4$ in the MS^2 spectrum. This suggests the existence of peroxyl group in the β-pinene derived ions while those generated from other BVOCs exhibit similar fragment pattern with lower RA. And 3-carene tends to produce another species retains longer in the LC column and its structure information needs to be studied with MS^3. Comparatively, formula assigned to $C_9H_{13}O_4^-$ at m/z 185.08 ($C_9H_{13}O_4^-$) were found to be attributed to different chemical structure eluted at different RT for BVOCs. cis-Pinic acid, which is formed during ozonolysis of α-/β-pinene[19,34], is detected in both of their SOA samples with the same RT (10.6 min). The lactone-containing homoterpenylic species of both α- and β-pinene derived SOA reported previously[25,27] was not detected in the spectrum. For d-limonene, the SOA sample yields two IC peaks (at 9.1 and 11.7 min) which might be attributed to ketolimononic acid and limonic acid according to the literature data.[34,47,48] Another major IC peak at 10.6 min was found to yield the same fragmentation pattern as pinic acid. And the 3-carene SOA sample contains single m/z 185 peak, of which the major one elutes at 13.3 min might be assigned to cis-caric acid as reported before.[34,49] $C_{10}H_{17}O_4^-$ and $C_8H_{11}O_4^-$ were displayed in the figure as well. Some of their isomers were commonly observed in multiple BVOC derived SOA samples while the rest of them are unique structure confirmed with MS^2. These unique species can potentially serve as markers for the SOA source characterization especially investigating aerosols derived from mixed BVOCs (e.g. ambient aerosols). However,

as mentioned above, further identification and structure elucidation is essential with the use of higher orders of MS^n.

Figure 4.10. Examples of highly oxidized monomers in SOA derived from various BVOCs.

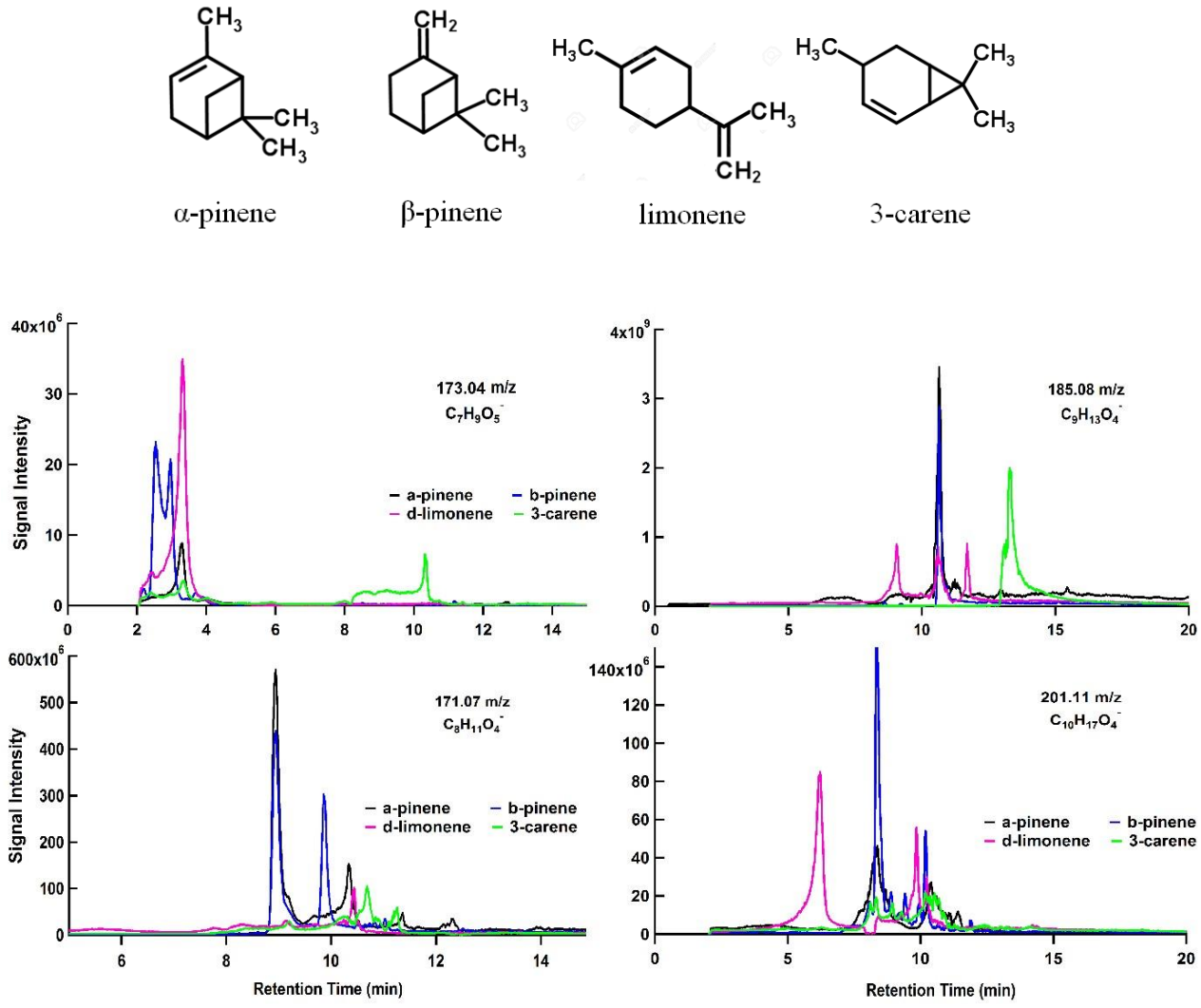

4.6 Conclusions

In this chapter, complicated SOA samples with more than a thousand molecular formulas were separated and tentatively identified with various analytical methods. Analytical methods developed for the separation of monomers/oligomers and isobaric/isomeric species were discussed and compared. Chemical structure and functional groups bearing in the components were investigated and their relative abundances were tracked during the different formation stages of SOA.

Separation by ion-mobility spectrometry coupled with high resolution mass spectrometry was applied based on the size and shape of the analytes. Singly charged ions are found to separate based on their size (i.e. molecular formula) so a linear correlation was displayed to separate the species into monomer, dimers and higher orders of oligomers. Multiply charged ions with much lower relative abundance were also detected with a lower slope of linear correlation displayed. The drift time (DT) of molecular components of SOA in the IMS drift cell was recorded and the smallest change in DT (~0.2 ms) results from the addition of two hydrogen atoms to the formula, which demonstrate the difficulty for IMS-MS to separate isobaric/isomeric species.

Separation with gas and liquid chromatography were applied as well. Unfortunately, due to the low/non-volatility of most SOA components, employment of GC-MS is not suitable for the detection since it favors the detection of species with much higher vapor pressure and lower boiling point. Application of liquid chromatography coupled with high resolution mass spectrometry was suggested to be able to separate isomeric/isobaric components of SOA. With the use of reverse phase column with optimized analytical method (e.g. elution gradient, oven temperature, pH of the solution and solvents used as mobile phase), the separation of isomeric and isobaric components were achieved and the attention was drawn on the monomers

detected in the negative ion mode. Ions that assigned to specific formulas were found to elute at multiple time points which suggest the existence of isomers. Additionally, isobaric species that elute at various RT demonstrate the efficiency of LC separation as well.

Further application of Tandem Mass Spectrometry to confirm the existence of isomeric species is essential. In my research, employment of MS^2 with orbitrap allows the determination of the neutral loss from its parent ion. And the type/RA of the neutral loss shed lights upon the functional groups bearing in the chemical structure. Molecular formulas detected with different neutral small loss under the exact same CID conditions are believed to have isomeric structures. Isotopic labeling using H/D exchange method was applied to be a complimentary method to confirm the type of neutral loss from MS^2 spectra. However, the tentative identification needs to combine with further investigation on the position of the functional groups on the backbone of carbon skeleton. Therefore, mass spectrometry with the appropriate mass analyzer that allows the MS^n to perform is necessary (e.g. ion trap).

Thirty formulas with peroxy acid and carboxylic acid groups in them were tentatively identified. Their high degree of oxidation and relatively low volatility causes them to irreversibly condense onto the particle phase and might be involved in further particle-phase reaction (aging) in the atmosphere to affect the fate of SOA. Therefore, their isomeric species and relative abundance were tracked during the growth and further aging process. The derivation of carboxylic acid to peroxy acids of which produce more highly oxidized species were observed during the formation/ growth of smaller SOA particles. Additionally, photochemical aging with OH radicals was found to yield larger number of peroxy acids which might be produced between fresh SOA and OH radicals with a similar reaction mechanism to auto-oxidation[40]. The separation method using HPLC-MS was applied to the SOA derived from other BVOCs as well and the results turned out that different formulas with isomers that

elute at different RT from those derived from β-pinene were observed. Further structure elucidation with MS^n is still essential as mentioned above.

REFERENCES

(1) Hallquist, M.; Wenger, J. C.; Baltensperger, U.; Rudich, Y.; Simpson, D.; Claeys, M.; Dommen, J.; Donahue, N. M.; George, C.; Goldstein, A. H.; Hamilton, J. F. *Atmos. Chem. Phys. Atmos. Chem. Phys.* **2009**, *9*, 5155–5236.

(2) Chan, A. W. H.; Isaacman, G.; Wilson, K. R.; Worton, D. R.; Ruehl, C. R.; Nah, T.; Gentner, D. R.; Dallmann, T. R.; Kirchstetter, T. W.; Harley, R. A.; Gilman, J. B.; Kuster, W. C.; De Gouw, J. A.; Offenberg, J. H.; Kleindienst, T. E.; Lin, Y. H.; Rubitschun, C. L.; Surratt, J. D.; Hayes, P. L.; Jimenez, J. L.; Goldstein, A. H. *J. Geophys. Res. Atmos.* **2013**, *118* (12), 6783–6796.

(3) Goldstein, A. H.; Galbally, I. E. *Environ. Sci. Technol.* **2007**, *41* (5), 1514–1521.

(4) Putman, A. L.; Offenberg, J. H.; Fisseha, R.; Kundu, S.; Rahn, T. A.; Mazzoleni, L. R. *Atmos. Environ.* **2012**, *46*, 164–172.

(5) Heaton, K. J.; Sleighter, R. L.; Hatcher, P. G.; Hall IV, W. A.; Johnston, M. V. *Environ. Sci. Technol.* **2009**, *43* (20), 7797–7802.

(6) Ma, Y.; Marston, G. *Phys. Chem. Chem. Phys.* **2008**, *10* (40), 6115–6126.

(7) Walser, M. L.; Desyaterik, Y.; Laskin, J.; Laskin, A.; Nizkorodov, S. A. *Phys. Chem. Chem. Phys.* **2008**, *10* (7), 1009–1022.

(8) Steimer, S. S.; Kourtchev, I.; Kalberer, M. *Anal. Chem.* **2017**, *89* (5), 2873–2879.

(9) Steimer, S. S.; Pitton, D.; Hoffmann, Y.; Kalberer, M. *European Aerosol Conference*, August **2017**.

(10) Mutzel, A.; Poulain, L.; Berndt, T.; Iinuma, Y.; Rodigast, M.; Böge, O.; Richters, S.; Spindler, G.; Sipilä, M.; Jokinen, T.; Kulmala, M.; Herrmann, H. *Environ. Sci. Technol.* **2015**, *49* (13), 7754–7761.

(11) Ma, Y.; Luciani, T.; Porter, R. a; Russell, A. T.; Johnson, D.; Marston, G. *Phys. Chem. Chem. Phys.* **2007**, *9* (37), 5084–5087.

(12) Glasius, M.; Duane, M.; Larsen, B. R. *J. Chromatography.* **1999**, *833*, 121–135.

(13) Mentel, T. F.; Springer, M.; Ehn, M.; Kleist, E.; Pullinen, I.; Kurtén, T.; Rissanen, M.; Wahner, A.; Wildt, J. *Atmos. Chem. Phys.* **2015**, *15* (12), 6745–6765.

(14) Donahue, N. M.; Epstein, S. A.; Pandis, S. N.; Robinson, A. L. *Atmos. Chem. Phys.* **2011**, *11* (7), 3303–3318.

(15) Hall IV, W. A.; Johnston, M. V. *J. Am. Soc. Mass Spectrom.* **2012**, *23* (6), 1097–1108.

(16) Perraud, V.; Bruns, E. a; Ezell, M. J.; Johnson, S. N.; Yu, Y.; Alexander, M. L.; Zelenyuk, A.; Imre, D.; Chang, W. L.; Dabdub, D.; Pankow, J. F.; Finlayson-Pitts, B. J. *Proc. Natl. Acad. Sci. U. S. A.* **2012**, *109* (8), 2836–2841.

(17) Winterhalter, R.; Neeb, P.; Grossmann, D. **2000**, 165–197.

(18) Jaoui, M.; Kamens, R. M. *J. Atmos. Chem.* **2003**, *43*, 101–141.

(19) Yasmeen, F.; Szmigielski, R.; Vermeylen, R.; Gómez-González, Y.; Surratt, J. D.; Chan, A. W. H.; Seinfeld, J. H.; Maenhaut, W.; Claeys, M. *J. Mass Spectrom.* **2011**, *46* (4), 425–442.

(20) Yasmeen, F.; Vermeylen, R.; Maurin, N.; Perraudin, E.; Doussin, J.-F.; Claeys, M. *Environ. Chem.* **2012**, *9* (3), 236–246.

(21) Iinuma, Y.; Mller, C.; Berndt, T.; Bge, O.; Claeys, M.; Herrmann, H. **2007**, *41* (19), 6678–6683.

(22) Glasius, M.; Lahaniati, M.; Calogirou, A.; Bella, D. D. I.; Jensen, N. R.; Hjorth, J.; Larsen, B. O. R. **2000**, *34* (6), 1001–1010.

(23) Glasius, M.; Duane, M.; Larsen, B. R. **1999**, *833*, 121–135.

(24) Winterhalter, R.; Van Dingenen, R.; Larsen, B. R.; Jensen, N. R.; Hjorth, J. *Atmos.Chem. Phys. Discuss.* **2003**, *3* (1), 1–39.

(25) Yasmeen, F.; Vermeylen, R.; Szmigielski, R.; Iinuma, Y.; Böge, O.; Herrmann, H.; Maenhaut, W.; Claeys, M. *Atmos. Chem. Phys.* **2010**, *10* (19), 9383–9392.

(26) Gao, S.; Surratt, J. D.; Knipping, E. M.; Edgerton, E. S.; Shahgholi, M.; Seinfeld, J. H. *J. Geophys. Res. Atmos.* **2006**, *111* (14).

(27) Claeys, M.; Iinuma, Y.; Szmigielski, R.; Surratt, J. D.; Blockhuys, F.; Van Alsenoy,

C.; Böge, O.; Sierau, B.; Gómez-González, Y.; Vermeylen, R.; Van der Veken, P.; Shahgholi, M.; Chan, A. W. H.; Herrmann, H.; Seinfeld, J. H.; Maenhaut, W. *Environ. Sci. Technol.* **2009**, *43* (18), 6976–6982.

(28) Szmigielski, R.; Surratt, J. D.; Gómez-González, Y.; van der Veken, P.; Kourtchev, I.; Vermeylen, R.; Blockhuys, F.; Jaoui, M.; Kleindienst, T. E.; Lewandowski, M.; Offenberg, J. H.; Edney, E. O.; Seinfeld, J. H.; Maenhaut, W.; Claeys, M. *Geophys. Res. Lett.* **2007**, *34* (24).

(29) Iinuma, Y.; Boge, O.; Kahnt, A.; Herrmann, H. *Phys. Chem. Chem. Phys.* **2009**, *11*(36), 7985–7997.

(30) Renard, P.; Tlili, S.; Ravier, S.; Quivet, E.; Monod, A. *Atmos. Environ.* **2015**, *130*, 153–162.

(31) Krechmer, J. E.; Groessl, M.; Zhang, X.; Junninen, H.; Massoli, P.; Lambe, A. T.; Kimmel, J. R.; Cubison, M. J.; Graf, S.; Lin, Y. H.; Budisulistiorini, S. H.; Zhang, H.; Surratt, J. D.; Knochenmuss, R.; Jayne, J. T.; Worsnop, D. R.; Jimenez, J. L.; Canagaratna, M. R. *Atmos. Meas. Tech.* **2016**, *9* (7), 3245–3262.

(32) Renard, P.; Siekmann, F.; Gandolfo, A.; Socorro, J.; Salque, G.; Ravier, S.; Quivet, E.; Clément, J. L.; Traikia, M.; Delort, A. M.; Voisin, D.; Vuitton, V.; Thissen, R.; Monod, A. *Atmos. Chem. Phys.* **2013**, *13* (13), 6473–6491.

(33) Winterhalter, R.; Neeb, P.; Grossmann, D.; Kolloff, A.; Horie, O.; Moortgat, G. *J. Atmos. Chem.* **2000**, *35* (2), 165–197.

(34) Glasius, M.; Lahaniati, M.; Calogirou, A.; Di Bella, D.; Jensen, N. R.; Hjorth, J.; Kotzias, D.; Larsen, B. R. *Environ. Sci. Technol.* **2000**, *34* (6), 1001–1010.

(35) Orata, F. *Adv. Gas Chromatogr. - Prog. Agric. Biomed. Ind. Appl.* **2012**, 83–156.

(36) Chapman, J. D.; Goodlett, D. R.; Masselon, C. D. *Mass Spectrom. Rev.* **2014**, *33* (6), 452–470.

(37) Yasmeen, F.; Szmigielski, R.; Vermeylen, R.; Gõmez-González, Y.; Surratt, J. D.; Chan, A. W. H.; Seinfeld, J. H.; Maenhaut, W.; Claeys, M. *J. Mass Spectrom.* **2011**,

46 (4), 425–442.

(38) Kundu, S.; Fisseha, R.; Putman, A. L.; Rahn, T. A.; Mazzoleni, L. R. *Atmos. Chem. Phys.* **2012**, *12* (12), 5523–5536.

(39) Ehn, M.; Thornton, J. A.; Kleist, E.; Sipilä, M.; Junninen, H.; Pullinen, I.; Springer, M.; Rubach, F.; Tillmann, R.; Lee, B.; Lopez-Hilfiker, F.; Andres, S.; Acir, I.-H.; Rissanen, M.; Jokinen, T.; Schobesberger, S.; Kangasluoma, J.; Kontkanen, J.; Nieminen, T.; Kurtén, T.; Nielsen, L. B.; Jørgensen, S.; Kjaergaard, H. G.; Canagaratna, M.; Maso, M. D.; Berndt, T.; Petäjä, T.; Wahner, A.; Kerminen, V.-M.; Kulmala, M.; Worsnop, D. R.; Wildt, J.; Mentel, T. F. *Nature* **2014**, *506* (7489), 476–479.

(40) Zhang, X.; Lambe, A. T.; Upshur, M. A.; Brooks, W. A.; Gray Bé, A.; Thomson, R. J.; Geiger, F. M.; Surratt, J. D.; Zhang, Z.; Gold, A.; Graf, S.; Cubison, M. J.; Groessl, M.; Jayne, J. T.; Worsnop, D. R.; Canagaratna, M. R. *Environ. Sci. Technol.* **2017**, *51* (11), 5932–5940.

(41) Crounse, J. D.; Nielsen, L. B.; Jørgensen, S.; Kjaergaard, H. G.; Wennberg, P.O. *J. Phys. Chem. Lett.* **2013**, *4* (20), 3513–3520.

(42) Larsen, B. R.; Di Bella, D.; Glasius, M.; Winterhalter, R.; Jensen, N. R.; Hjorth, J. *J. Atmos. Chem.* **2001**, *38* (3), 231–276.

(43) Crounse, J. D.; Nielsen, L. B.; Jørgensen, S.; Kjaergaard, H. G.; Wennberg, P. O. *J. Phys. Chem. Lett.* **2013**, *4* (20), 3513–3520.

(44) Lightfoot, P. D.; Cox, R. A.; Crowley, J. N.; Destriau, M.; Hayman, G. D.; Jenkin, M. E.; Moortgat, G. K.; Zabel, F. *Atmos. Environ. Part A, Gen. Top.* **1992**, *26* (10), 1805–1961.

(45) Tu, P.; Johnston, M. V. *Atmos. Chem. Phys.* **2017**, 17, 7593-7603.

(46) Jaoui, M.; Kamens, R. M. *Sect. Title Air Pollut. Ind. Hyg.* **2003**, *44* (3), 259–297.

(47) Warnke, J.; Bandur, R.; Hoffmann, T. *Anal. Bioanal. Chem.* **2006**, *385* (1), 34–45.

(48) Jaoui, M.; Corse, E.; Kleindienst, T. E.; Offenberg, J. H.; Lewandowski, M.; Edney,

E. O. *Environ. Sci. Technol.* **2006**, *40* (12), 3819–3828.

(49) Yu, J.; Cocker III, D.; Griffin, R. J.; Flagan, R. C. *J. Atmos. Chem.* **1999**, No. 3, 207–258.

Chapter 5

CONCLUSIONS

This dissertation is a detailed study of secondary organic aerosol (SOA) derived from various biogenic precursors on a molecular level. Multiple methods of SOA generation and chemical characterization were used allowed the study of SOA at different formation stages during its lifetime and under varied reaction conditions, and various analytical techniques were applied in this study.

The photooxidation reaction with OH radical (aging) alters the chemical composition of SOA after it is freshly formed. The work in chapter 2 simulated the aging process taking place in the atmosphere by using the photochemical chamber in which OH radicals with a constant concentration were generated under the irradiation of the ultraviolet light. The chemical composition of fresh and aged SOA was analyzed with off-line high resolution mass spectrometry techniques. The results showed that some highly-oxidized species (detected in both positive and negative ion mode) were produced during aging process as a result of functionalization. In the meantime, fragmentation of the carbon to carbon bond leads to the decrease of the aerosol mass concentration as detected by SMPS. The great change in both chemical composition and physical properties of SOA as aging proceeds emphasizes the important role of OH radical in the atmosphere and shed light upon the fate of SOA in the atmosphere.

The off-line analysis of fresh/aged SOA allows the non-target screening of its chemical composition. With the high-resolution mass spectrometry, hundreds to thousands ions with formulas assigned within 5 ppm were displayed in Chapter 2.

Among these, the highly oxidized components in the particle phase, also called HOMs, are found to play an important role at different formation stages of SOA. In Chapter 2, methods and criterions to characterize HOMs are developed and applied in both fresh and aged SOA derived from α-pinene, β-pinene and limonene. HOMs that categorized into three groups are discussed and compared with similar study of ELVOCs and LV-OOA elsewhere. It turned out that the average formula of HOMs identified in this study resembles that of ambient LV-OOA based on field measurement at 10 sites; and only a few of HOMs are found to be consistent with ELVOCs that detected in gas phase. Aged HOMs derived from three precursors exhibited similar change comparing with their corresponded fresh HOMs which suggests the occurrence of functionalization.

Formation of SOA is initiated by the oxidation of volatile organic compounds (VOCs) in the gas phase. Mass transfer to the particle phase is thought to occur primarily by a combination of condensational growth of non-volatile products and partitioning of semi- volatile products, though particle phase chemistry may also help grow the particle if it transforms semi-volatile reactants into non-volatile products. In principle, changes in particle composition as a function of particle size allow the relative contributions of e.g. condensation (a surface-limited process) and particle phase reaction (a volume-limited process) to be distinguished. Chapter 3 focused on the study of size selected SOA particles within size range of 30-110 nm. Aerosol exiting the reactor was size-selected with a differential mobility analyzer, and individual particle sizes between 35 and 110 nm in diameter were characterized by on- and off- line mass spectrometry. Both the average oxygen-to-carbon (O/C) ratio and carbon oxidation state (OSc) were found to decrease with increasing particle size, while the relative signal intensity of oligomers increased with increasing particle size. These results are consistent with oligomer formation in the particle phase i.e. accretion reactions, which become more favored as the surface-to-volume ratio of the particle

decreases. Analysis of a series of polydisperse SOA samples showed similar dependencies: as the mass loading increased (and average surface-to-volume ratio decreased), the average O/C ratio and OSc decreased while the relative intensity of oligomer ions increased. The results illustrate the potential impact that particle phase chemistry can have on biogenic SOA formation and the particle size range where this chemistry becomes important.

With respect to the complex chemical composition of SOA, subsequent steps of separation and structure elucidation are necessary allowing the further study (e.g. toxicity and biogeochemical study of aerosol) based on its chemical structure. Chapter 4 described the multiple separation methods applied on SOA derived from various BVOCs. First, separation with ion mobility spectrometry coupled with MS was applied based on the size and molecular formula of SOA. And it turned out that IMS separation is not capable to separate the large amount of isobaric and isomeric components in SOA. Second, gas chromatography coupled with electron ionization MS was utilized and the authentic standard with similar structure of monomeric components of SOA were used as reference. Unfortunately, most of the SOA components, due to their low-volatility, were hardly detected with GC. Lastly, HPLC coupled with high resolution mass spectrometry was used and are found to provide the best separation efficiency among the three methods. With the optimized elution gradient and reverse phase column, isomeric/ isobaric components of SOA were separated. In this case, authentic standards were used as well as an aid to identify the isomeric species that elutes at a separate retention time.

In the meantime, tandem mass spectrometry applied after LC separation was used as a complimentary method to confirm the existence of isomers. MS^2 spectra provide information of the neutral small loss from the parent ions thus helped to distinguish the isomers that contained different types of functional groups suggested by the neutral loss. Additionally, H/D exchange method was applied combing with

MS^2 to confirm the functional groups contained in the formulas. Therefore, 30 formulas (mostly peroxy and carboxylic acid in monomer region of SOA and detected in negative ion mode) with isomers tentatively identified in 12 of them were reported. Additionally, these species were tracked during the formation/growth and further aging process of SOA and were found to play an important role in the particle phase chemistry. However, further structure elucidation (e.g. the position of the functional groups on the carbon skeleton, ring structure) is limited due to the incapability of Orbitrap mass analyzer to perform higher orders of tandem mass spectrometry (e.g. MS^3), which would be essential to identify the complete structure of SOA components (and their isomers).

Appendix

A LIST OF HIGHLY OXIDIZED FORMULAS (REGION 1 AND 2) IN FRESH/AGED SOA (CHAPTER 2)

MW_{fresh}	$Neutral_{fresh}$	MW_{aged}	$Neutral_{aged}$
134.06	C5H10O4	114.033	C5H6O3
150.055	C5H10O5	130.028	C5H6O4
114.033	C5H6O3	146.023	C5H6O5
130.028	C5H6O4	162.018	C5H6O6
146.023	C5H6O5	116.049	C5H8O3
116.049	C5H8O3	132.044	C5H8O4
132.044	C5H8O4	148.039	C5H8O5
148.039	C5H8O5	164.034	C5H8O6
164.034	C5H8O6	118.065	C5H10O3
146.06	C6H10O4	134.06	C5H10O4
162.055	C6H10O5	150.055	C5H10O5
178.05	C6H10O6	144.044	C6H8O4
148.076	C6H12O4	160.039	C6H8O5
144.044	C6H8O4	176.034	C6H8O6
160.039	C6H8O5	192.029	C6H8O7
176.034	C6H8O6	146.06	C6H10O4
174.055	C7H10O5	162.055	C6H10O5
190.05	C7H10O6	178.05	C6H10O6
206.045	C7H10O7	194.045	C6H10O7
176.071	C7H12O5	148.076	C6H12O4
192.066	C7H12O6	164.071	C6H12O5
186.055	C8H10O5	174.055	C7H10O5
202.05	C8H10O6	190.05	C7H10O6
218.045	C8H10O7	206.045	C7H10O7
188.071	C8H12O5	222.04	C7H10O8
204.066	C8H12O6	176.071	C7H12O5
220.061	C8H12O7	192.066	C7H12O6
190.087	C8H14O5	208.061	C7H12O7
206.082	C8H14O6	178.087	C7H14O5
216.066	C9H12O6	186.055	C8H10O5

232.061	C9H12O7	202.05	C8H10O6
248.056	C9H12O8	218.045	C8H10O7
218.082	C9H14O6	234.04	C8H10O8
234.077	C9H14O7	188.071	C8H12O5
250.072	C9H14O8	204.066	C8H12O6
220.098	C9H16O6	220.061	C8H12O7
236.093	C9H16O7	236.056	C8H12O8
228.066	C10H12O6	190.087	C8H14O5
244.061	C10H12O7	206.082	C8H14O6
260.056	C10H12O8	222.077	C8H14O7
230.082	C10H14O6	216.066	C9H12O6
246.077	C10H14O7	232.061	C9H12O7
262.072	C10H14O8	248.056	C9H12O8
231.09	C10H15O6	264.051	C9H12O9
232.098	C10H16O6	218.082	C9H14O6
248.093	C10H16O7	234.077	C9H14O7
234.114	C10H18O6	250.072	C9H14O8
250.109	C10H18O7	220.098	C9H16O6
258.077	C11H14O7	236.093	C9H16O7
274.072	C11H14O8	228.066	C10H12O6
260.093	C11H16O7	244.061	C10H12O7
276.088	C11H16O8	260.056	C10H12O8
292.083	C11H16O9	276.051	C10H12O9
262.109	C11H18O7	292.046	C10H12O10
278.104	C11H18O8	230.082	C10H14O6
264.125	C11H20O7	246.077	C10H14O7
288.088	C12H16O8	262.072	C10H14O8
304.083	C12H16O9	278.067	C10H14O9
290.104	C12H18O8	294.062	C10H14O10
306.099	C12H18O9	232.098	C10H16O6
292.12	C12H20O8	248.093	C10H16O7
300.088	C13H16O8	264.088	C10H16O8
316.083	C13H16O9	280.083	C10H16O9
302.104	C13H18O8	297.086	C10H17O10
318.099	C13H18O9	234.114	C10H18O6
334.094	C13H18O10	250.109	C10H18O7

304.12	C13H20O8	258.077	C11H14O7
320.115	C13H20O9	274.072	C11H14O8
306.136	C13H22O8	290.067	C11H14O9
330.099	C14H18O9	306.062	C11H14O10
346.094	C14H18O10	260.093	C11H16O7
332.115	C14H20O9	276.088	C11H16O8
348.11	C14H20O10	292.083	C11H16O9
334.131	C14H22O9	308.078	C11H16O10
350.126	C14H22O10	262.109	C11H18O7
336.147	C14H24O9	278.104	C11H18O8
342.099	C15H18O9	294.099	C11H18O9
344.115	C15H20O9	310.094	C11H18O10
360.11	C15H20O10	327.097	C11H19O11
346.131	C15H22O9	264.125	C11H20O7
362.126	C15H22O10	288.088	C12H16O8
378.121	C15H22O11	304.083	C12H16O9
348.147	C15H24O9	320.078	C12H16O10
364.142	C15H24O10	336.073	C12H16O11
350.163	C15H26O9	290.104	C12H18O8
372.11	C16H20O10	306.099	C12H18O9
374.126	C16H22O10	322.094	C12H18O10
390.121	C16H22O11	338.089	C12H18O11
376.142	C16H24O10	355.092	C12H19O12
392.137	C16H24O11	292.12	C12H20O8
378.158	C16H26O10	308.115	C12H20O9
394.153	C16H26O11	324.11	C12H20O10
380.174	C16H28O10	341.113	C12H21O11
402.121	C17H22O11	357.108	C12H21O12
404.137	C17H24O11	294.136	C12H22O8
406.153	C17H26O11	300.088	C13H16O8
422.148	C17H26O12	316.083	C13H16O9
408.169	C17H28O11	332.078	C13H16O10
414.121	C18H22O11	348.073	C13H16O11
416.137	C18H24O11	302.104	C13H18O8
418.153	C18H26O11	318.099	C13H18O9
434.148	C18H26O12	334.094	C13H18O10

420.169	C18H28O11	350.089	C13H18O11
436.164	C18H28O12	304.12	C13H20O8
422.185	C18H30O11	320.115	C13H20O9
446.148	C19H26O12	336.11	C13H20O10
448.164	C19H28O12	352.105	C13H20O11
450.18	C19H30O12	353.113	C13H21O11
460.164	C20H28O12	369.108	C13H21O12
462.18	C20H30O12	385.103	C13H21O13
464.196	C20H32O12	306.136	C13H22O8
492.191	C21H32O13	322.131	C13H22O9
534.202	C23H34O14	338.126	C13H22O10
		323.139	C13H23O9
		339.134	C13H23O10
		355.129	C13H23O11
		371.124	C13H23O12
		387.119	C13H23O13
		330.099	C14H18O9
		346.094	C14H18O10
		362.089	C14H18O11
		378.084	C14H18O12
		332.115	C14H20O9
		348.11	C14H20O10
		364.105	C14H20O11
		380.1	C14H20O12
		334.131	C14H22O9
		350.126	C14H22O10
		366.121	C14H22O11
		367.129	C14H23O11
		383.124	C14H23O12
		399.119	C14H23O13
		415.114	C14H23O14
		336.147	C14H24O9
		352.142	C14H24O10
		337.155	C14H25O9
		353.15	C14H25O10
		369.145	C14H25O11

		385.14	C14H25O12
		401.135	C14H25O13
		417.13	C14H25O14
		342.099	C15H18O9
		358.094	C15H18O10
		374.089	C15H18O11
		390.084	C15H18O12
		344.115	C15H20O9
		360.11	C15H20O10
		376.105	C15H20O11
		392.1	C15H20O12
		346.131	C15H22O9
		362.126	C15H22O10
		378.121	C15H22O11
		394.116	C15H22O12
		348.147	C15H24O9
		364.142	C15H24O10
		380.137	C15H24O11
		396.132	C15H24O12
		381.145	C15H25O11
		397.14	C15H25O12
		413.135	C15H25O13
		429.13	C15H25O14
		445.125	C15H25O15
		350.163	C15H26O9
		366.158	C15H26O10
		367.166	C15H27O10
		383.161	C15H27O11
		399.156	C15H27O12
		415.151	C15H27O13
		431.146	C15H27O14
		447.141	C15H27O15
		372.11	C16H20O10
		388.105	C16H20O11
		404.1	C16H20O12
		420.095	C16H20O13

		374.126	C16H22O10
		390.121	C16H22O11
		406.116	C16H22O12
		422.111	C16H22O13
		376.142	C16H24O10
		392.137	C16H24O11
		408.132	C16H24O12
		424.127	C16H24O13
		378.158	C16H26O10
		394.153	C16H26O11
		410.148	C16H26O12
		380.174	C16H28O10
		382.19	C16H30O10
		402.121	C17H22O11
		418.116	C17H22O12
		434.111	C17H22O13
		404.137	C17H24O11
		420.132	C17H24O12
		436.127	C17H24O13
		406.153	C17H26O11
		422.148	C17H26O12
		438.143	C17H26O13
		408.169	C17H28O11
		424.164	C17H28O12
		414.121	C18H22O11
		430.116	C18H22O12
		446.111	C18H22O13
		416.137	C18H24O11
		432.132	C18H24O12
		448.127	C18H24O13
		464.122	C18H24O14
		465.13	C18H25O14
		481.125	C18H25O15
		418.153	C18H26O11
		434.148	C18H26O12
		450.143	C18H26O13

		466.138	C18H26O14
		483.141	C18H27O15
		420.169	C18H28O11
		436.164	C18H28O12
		452.159	C18H28O13
		422.185	C18H30O11
		438.18	C18H30O12
		444.132	C19H24O12
		460.127	C19H24O13
		476.122	C19H24O14
		446.148	C19H26O12
		462.143	C19H26O13
		478.138	C19H26O14
		448.164	C19H28O12
		464.159	C19H28O13
		480.154	C19H28O14
		450.18	C19H30O12
		466.175	C19H30O13
		482.17	C19H30O14
		452.196	C19H32O12
		456.132	C20H24O12
		472.127	C20H24O13
		488.122	C20H24O14
		458.148	C20H26O12
		474.143	C20H26O13
		490.138	C20H26O14
		460.164	C20H28O12
		476.159	C20H28O13
		492.154	C20H28O14
		508.149	C20H28O15
		462.18	C20H30O12
		478.175	C20H30O13
		494.17	C20H30O14
		464.196	C20H32O12
		480.191	C20H32O13
		496.186	C20H32O14

		466.212	C20H34O12
		482.207	C20H34O13
		486.143	C21H26O13
		502.138	C21H26O14
		488.159	C21H28O13
		504.154	C21H28O14
		520.149	C21H28O15
		490.175	C21H30O13
		506.17	C21H30O14
		522.165	C21H30O15
		492.191	C21H32O13
		508.186	C21H32O14
		494.207	C21H34O13
		510.202	C21H34O14
		516.154	C22H28O14
		532.149	C22H28O15
		518.17	C22H30O14
		534.165	C22H30O15
		520.186	C22H32O14
		536.181	C22H32O15
		522.202	C22H34O14
		538.197	C22H34O15
		558.224	C22H38O16
		574.219	C22H38O17
		528.154	C23H28O14
		544.149	C23H28O15
		530.17	C23H30O14
		546.165	C23H30O15
		532.186	C23H32O14
		548.181	C23H32O15
		564.176	C23H32O16
		534.202	C23H34O14
		550.197	C23H34O15
		536.218	C23H36O14
		552.213	C23H36O15
		558.165	C24H30O15

		574.16	C24H30O16
		560.181	C24H32O15
		576.176	C24H32O16
		562.197	C24H34O15
		578.192	C24H34O16
		564.213	C24H36O15
		580.208	C24H36O16
		566.229	C24H38O15
		584.24	C24H40O16
		570.165	C25H30O15
		586.16	C25H30O16
		572.181	C25H32O15
		588.176	C25H32O16
		574.197	C25H34O15
		590.192	C25H34O16
		576.213	C25H36O15
		592.208	C25H36O16
		578.229	C25H38O15
		594.224	C25H38O16
		580.245	C25H40O15
		612.235	C25H40O17
		602.192	C26H34O16
		604.208	C26H36O16
		620.203	C26H36O17
		606.224	C26H38O16
		608.24	C26H40O16
		640.23	C26H40O18
		698.295	C26H50O21
		634.219	C27H38O17
		654.246	C27H42O18
		646.219	C28H38O17
		648.235	C28H40O17
		650.251	C28H42O17
		652.267	C28H44O17
		690.246	C30H42O18
		744.279	C30H48O21

		768.338	C30H56O22
		784.333	C30H56O23
		800.328	C30H56O24
		722.273	C31H46O19
		742.3	C31H50O20
		752.284	C32H48O20
		770.295	C32H50O21
		768.316	C33H52O20
		784.311	C33H52O21
		798.327	C34H54O21